

1  
2  
3  
4  
5  
6  
7  
8  
9  
10  
11  
12  
13  
14  
15  
16  
17  
18  
19  
20  
21  
22

**Active WNT vampirization by glioblastoma network leads to  
brain tumor growth and neurodegeneration**

Marta Portela<sup>1\*</sup>, Varun Venkataramani<sup>2,3,4</sup>, Natasha Fahey-Lozano<sup>1</sup>, Esther Seco<sup>1</sup>,  
Maria Losada-Perez<sup>1</sup>, Frank Winkler<sup>2,3</sup> and Sergio Casas-Tintó<sup>1\*</sup>

1- Instituto Cajal-CSIC. Av. del Doctor Arce, 37. 28002. Madrid. Spain

2- Neurology Clinic and National Center for Tumor Diseases, University Hospital  
Heidelberg, INF 400, 69120 Heidelberg, Germany

3- Clinical Cooperation Unit Neurooncology, German Cancer Consortium (DKTK),  
German Cancer Research Center (DKFZ), 69120 Heidelberg, Germany

4- Institute for Anatomy and Cell Biology, Heidelberg University, 69120 Heidelberg,  
Germany.

Corresponding author: [scasas@cajal.csic.es](mailto:scasas@cajal.csic.es) and [m.portela@cajal.csic.es](mailto:m.portela@cajal.csic.es)

Running title: Glioma-induced neurodegeneration

## 23 **Summary**

24 Glioblastoma (GB) is the most lethal brain tumor due to its high proliferation,  
25 aggressiveness, infiltration capacity and resilience to current treatments. Activation of  
26 the Wingless-related-integration-site (WNT) pathway is associated with a bad  
27 prognosis. Using *Drosophila* and primary xenograft models of human GB, we describe  
28 a mechanism that leads to the activation of WNT signaling [Wingless (Wg) in  
29 *Drosophila*] in tumor cells. GB cells display a network of tumor microtubes (TMs) which  
30 enwraps neurons, accumulates Wg receptor Frizzled1 (Fz1), and, thereby, actively  
31 depletes Wg from the neurons. Consequently, GB cells proliferate due to  $\beta$ -catenin  
32 activation, and neurons degenerate due to Wg signaling extinction. This novel view  
33 explains both neuron-dependent tumor progression, and also the neural decay  
34 associated with GB.

## 35 **Keywords**

36 Neuron, Glia, Cancer, Synapse-loss, wingless, Frizzled, beta-catenin, Glioblastoma,  
37 Cytoneme, Wg-depletion.

38

## 39 **Introduction**

40 The evolution of glioblastoma (referred here as GB) is accompanied by broad  
41 neurological dysfunctions, including neurocognitive disturbances, that compromise  
42 quality of life during the short life span of patients, one year usually <sup>1</sup>. These tumors are  
43 often resistant to standard treatments which include resection, radiotherapy and  
44 chemotherapy with temozolomide <sup>2</sup>. Numerous studies are focused on new molecular  
45 targets to treat GBs <sup>3-6</sup>; however, none of them has proven effective yet, which is in  
46 stark contrast to the considerable progress made in other tumor types. It is therefore  
47 necessary to explore new biological concepts that can lead to additional therapeutic  
48 strategies against GBs.

49 The WNT canonical pathway is activated upon the ligand “Wingless-related integration  
50 site” (WNT) binding to specific receptors (LRPs and FZD) in the plasma membrane. As  
51 a consequence, the destruction complex (APC and Axin) is inactivated and  $\beta$ -catenin  
52 (armadillo in *Drosophila*) is released. Further,  $\beta$ -catenin translocates into the cell  
53 nucleus where it promotes the expression of target genes (*i.e.* *Cyclin D1* and *Myc*)<sup>7-8</sup>.  
54 The WNT pathway is conserved through metazoans and it plays a central role in brain  
55 development<sup>9</sup>, adult neuronal physiology<sup>10</sup> and synaptogenesis<sup>11</sup>. Perturbations in  
56 WNT signaling are associated with neural deficits, Alzheimer’s disease and brain  
57 cancer, most notably GB<sup>12</sup>. WNT and FZD signaling can be deregulated in  
58 glioblastoma<sup>13-14</sup> (reviewed in<sup>15</sup>). In particular, one of the hallmarks of bad prognosis is  
59 the accumulation of  $\beta$ -catenin in tumoral cells<sup>16-17</sup>, indicating an activation of WNT/FZD  
60 pathway<sup>18</sup>.

61 GB cells extend ultra-long membrane protrusions that interconnect tumor cells<sup>19</sup>.  
62 These tumor microtubes (TMs) are associated with the worst prognosis in molecular  
63 subtypes of human gliomas. TMs contribute to invasion and proliferation, resulting in  
64 effective brain colonization by GB cells. Moreover, TMs constitute a multicellular  
65 network that connects GB cells over long distances, a feature that likely provides  
66 resistance against radiotherapy, chemotherapy and surgery<sup>19-20</sup>. Considering the many  
67 cytological similarities of TMs and tunneling nanotubes (TNTs)<sup>21</sup>, it seems that TMs in  
68 aggressive gliomas are the *in vivo* correlate of TNTs described in cell culture. In  
69 addition, TMs seem akin to a basic mechanism of cell-cell connection and molecular  
70 communication called “cytonemes” in *Drosophila*<sup>22</sup>. *Growth Associated Protein-43*  
71 (*GAP43*) is essential for the development of TMs and, thus, the tumor cell network  
72 which is associated with GB progression<sup>19</sup>. However, many aspects of this  
73 paradigmatic finding in glioma biology are still unexplored, including its impact on  
74 neighboring neurons.

75 Here, we report that *Drosophila* glial cells develop a TM network upon oncogenic  
76 transformation, akin to what is known from refined mouse glioma models, and from  
77 patients<sup>19</sup>. These TMs share characteristics in common with *Drosophila* epithelial  
78 cytonemes<sup>22-23</sup> which are also dependent on *Gap43* expression. TMs relocate Frizzled  
79 (Fz1) receptor in the glia-neuron interphase, depleting Wingless (Wg) from neighboring  
80 neurons. As a consequence, the number of glioma cells increases, while neuronal  
81 synapse number decreases and neurodegeneration ensues. The concept of a Wg/Fz1  
82 signaling equilibrium between glioma cells and neurons is relevant because it redefines  
83 GB as a neurodegenerative disease, and because it reveals a potential novel strategy  
84 against GB.

85

## 86 **Results**

### 87 ***Drosophila* glioma network**

88 To study the mechanisms of communication among malignant glial cells and  
89 neighboring neurons, we used a previously described *Drosophila* GB model<sup>24</sup>, which  
90 consists in the co-overexpression of constitutively active forms of EGFR (dEGFR $\lambda$ ) and  
91 the PI3K catalytic subunit p110 $\alpha$  (PI3K92E) driven by the glial specific *repo-Gal4*. This  
92 combination stimulates malignant transformation of post-embryonic larval glia, leading  
93 to lethal glial neoplasia<sup>24-25</sup> which is measured by the increase of glial cell number  
94 (Repo positive) compared with a control brain (Figure 1A-C). Based on  
95 this *Drosophila* GB model we have evaluated the impact of glial tumor cell proliferation  
96 on neighboring neurons.

97 To visualize the glial network, a myristoylated form of red fluorescent protein  
98 (expressed via *UAS-myrRFP*), which accumulates in the plasma membrane, was  
99 expressed in glial cells. RFP signal in control brains shows glial soma and the network

100 formed in WT larval brains (Figure 1D). Relative to the control brain, the glioma brain  
101 shows a significant enlargement in glial membrane projections (Figure 1E).

102 To define the nature of these projections, we expressed a *UAS-Ihog-RFP* construct in  
103 glial cells. Ihog (*interference hedgehog*) is a type 1 membrane protein shown to  
104 mediate the response to the active Hedgehog (Hh) protein signal<sup>26</sup>, which accumulates  
105 in the epithelial cell filopodia, termed cytonemes<sup>27</sup>. This red fluorescent tagged form of  
106 Ihog-RFP in epithelial cells labels cellular processes (filopodia) in the basal region of  
107 the wing imaginal discs<sup>27-28</sup>. The expression of *UAS-Ihog-RFP* under the control of  
108 *repo-Gal4* allows the visualization of cytonemes in glial cells (Figure 1F) as part of a  
109 wild type glial interconnecting network. The accumulation of Ihog in the cellular  
110 projections of transformed glial cells allowed labeling the tumor microtubule-like  
111 processes of these cells. Since the term tumor microtubule (TM) is the now established  
112 terminology to describe thin membrane protrusions from malignant glioma cells in  
113 human and murine tumors, we decided to also use this term from here on<sup>19</sup>. In glioma,  
114 TMs are observed across the brain (Figure 1G) suggesting a larger volume of TMs.  
115 Quantifications (Figure 1H) including the ratio of glioma cells number vs the volume of  
116 glioma TMs network show that TMs growth is higher in glioma cells and therefore that  
117 the network expands more than the proportional glial number in GB.

118 A detailed analysis of this glioma network revealed that glial TMs wrap clusters of  
119 neurons in individual GB “nests” (Figure 1J compared with I, Figure S1 A-B’’ and see  
120 video S1 and S2) comparable to previously described perineuronal nests in patients<sup>29</sup>.  
121 To further identify the identity of the TMs, we took advantage of the LifeAct-GFP  
122 reporter as a validated marker of human TMs<sup>19</sup> (Figure S1C). Additionally we  
123 characterized the TMs with previously described markers for cytonemes in *Drosophila*  
124<sup>28</sup> and orthologues markers of human TMs<sup>19,28</sup> (Figure S1D-G). Moreover, we  
125 performed functional experiments where the TMs are defective after the  
126 downregulation of *neuroglian (nrg-RNAi)* as it has been previously described in

127 epithelial cytonemes<sup>30</sup> (Figure S1 H-I). This characteristic morphology suggests that  
128 glioma cells build an organized TMs network around the neurons which segregates  
129 neuronal populations.

130 Next we sought to clarify whether similar molecular machineries are involved in human  
131 and *Drosophila* TMs. GAP43 is necessary for TMs formation and function, and drives  
132 microtubule-dependent tumor cell invasion, proliferation, interconnection, and  
133 radioresistance<sup>19</sup>. We have reproduced this specific and unique characteristic of  
134 human GB in the *Drosophila* model. To determine whether the *Drosophila* glial network  
135 is susceptible to *GAP43* depletion, as it has been described in human tumor cells<sup>19</sup>,  
136 we knocked down igloo-the *Drosophila Gap43* homologous gene<sup>31</sup>, in glioma cells.  
137 Confocal images of larval brains show that the glioma network does not develop upon  
138 *Gap43* silencing and, as a consequence, glial TMs do not enwrap neurons showing a  
139 phenotype similar to the control (Figure 1K and video S3).

140 In addition, we obtained scan electron microscopy (SEM) images to visualize glia  
141 morphology (Figure 2A-G). High magnification SEM images show an enlargement of  
142 glial cells surface in glioma samples (Figure 2D). Higher magnifications show  
143 perineuronal nests of TMs which surround neurons (Figure 2E-F). Longitudinal sections  
144 of glial cells show the intercalation of glioma TMs in neuronal tissue (G). Moreover, 3D  
145 reconstructions of Control and glioma brains with the glial network marked with ihog-  
146 RFP and LifeAct-GFP showed similar phenotypes (Figure 2H-I and Videos S4-S5).

147 To exclude the possibility that suppression was due to a titration of GAL4 activity  
148 caused by introducing an additional UAS-transgene, we also tested whether co-  
149 expression of *UAS-lacZ* or *UAS-yellow-RNAi* had any rescuing ability in glioma brains.  
150 The observed phenotypes such as the number of glial cells and the GB nests were  
151 unchanged in the presence of an additional UAS-transgene (Figure S2A-B). This

152 observation indicates that in *Drosophila* glioma Gap43 reproduces the function  
153 previously described in human samples.

154 The genetic disruption of *Gap43* prevents the tumoral network of TMs and halts the  
155 overgrowth of glioma cell membranes. Moreover, the direct consequence on flies  
156 developing a glioma is larval/pupal lethality. Upon *Gap43* knockdown, however, the  
157 glioma-induced lethality is prevented allowing the emergence of adults (Figure 1L).  
158 Interestingly, *Gap43* knockdown in wild type glial cells neither affects the normal  
159 development of neurons and glia, nor their viability (Figure S2C-G). Taking all data  
160 together, transformed glial cells take advantage of the Gap43-dependent tumoral  
161 network to proliferate and enwrap neurons and, as a consequence, cause death. Thus,  
162 the dependency of TMs on GAP43 is conserved between flies and gliomas originated  
163 from human tumor cells.

#### 164 **Wingless signaling in glioma**

165 GB is characterized by the deregulation of many key signaling pathways involving  
166 growth, proliferation, survival, and apoptosis, such as p53, pRB, EGFR, PI3K, STAT3  
167 or WNT<sup>32-33</sup>. WNT signaling has long been suggested as a hallmark in gliomagenesis  
168 associated with the proliferation of stem-like cells in human GBs<sup>34</sup>. WNT signaling  
169 promotes tumoral cell proliferation and dissemination as well as resistance to chemo  
170 and radiotherapy (reviewed in<sup>15,35</sup>). To assess the prevalence of WNT genes/pathway  
171 deregulation in GB, we searched for mutations related to WNT pathway in the  
172 Collection of Somatic Mutations in Cancer (COSMIC). We analyzed data from 922  
173 samples of grade IV astrocytomas (GB) searching for gain of expression or  
174 duplications. First, we analyzed *Wnt* family genes, which encode the ligands of the  
175 WNT pathway. In particular, we analyzed WNT6 that is related to the self-renewal  
176 ability of GB cells<sup>36</sup>, WNT3A and WNT1 overexpression that is detected in glial stem  
177 cells<sup>37</sup> and WNT5A and WNT2 that were shown to induce migration of GB cells<sup>38-39</sup>.

178 Our analysis of the COSMIC database revealed that WNT1, WNT3A, WNT6 or WNT5A  
179 genes do not appear mutated in GB samples and only 6 cases showed mutations in  
180 WNT2 (0,6%) (Figure S3A). WNT signaling is a hallmark of GBs, but as no evident  
181 changes in WNT expression were found, we searched for mutations in FZD genes, that  
182 encode the receptors of WNT. In particular, we analyzed FZD2 and FZD9 that are  
183 linked to self-renewal ability in GB <sup>36,39-40</sup> and FZD4, a positive WNT regulator, which is  
184 a causative effector for invasive phenotypes of GB cells <sup>41</sup>. We did not find any case of  
185 a GB patient with a gain of expression in FZD2 or FZD4, and barely 4 cases (0,4%)  
186 showed a mutation for FZD9. The total number of mutations related with WNT or FZD  
187 genes accounts for 5% of the total GB samples analyzed (Supp. Table 1). In addition,  
188 we analyzed data from GB in The Cancer Genome Atlas (TGAC) for WNT ligands, FZD  
189 receptors and transcriptional targets of WNT pathway databases Figure S3C-D  
190 through the Xena Functional Genomics Explorer (<https://xenabrowser.net/>). We  
191 analyzed expression levels in primary GB tissue and non tumoral tissue, transcriptional  
192 targets for WNT pathway (Figure S3B) are upregulated in GB samples. However, WNT  
193 ligands from the canonical WNT pathway are not upregulated (Figure S3C) and among  
194 FZD receptors, only FZD7 shows significant changes in GB tissue (Figure S3D).  
195 Taking all these data together, in spite of WNT pathway activation in GB tissue, there is  
196 no correlation between overexpression of WNT ligands and GB development.

197 Nevertheless, previous reports indicate that WNT targets, such as FoxM1 which  
198 promotes nuclear localization of  $\beta$ -catenin, or  $\beta$ -catenin itself are related with Glial  
199 Stem Cells (GSC) maintenance and tumorigenesis. Indeed, they are standard  
200 biomarkers for GB bad prognosis <sup>16,42-45</sup>.  $\beta$ -catenin activation (translocation to the  
201 nuclei) is a downstream event of WNT pathway. It has been identified in 19% of  
202 surgical samples from adult GB patients and in 30% of surgical samples from pediatric  
203 patients. Moreover, WNT inhibition leads to suppression of tumor growth, proliferation  
204 in cultures, and a modest induction of cell death <sup>34</sup>.



205 Given the discrepancy between the presence of WNT pathway markers and the lack of  
206 mutations in GB samples, we decided to study *Wingless* (*wg*) expression, the fly  
207 homologue to human WNT, in our glioma model. The results showed that Wg protein is  
208 homogeneously distributed in control larval brains with a slight increase in glial  
209 membranes (Figure 3A-A'', C) but glioma brains showed accumulation of Wg in  
210 tumoral cells (Figure 3B-B'', C), in line with human GBs<sup>38,46</sup>. To determine whether Wg  
211 could be signaling to the glial cells, we assessed the presence of Frizzled (Fz)  
212 receptors in glial membranes. Monoclonal antibodies were used to visualize the Fz1  
213 and Fz2 receptors in control samples, Fz1 receptors are localized homogeneously  
214 across the brain and partially accumulated in glial membranes (Fz1, Figure 3D-3D''  
215 and Fz2, showing the expected pattern in the wing disc<sup>47</sup> Figure S4A and localized  
216 homogeneously in the brain S4B-B'''). And glioma samples where Fz1 is highly  
217 accumulated in glial membranes (Figure 3E-E'', H). No changes for Fz2 were detected  
218 in glioma brains (Figure S4C-C'''). In addition, a detailed analysis of glioma brains  
219 revealed that Fz1 protein specifically accumulated in TMs (iHog<sup>+</sup>) (Figure 3E'').  
220 Furthermore, we used a Fz1-GFP protein reporter to determine the localization of Fz1  
221 protein in more detail (supp. Figure S4D-D''). The results indicate that Fz1 is  
222 preferentially accumulated in glial cells located at the border of the tumor, in direct  
223 contact with neighboring neurons. These data suggest that the glioma TMs network  
224 contributes to Wg/Fz1 signaling.

225 To evaluate the contribution of Fz1 to the progression of the glioma, we knocked down  
226 the Fz1 receptor (using *UAS-Fz1-RNAi*) in transformed glial cells. First we validated  
227 *UAS-Fz1-RNAi* tool in epithelial tissue from larvae wing imaginal discs. Even though  
228 Fz1 expression in wing imaginal disc is discrete, upon *UAS-Fz1-RNAi* expression in the  
229 posterior compartment (marked with GFP), there is a reduction in Fz1 protein signal  
230 compared with the anterior compartment from the same tissue (Figure S5A). Brains  
231 showed a significant reduction of Fz1 protein expression (Figure 3F, H). However, no

232 change was observed in glioma TMs network development (Figure 3F'). Furthermore,  
233 we inhibited the development of the glioma network by expressing *UAS-Gap43-RNAi*  
234 and stained the brains for Fz1. Under these conditions the network does not expand,  
235 Fz1 does not accumulate in TMs and it shows a homogeneous distribution similar to  
236 control brains (Figure 3G-G', H). These results indicate that Fz1 accumulation in TMs  
237 is a consequence of the glioma network but the glioma network formation does not  
238 require Fz1 accumulation in the TMs.

### 239 **Glial Fz1 interacts with neuronal Wg**

240 The abnormal distribution of Wg and Fz1 in glioma brains could be due to either an  
241 increase in gene expression or to redistribution of the protein. First, to determine *wg*  
242 and *Fz1* transcription levels in glioma, we performed quantitative PCR experiments  
243 from brain RNA extracts. The results showed that *wg* and *Fz1* transcription levels are  
244 comparable in control and gliomas (supp. Figure S6A). To consider the mRNA  
245 translation or protein stability and degradation, we measured total Fz1 and Fz2 protein  
246 levels in Western blot experiments. Control and glioma brain protein extracts were  
247 blotted and incubated with anti-Fz1 or Fz2 antibodies; Tubulin was used as a loading  
248 control (Supp. Figure S6B). Quantification of the membranes showed no significant  
249 changes for Fz1 protein levels in glioma (Supp. Figure S6B). Moreover, we performed  
250 *in situ* hybridization experiments to detect Wg and Fz1 mRNA expression in control and  
251 glioma brains. The results are consistent with the qPCRs results (Figure S6A) showing  
252 no differences for *wg* or *Fz1* transcription between controls and gliomas (Figure S6C).

253 The data indicate that in spite of a higher signal for Wg and Fz1 proteins in glioma cells  
254 by immunofluorescence, there are no changes in gene expression. We hypothesized  
255 that Fz1 is transported and accumulated along glioma TMs, which contact neighboring  
256 neurons and receive Wg from them.

257 According to this hypothesis, the glial membranes would be in close proximity to  
258 neuronal membranes to allow Fz1-Wg interaction. To assess this, we performed  
259 GRASP experiments<sup>48</sup>. This technique determines intimate physical interaction among  
260 glia and neurons, in the range of 20-40nm (synaptic distance) which is compatible with  
261 protein-protein interaction<sup>48</sup>. Each split fragment of the green fluorescent protein (GFP)  
262 was expressed in neurons (*elav-lexA*) or glial (*repo-Gal4*) cells, respectively (see  
263 Material and Methods). Only upon intimate contact between the two split fragments  
264 GFP fluorescence is reconstituted. Control samples (Figure 4A-C'') showed a discrete  
265 signal corresponding to the physiological interaction between glia and neurons,  
266 nevertheless, upon glioma induction a massive GFP signal from GRASP reporter was  
267 detected (Figure 4D-F''). This result indicates that, in a glioma condition, there is a  
268 significant increase of glia-neuron membrane interaction.

269 We had observed specific signal localization for Wg and Fz1 in glioma membranes  
270 (*myr-RFP/ihog-RFP*) (Figure 3B-B'', E-E''). However, to determine if Fz1 (receptor)  
271 and Wg (ligand) co-localized in glioma brains we conducted co-staining with Wg and  
272 Fz1 antibodies. The confocal images showed Fz1 and Wg accumulation in glioma TMs  
273 compared to controls (*ihog-RFP* marked) (Figure 4G-G''-H-H''). Moreover, a detailed  
274 inspection of the images revealed that Wg protein accumulated at the border between  
275 neuron and glioma cells (Figure 4H-H''), which is consistent with our hypothesis of glial  
276 cells receiving Wg from neighboring neurons. To confirm the physical interaction of Fz1  
277 and Wg proteins we performed proximity ligation assays (PLA) (see Materials and  
278 Methods)<sup>49</sup>. This quantitative method reports the interactions between two proteins  
279 with a resolution of 40nm<sup>50</sup>. Control brains showed a discrete number of puncta  
280 showing the physiological interactions (Figure 4I-I'', K). However, glioma brains  
281 showed a fivefold increase in the number of puncta (Figure 4-J'', K) indicating a  
282 significant increase in Fz1-Wg number of interactions. These results confirm that  
283 glioma cells accumulate Fz1 receptor in TMs, and then this specific receptor interacts

284 with Wg. But Wg is not upregulated in the glioma brain so we hypothesize that Wg  
285 comes from neighboring neuronal membranes and it accumulates in glioma cell  
286 membranes.

### 287 **Wg/Fz1 pathway targets are active in glioma and inactive in neurons**

288 Wg targets are indicators of Wg/Fz1 activity in the recipient cell. Armadillo/ $\beta$ Catenin is  
289 a cytoplasmic protein which, upon activation of Wg pathway, translocates into the  
290 nucleus and activates transcription of target genes<sup>12,51</sup>. To determine if Fz1 is signaling  
291 in gliomas as a consequence of Wg-Fz1 interaction, we stained control and glioma  
292 brains for Armadillo (Arm) with a specific antibody that detects preferentially its  
293 cytoplasmic inactive form (Cyt-Arm)<sup>52</sup>. Cyt-Arm was homogeneously distributed along  
294 the brain in control samples (Figure 5A, D). However, glioma brains showed  
295 accumulation of Cyt-Arm in the cytoplasm of the neurons and a reduction in glioma  
296 cells (Figure 5B, D). This result suggests that, in glioma brains, Wg/Fz1 pathway is  
297 inactive in neurons and active in glioma cells. More importantly, this data shows that  
298 the network expansion and the accumulation of Fz1 in the TM projections have an  
299 effect on neighboring neurons. Further, we dismantled the glioma network expressing  
300 *UAS-Gap43-RNAi* or down<sup>53</sup>regulated Fz1 (*UAS-Fz1-RNAi*) and stained for Cyt-Arm.  
301 Under this condition, Cyt-Arm was homogeneously distributed along the brain similar to  
302 the control (Figure 5C, D and S7A) demonstrating that the network is required to  
303 promote Wg signaling in the transformed glia.

304 To further confirm that Wg pathway is active in the glial transformed cells and silenced  
305 in neurons, we used several additional Wg pathway reporters, namely *arm-GFP*, *nkd-*  
306 *lacZ*, *tsh-lacZ*, *fz4-GFP* and *dally-LacZ*<sup>54-55</sup>. The results showed that all these reporters  
307 were active in glioma cells and inactive in neurons compared to control brains (Figure  
308 5E-H'' and Figure S7B-G'') which confirm that the Wg/Fz1 pathway is inactive in  
309 neurons and active in glioma cells.

310 Since we observed specific signal localization and accumulation of Wg and Fz1 in  
311 glioma membranes and consequently the activation of the pathway in glioma cells, we  
312 wondered if these results were conserved in human glioma cells. Therefore, we used a  
313 primary patient-derived glioblastoma culture xenograft model using S24 cells kept  
314 under stem-like conditions (see Materials and Methods), which reproduce previously  
315 described Scherer modes, perivascular migration and spread<sup>29,56</sup>. GFP-marked S24  
316 cells were injected in the brain of NMRI nude mice, and brains were removed and  
317 analyzed 90 days later (as previously described in<sup>19</sup>). To validate our data, we  
318 performed a series of more diffuse tumor parts (history grade II-like tumor periphery  
319 where normal brain has just been colonized) and denser tumor parts (grade III-IV like,  
320 from central areas) GB images from S24 xenografts brain sections.

321 We stained the samples for  $\beta$ -catenin and WNT1 proteins in S24 xenograft brain  
322 sections and compared them to control samples (Figure 5-I-N and Figure S8G-H). We  
323 observed a significant increase of both proteins in GB cells, in line with previous  
324 observations. These data indicate that WNT1 is deposited in GB cells and activates  
325 WNT pathway; consequently  $\beta$ -Catenin is upregulated to mediate GB cells malignancy  
326<sup>16</sup>. Moreover, images of the WNT1 and  $\beta$ Catenin staining of grade II and III GB images  
327 from S24 xenografts brain sections and quantification of the pixel intensity indicates  
328 that the accumulation of WNT1 and activation of  $\beta$ Catenin correlates with the growth of  
329 the tumor (Figure S8A-F).

330 To determine Fz1's contribution to the proliferation of *Drosophila* gliomas we quantified  
331 the number of transformed glial cells upon *Fz1* downregulation. A specific Repo  
332 antibody was used to mark glial cell nuclei in the brains. The data show a significant  
333 increase of glial cell number in glioma brains, which is prevented by *Fz1*  
334 downregulation or TM network dismantlement (Figure 6A-E). In addition, we studied  
335 the adult survival by quantifying the number of flies with glioma and/or *Fz1-RNAi*  
336 expression. First, Fz1 downregulation in normal glial cells allows 80% adult survival.

337 On the other hand, the glioma caused 100% lethality in larval or pupal stages. By  
338 contrast, glioma lethality was reverted upon *Fz1* downregulation in repo cells, and 70%  
339 of the animals reached adulthood (Figure 6F). In conclusion, *Fz1* is not necessary for  
340 the glioma network overgrowth but *Wg/Fz1* signaling is necessary for the increase in  
341 the number of tumoral cells and the associated lethality.

342

### 343 **Wg/Fz1 pathway disruption in adult brains**

344 To discard that these results are restricted to a developmental process, we performed  
345 similar experiments in adult brains. We included a *tub>Gal80<sup>TS</sup>* system to repress *Gal4*  
346 activation during all developmental stages (see Materials and Methods), glioma was  
347 induced 4 days after adult eclosion when adult brain is fully differentiated. Analysis of  
348 adult flies survival indicate that animals with glioma start dying at day 9 after the glioma  
349 induction until the 14th day, significantly earlier than control flies. (Figure S9A). 7 days  
350 after glioma induction we stained for Arm, *Fz1* and *Wg* control and glioma adult brain  
351 samples and quantified ( $n > 15$ ) the average pixel intensity ratio (Glial cells membranes  
352 RFP+ vs neuronal tissue (Figure S9B-H). The results reproduce the findings from larval  
353 brains: *Fz1* and *Wg* proteins are accumulated in glioma tissue and Cyt-Arm signal  
354 shows an increase of *wg*-pathway activity in glioma cells. Therefore, there are no  
355 differences between larval and adult brains regarding *Wg*-pathway in glioma cells and  
356 neurons. Moreover, we analyzed *Drosophila* adult negative geotaxis behavior (climbing  
357 assay), as an indication for possible motor defects associated with neurodegeneration.  
358 The results showed symptoms of neurodegeneration in glioma flies compared to  
359 controls (Video S6).

### 360 **Gliomas cause Neurodegeneration**

361 Previous results suggest that a neurodegeneration process is taking place in glioma  
362 brains. To determine whether the glioma is causing neurodegeneration we quantified

363 the number of active zones (synapses) in the neuromuscular junction (NMJ). This well-  
364 established system has been used for decades to study neurodegeneration in  
365 *Drosophila*<sup>57-60</sup>, motor neuron soma is located in the central nervous system, but  
366 synapse counting can be accurately done in synaptic buttons located in adult or larva  
367 muscular wall. Adult NMJs Quantification of confocal images stained with anti-  
368 bruchpilot (Nc82) revealed a significant reduction in the number of synapses in glioma  
369 adult (Figure S9I) or larval NMJs compared to controls (Figure 7A-B, F) and therefore,  
370 a neurodegenerative process, which is prevented by Fz1 downregulation or TM  
371 network dismantlement (Figure 7C-D, F).

372

### 373 **Wg expression in glioma cells is dispensable for tumor progression**

374 Fz1 receptor is accumulated in glioma TMs and contribute to Wg depletion and  
375 pathway equilibrium disruption. To determine whether the source of Wg is neuronal or  
376 glial, we silenced *wg* expression in neurons exposed to glioma, or in glioma cells. First  
377 we validated *UAS-wg-RNAi* tool in epithelial tissue, wing imaginal discs. Activation of  
378 *UAS-wg-RNAi* in the posterior compartment (marked with GFP) cause a reduction of  
379 specific monoclonal anti *wg* (Figure S5B). Pan-neuronal *wg* silencing (*elav>wg RNAi*)  
380 is lethal in line with our hypothesis regarding the requirement of Wg in neuronal  
381 biology. Besides, *wg* knockdown (*wg-RNAi*) in glioma cells (*Repo>PI3K; EGFR; wg-*  
382 *RNAi*) does not prevent glioma cell number increase (Figure 7G-I, K) nor glioma TMs  
383 volume expansion (Figure 7G-I, L), these results suggest that *wg* expression in glioma  
384 cells is not relevant for glioma progression.

385 Moreover, to stress on the contribution of Fz1 receptor as mediator for Wg depletion,  
386 we generated glioma cells and silenced *Fz1* expression, in addition we expressed a  
387 constitutively active form of *armadillo* (*UAS-armS10*)<sup>61</sup> to activate Wg pathway  
388 downstream Wg-Fz1 in these gliomas (Figure 7E-F and J-L). We counted the number

389 of synapses and observed that it is comparable to glioma + *Fz1RNAi* (Figure 7A-F).  
390 This result suggests that the reduction in the number of synapses is specifically  
391 mediated by Fz1 accumulation. To confirm that the Fz1 depletion and Arm signaling  
392 produces a glioma like condition we counted the number of glial cells and network  
393 volume (Figure 7G-L). We observed that in this case the number of glioma cells  
394 increased and expanded TMs (Figure 7J-L) similar to a glioma (Figure 7JH).

### 395 **Wg/Fz1 pathway disruption causes neurodegeneration**

396 Neuronal development and physiology are dependent on Wg/Fz1 signaling and  
397 disruptions in this signaling pathway lead to synapse loss, an early symptom of  
398 neurodegeneration (reviewed in <sup>62-65</sup>. To determine if an imbalance in Wg distribution  
399 caused by glioma cells can affect the neighboring neurons, we aimed to determine the  
400 contribution of Fz1/Wg pathway to neuronal physiology. To inhibit Wg/Fz1 pathway  
401 signaling we expressed *UAS-fz1-RNAi* or *UAS-wg-RNAi* in motor neurons under the  
402 control of a *D42-Gal4* driver <sup>66</sup> and quantified the number of active zones (synapses) in  
403 the neuromuscular junction (NMJ). Quantification of confocal images stained with anti-  
404 bruchpilot (Nc82) revealed a significant reduction in the number of synapses and  
405 therefore, a neurodegenerative process (Figure 8A-D). These data suggest that  
406 Wg/Fz1 signaling pathway activity in neurons is necessary in for synaptogenesis.

407 So far, we have demonstrated that glioma cells cause a disruption of Wg/Fz1 signaling  
408 in neurons (Figure 5) and our data suggest that this is dependent on Fz1 accumulation  
409 in glioma cells (Figure 3 and 4H). Next, we decided to restore this signaling equilibrium  
410 by overexpressing Fz1 receptor in neurons surrounded by glioma cells. To avoid  
411 crossed expression we generated Fz1 transgenic flies based on the LexA-LexAop  
412 expression system <sup>67</sup>, which is independent of the Gal4-UAS system used to generate  
413 the glioma. We validated this newly generated tool in *Drosophila* brains. *LexAop-Fz1*  
414 was activated in neurons under the control of *elav-LexA* and monoclonal anti-Fz1



415 showed higher signal in neurons and functional activity revealed by anti-Arm staining  
416 (Figure S5C-D). Oversized glioma brains showed the expected glioma network  
417 compartmentalizing neurons in the brain (Figure 8E-F´). However, Fz1 overexpression  
418 in neurons restored homogeneous Fz1 protein distribution in the brain (Figure 8G, H),  
419 rescued brain size (Figure 8G-G´) and neuron distribution and morphology (Figure  
420 8H´-H´). In addition, Fz1 equilibrium restoration partially rescued lethality and most  
421 animals reached adulthood. To verify Fz1 activation of the pathway we stained for Wg  
422 and Cyt-Arm (Figure S10). As previously shown, glioma brains showed a  
423 heterogeneous distribution for Wg protein (Figure S10A-A´) and, as a consequence,  
424 an imbalance in pathway activation reported by Arm accumulation (Figure S10 C-C´).  
425 As expected, neuronal Fz1 overexpression in glioma brains restored Wg distribution  
426 and Arm signal to a control situation (Figure S10B-B´, D-D´)

427 To further determine the effect of Wg/Fz1 signal restoration in neurons, we quantified  
428 the number synapses in their NMJs. Neuronal morphology is disrupted by glioma  
429 (Figure 8I, J) and restored by Fz1 overexpression in neurons neighboring glioma cells  
430 (Figure 8J, K). Moreover, synapse number reduction upon glioma induction is restored  
431 by Fz1 overexpression in neurons (Figure 8L). All these results indicate that the  
432 Wg/Fz1 pathway disruption caused by glioma is responsible of the synapse loss.  
433 Restoration of the signaling equilibrium between glia and neurons prevents synapse  
434 loss and therefore, neurodegeneration.

### 435 **Glioma depletes Wg from neuronal membranes**

436 The actual mechanisms of Wingless delivery have been under debate. This protein  
437 was initially described as a diffusible secreted protein <sup>68</sup>. Recent studies have proved  
438 that Wg secretion is not necessary for *Drosophila* development <sup>69</sup>. A membrane-  
439 tethered version of Wg protein <sup>70</sup> (*Wg<sup>NRT</sup>*) can substitute the endogenous gene, mimic  
440 Wg normal functions and produce viable organisms <sup>69</sup>. We took advantage of this tool

441 to determine the cellular mechanisms mediating glioma Wg retrieval from neurons. We  
442 created a genetic combination to substitute one copy of endogenous Wg with one copy  
443 of  $wg^{NRT}$  exclusively in neurons (by using the LexAop system). In addition, upon LexA  
444 system activation, neurons are marked with membranous GFP (CD8-GFP) while the  
445 rest of the cells are wild type. Moreover, this  $Wg^{NRT}$  is tagged with an HA which allows  
446 to discriminate from the endogenous Wg protein. We induced a glioma and marked the  
447 glial cells in red (ihog-RFP) (see materials and methods and Figure 9G). First, we  
448 studied normal control brains that express  $Wg^{NRT}$  exclusively in neurons in the absence  
449 of glioma. We stained with anti-HA and observed a positive signal both in neurons and  
450 glial cells but not in the control without the elav-LexA driver, indicating that the HA  
451 signal is not a false positive (Figure 9A-B, H). Finally, we performed the experiment in  
452 the glioma model to examine the interaction of glioma cells with  $Wg^{NRT}$  expressing  
453 neurons (Figure 9E-F-I) and stained with anti-HA. The images show a homogeneous  
454 signal for HA throughout the brain in glia and in neurons (See figure H-I magnifications  
455 for more detail), suggesting that glioma cells can deplete this non-  
456 secretable/membrane tethered version of Wg from neurons. We have quantified the  
457 number of HA<sup>+</sup> puncta in glia and neuron from control and glioma samples. The results  
458 suggest that glial cells sequester  $Wg^{NRT}$  from neuronal membranes at comparable  
459 rates under both physiological and glioma conditions (Figure 9J). Noticeably, however,  
460 there was a detectable reduction in the number of glioma cells, similar to previous  
461 results when Wg/Fz1 equilibrium in glial vs neurons was restored (Figure 8C, E and  
462 Figure 8G-H'). Since  $Wg^{NRT}$  is anchored to neuronal membranes, it would be expected  
463 to reduce the total Wg signaling in glioma cells thereby decreasing cell  
464 proliferation/survival, thus resulting in a rather normal sized brain (Figure 9A, C, E).  
465 Moreover, heterozygous  $wg^{NRT}/wg$  prevented glioma network progression (Figure  
466 9D'vs F'). In conclusion, glioma cells produce a network TMs that reach neighboring  
467 neurons, increasing intimate membrane contact that facilitates neuronal-Wg  
468 sequestering mediated by the Fz1 receptor in glioma TMs. Since Wg/Fz1 signaling in

469 glioma mediates cell number and tumor progression, targeting this cellular interaction  
470 may be a new candidate for future therapies.

471

## 472 **Discussion**

473 In addition to cell autonomous features of tumor cells, including founder mutations,  
474 recent evidences indicate that microenvironment signals contribute to glioma  
475 progression. Neuroligin-3 (NLGN3) is a synaptic protein cleaved and secreted after  
476 neuronal activity which promotes PI3K-mTOR signaling stimulating glioma growth.  
477 Thus, NLGN3 mediates an autocrine/paracrine loop in glioma cells which perpetuates  
478 tumoral features <sup>71</sup> (reviewed in <sup>72</sup>). Also, neural precursor cells (NPC) from the  
479 subventricular zone (SVZ) produce chemoattractants (SPARC/SPARCL1, HSP90B and  
480 pleiotrophin) which facilitate glioma invasion of the SVZ through Rho/ROCK signaling  
481 <sup>73</sup>.

482 We showed recently that TM network formation determines GB tumor malignancy,  
483 confers radiotherapy resistance and influences patient's prognosis <sup>19</sup>. TMs stability in  
484 GB is sensitive to *Gap43* expression in tumoral cells <sup>19</sup>. Also, *Tweety homologue-1*  
485 (*TTHY1*) expression in GB cells, mediated by NLGN3 regulates TM formation <sup>74</sup>.

486 This study shows that TMs intercalate among neurons and enwrap them in  
487 perineuronal nests <sup>29</sup> structures establishing an intimate link glioma-neuron. Then GB  
488 cells make direct contact via TMs and deprive neurons of WNT.

489 Expression data from human cancer databases indicate that glioma cells do not  
490 upregulate *Wnt* expression, neither upregulate its receptors. Instead, the results in the  
491 fly model show that glioma cells relocate Fz1 receptor in the TMs allowing to vampirize  
492 Wg from neurons. Consistent with these data, in the patient-derived GB xenograft  
493 model, where WNT1 is deposited in GB cells and the WNT pathway is activated,  $\beta$ -

494 catenin is upregulated. The available data suggest that GB TMs grow towards the  
495 source of Wg. However, as TMs expand upon Fz1/Wg signaling, the question  
496 regarding the exact order of events remains open. Do TMs require some initial stimuli  
497 from the source of Wg to grow? Alternatively, do TMs initiate growth triggered by glial  
498 internal signals and directed through a gradient of neuron-secreted attractants?

499

500 Concerning the mechanism of Wg vampirization, we have expressed a non secretable,  
501 HA- tagged version of membrane- tethered Wg<sup>NRT</sup> in neurons. In that experiment Wg is  
502 detected within glial cells demonstrating that GB cells can take Wg directly from the  
503 neuronal membrane. However, further studies are still required to determine the  
504 precise mechanism of neuronal Wg depletion by GB cells TMs.

505

506 It is widely observed that brain tumors and related ailments can cause cognitive decline  
507 and neuronal dysfunction (reviewed in <sup>75</sup>). High-grade glioma patients continue to  
508 display cognitive deficits after surgery, radiotherapy or chemotherapy <sup>76-78</sup>. The most  
509 common deficits concern memory, executive functions and general attention beyond  
510 the effects of age, education and gender <sup>79</sup>. Nevertheless, the molecules mediating  
511 neuronal degeneration need to be determined.

512

513 Synapse loss is an early step in neurodegeneration <sup>80-82</sup> which is consistent with the  
514 cognitive defects observed in GB patients. Nonetheless, cognitive defects can be  
515 observed also in patients with excess of synapses as in the case of fragile X syndrome  
516 <sup>83-84</sup>. GB cells can stimulate aberrant synapses associated with seizures <sup>85</sup> which are  
517 compatible with cognitive dysfunctions. Neuronal death is a later event in  
518 neurodegenerative processes such as Alzheimers´ disease <sup>86-88</sup>. In GB patients,  
519 neuronal death is under debate and this issue should be addressed with further data.  
520 There is preclinical work <sup>88-89</sup> supporting Glioma-induced neuronal death due to  
521 glutamate cytotoxicity, in addition clinical studies from <sup>90</sup> support neuronal death in GB

522 patients. However, it is certainly very difficult to draw clear conclusions from clinical  
523 samples or clinical courses, considering that therapy, antiepileptics and the pure space  
524 occupation plus the edema contribute to the neuronal dysfunction, degeneration and  
525 cell death.

526

527 In particular, neuronal cell loss is typically found at and around glioblastomas, and  
528 neurocognitive disturbances are a frequent finding in glioma patients. Although  
529 evidences from our experience and from neuropathology expertise, this is an open  
530 debate which requires further attention.

531

532 The data also reveal that reestablishing Wg signaling equilibrium by Fz1  
533 overexpression in neurons, not only restores synapse number but also blocks GB  
534 progression. Functional disruption of the equilibrium between GB glia and neurons is  
535 described here for the first time. Possibly, this mechanism could be valid for other  
536 molecules related to tumor progression such as Notch, Hedgehog or TGF. Moreover,  
537 cytoneme-like structures play a role in development and other cell types<sup>91-93</sup>. Hence,  
538 we propose that cytoneme-like structures in physiological conditions and TMs in  
539 pathological GB conditions could redistribute limited amounts of signaling molecules  
540 among competing cell types, therefore long range redistribution of signaling molecules  
541 could be a general mechanism to compete for different resources.

542

543 This study integrates for the first time the oncogenic nature of glioma with the neuronal  
544 degeneration caused by Wg depletion. This innovative concept of glioma-induced  
545 neurodegeneration opens the possibility of combined treatments to fight GB  
546 progression and associated neurodegeneration at the same time. Our data  
547 demonstrate that making the neurons more competitive for secretable factors such as  
548 Wg already has an impact in GB tumor growth, although it remains to be demonstrated  
549 what type of drugs can carry out these actions.

550

551 The rapid transformation of GB cells and the heterogeneity of mutations in these  
552 tumors are a handicap for genetic therapies and monoclonal therapies. In our view,  
553 cellular features such as the network shared by GB cells emerge as an alternative to  
554 tackle tumor progression. Among the possible new strategies, TMs dynamic and  
555 cellular transport of receptors to the TMs could be a target to prevent GB proliferation  
556 and neurodegeneration. Gap43 has emerged as a functional component of GB network  
557 formation. Recent studies indicate that other proteins such as Flotilin<sup>28,94</sup>, participate in  
558 cytoneme dynamics. The discovery of molecules regulating TM/cytoneme biology  
559 arises as potential targets for cancer treatment.

560

561

#### 562 **Author contributions**

563 Conceptualization, S.C.T. M.P. and FW; Methodology, S.C.T., VR, M.P., M.L.P., E.S.  
564 and N.F.; Investigation, S.C.T., FW, VR, M.P. M.L.P, E.S and N.F.; Writing – Original  
565 Draft, M.P, FW and SCT.; Writing – Review & Editing, S.C.T. and M.P.; Funding  
566 Acquisition, S.C.T and FW.; Supervision, S.C.T.

567

#### 568 **Acknowledgements**

569 We thank Professor Alberto Ferrús, Professor Helena Richardson, Dr. Paco Martín, Dr.  
570 Elena Santana, Patricia Jarabo and anonymous reviewers for critiques of the  
571 manuscript and for helpful discussions. Clemencia Cuadrado for fly stocks  
572 maintenance. We want to thank JF de Célis and C. Martínez Ostalé for their critical  
573 help with *in situ* hybridizations. We are grateful to R. Read, I. Guerrero, M. Milan, A.  
574 Baena-López, E. Martín-Blanco, David Stutt, the Vienna *Drosophila* Resource Centre,  
575 the Bloomington *Drosophila* stock Centre and the Developmental Studies Hydridoma  
576 Bank for supplying fly stocks and antibodies, and FlyBase for its wealth of information.

577 We acknowledge the support of the Confocal Microscopy unit and Molecular Biology  
578 unit at the Cajal Institute and the *Drosophila* Transgenesis Unit at CBMSO for their help  
579 with this project. MP holds a fellowship from the Juan de la Cierva program IJCI-2014-  
580 19272 and SCT holds a contract from the Ramón y Cajal program RYC-2012-11410  
581 from the Spanish MICINN. Research has been funded by grant BFU2015-65685P.  
582 Authors declare no conflicts of interest.

583

## 584 **Experimental Procedures**

### 585 **Fly stocks**

586 Flies were raised in standard fly food at 25°C.

587 Fly stocks from the Bloomington stock Centre: *UAS-GFP<sup>nl5</sup>* (BL4776), *UAS-lacZ*  
588 (BL8529), *UAS-myr-RFP* (BL7119), *UAS-Gap43-RNAi* (BL29598), *arm-GFP* (BL8555),  
589 *nkd04869a-lacZ* (BL25111), *D42-Gal4* (BL8816), *GFP-fz1-GFP* (BL59780), *repo-Gal4*  
590 (BL7415), *puc-lacZ*, *UAS-CD8-GFP* (BL32186), *tub-gal80<sup>ts</sup>* (BL7019), *elav-lexA*  
591 (*BL52676*), *lexAop-CD8-GFP* (BL32205), *lexAop-flp* (BL-55819), *UAS-armS10*  
592 (*BL4782*), *sqh-GFP* (*BL57145*), *UAS-CD4-spGFP1-10*, *lexAop-CD4-spGFP11*  
593 (obtained from BL58755), *en-Gal4*, *UAS-GFP* (from BL25752). Fly stocks from the  
594 Vienna *Drosophila* Resource Centre: *UAS-fz1-RNAi* (v105493), *fz4-GFP* (v318152),  
595 *UAS-mmp1-RNAi* (v101505), *UAS-wg-RNAi* (v104579), *UAS-yellow-RNAi* (v106068),  
596 *UAS-nrg-RNAi* (v107991). *GFP-sls* (MLC, ZCL2144 from <http://flytrap.med.yale.edu> ),  
597 *UAS-dEGFR<sup>Δ</sup>*, *UAS-PI3K92E* (dp110<sup>CAAX</sup>) (A gift from R. Read), *UAS-ihog-RFP* (a gift  
598 from I. Guerrero), *tsh-lacZ* and *dally-lacZ* (gifts from M. Milan), *lexAop-fz1* (generated in  
599 this study), *FRT Wg FRT NRT-Wg-HA*, *pax -Cherry* (a gift from A. Baena-López) and  
600 *puc-lacZ* (a gift from E. Martín-Blanco), *lifeact-GFP* (a gift from I. Guerrero), for electron  
601 microscopy studies, we used the *UAS-HRP:CD2* as reporter <sup>95</sup>, *UAS-GPI-YFP* <sup>96</sup>,  
602 *UAS-GMA-GFP* <sup>97</sup>.

### 603 ***Drosophila* glioblastoma model**

604 The most frequent genetic lesions in human gliomas include mutation or amplification  
605 of the Epidermal Growth Factor Receptor (EGFR) gene. Glioma-associated EGFR  
606 mutant forms show constitutive kinase activity that chronically stimulates Ras signaling  
607 to drive cell proliferation and migration <sup>98-99</sup>. Other common genetic lesions include loss  
608 of the lipid phosphatase PTEN, which antagonizes the phosphatidylinositol-3 kinase  
609 (PI3K) signaling pathway, and mutations that activate PI3KCA, which encodes the  
610 p110a catalytic subunit of PI3K <sup>98-99</sup>. Gliomas often show constitutively active Akt, a



611 major PI3K effector. However, EGFR-Ras or PI3K mutations alone are not sufficient to  
612 transform glial cells. Instead, multiple mutations that coactivate EGFR-Ras and  
613 PI3K/Akt pathways are required to induce a glioma<sup>29</sup>. In *Drosophila*, a combination of  
614 EGFR and PI3K mutations effectively causes a glioma-like condition that shows  
615 features of human gliomas including glia expansion, brain invasion, neuron  
616 dysfunction, synapse loss and neurodegeneration<sup>24,100-101</sup>. Moreover, this model has  
617 proved to be useful in finding new kinase activities relevant to glioma progression.<sup>25</sup> To  
618 generate a glioma in *Drosophila melanogaster* adult flies, the Gal4/UAS system<sup>102</sup> was  
619 used as described above (*repo-Gal4>UAS-EGFRΔ,UAS-dp110*). To restrict the  
620 expression of this genetic combination to the adulthood, we used the thermo sensitive  
621 repression system Gal80<sup>TS</sup>. Individuals maintained at 17°C did not activate the  
622 expression of the UAS constructs, but when flies were switched to 29°C, the protein  
623 Gal80<sup>TS</sup> changed conformation and was not longer able to bind to Gal4 to prevent its  
624 interaction with UAS sequences, and the expression system was activated.

#### 625 **Generation of Transgenic flies**

626 *LexAop-Frizzled1* construct was generated by RECOMBINA S.L. Fz1 (CG17697) CDS  
627 was synthesized by overlapping g-block assembly. The complete 17665bp fragment  
628 was amplified using the high fidelity Phusion taq polymerase (Thermo fisher Scientific)  
629 and *Eco.Friz.Fw* and *Xba.Friz.Rv* primers. PCR amplicon was cloned in pJET entry  
630 vector (Thermo Fisher Scientific), then Frizzled fragment was released with *EcoRI/XbaI*  
631 restriction enzymes and sub-cloned into destination *pLOTattB* plasmid.

632 *Eco.Fz1.Fw* 5'-GAATTGGGAATTCATGTGGCGTCAAATCCTG-3'

633 *Xba.Fz1.Rv* 5'-TCTAGACTAGACGTACGCCTGCGCCC-3'

634 Transgenic flies were injected and *Frizzled1* fragment was inserted in the chromosome  
635 2L by the *Drosophila* microinjection service (CBMSO-CSIC) using the following stock:

636 *y[1] M{vas-int.Dm}ZH-2A w[\*]; M{3xP3-RFP.attP}ZH-22A* (BL24481). Transgenic flies  
637 were selected individually by eye color (w+) and balanced with *CyO*.

638

### 639 **Antibodies for Immunofluorescence**

640 Third-instar larval brains, were dissected in phosphate-buffered saline (PBS), fixed in  
641 4% formaldehyde for 30min, washed in PBS + 0.1 or 0.3% Triton X-100 (PBT), and  
642 blocked in PBT + 5% BSA.

643 Antibodies used were: mouse anti-Wg (DSHB 1:50), mouse anti-Repo (DSHB 1:50),  
644 mouse anti-Fz1 (DSHB 1:50), mouse anti-Fz2 (DSHB 1:50), Rabbit anti-Fz1<sup>103</sup>, 1:300),  
645 mouse anti-Arm (DSHB 1:50), mouse anti- $\beta$ -galactosidase (Sigma, 1:500), rabbit anti-  
646 GFP (Invitrogen A11122, 1:500), mouse anti-GFP (Invitrogen A11120, 1:500), mouse  
647 anti-Nc82 (DSHB 1:20), Rabbit anti-Hrp (Jackson ImmunoResearch 111-035-144,  
648 1:400) , mouse anti-HA (12CA5 Roche 11583816001 1:100), rat anti-HA (Roche  
649 11867423001, 1:200).

650 Secondary antibodies: anti-mouse Alexa 488, 647, anti-rabbit Alexa 488, 647  
651 (Thermofisher, 1:500). DNA was stained with 2-(4-amidinophenyl)-1H-indole-6-  
652 carboxamide (DAPI, 1 $\mu$ M).

653

### 654 **Cell culture, fixation and histology of S24 Xenograft model**

655 The S24 cell line was derived as a primary glioblastoma culture (Lemke et al., 2012;  
656 Osswald et al., 2015). For the S24 glioma model, 50.000 S24:GFP cells (stably  
657 transduced by lentivirus) were injected into the cortex in 8-10 week old male NMRI  
658 nude mice (Charles River, Sulzfeld, Germany, n=2). Cells were cultivated under serum-  
659 free conditions in DMEM-F12 as sphere cultures (Thermo Fisher Scientific Inc.,  
660 Waltham, MA, USA) supplemented with 2% B-27 (Thermo Fisher Scientific Inc.,  
661 Waltham, MA, USA), 5  $\mu$ g/ml human insulin (Sigma-Aldrich Corporation, St. Louis, MO,  
662 USA), 12.8 ng/ml heparin (Sigma-Aldrich), 0.4 ng/ml EGF (R&D Systems Inc.,

663 Minneapolis, MN, USA) and 0.4 ng/ml FGF (Thermo Fisher Scientific Inc., Waltham,  
664 MA, USA). Animals were sacrificed 90 days after glioma cell injection with age-  
665 matched wild-type NMRI nude mice (n=2) which were used as control.

666 Brains were fixed with transcardial perfusion with 40 ml PBS and 40 ml 4 % PFA. The  
667 brain was removed and postfixed in 4 % PFA for 4 hrs at room temperature. Afterwards  
668 the brains were stored in PBS at 4 °C in the dark.

669 For histology, S24:GFP tumor-bearing brains were coronally cut on a vibratome  
670 (Sigmann Elektronik, Hüffenhardt, Germany) into 100 µm sections. The sections were  
671 permeabilized with 1 % TX100 for 3 hrs and counterstained with primary antibodies  
672 against beta-catenin (abcam, ab32572) and WNT1 (abcam, ab15251) for 3 hrs in 0.2%  
673 TX100 and 5 % FCS. Sections were washed three times with 0.2% TX100 and 5 %  
674 FCS and counterstained with secondary antibodies couples to Alexa-647 and Alexa-  
675 546 (Invitrogen) as well as DAPI for 3 hrs. The sections were washed three times in 1 ×  
676 PBS, pH=7.4, and mounted on coverslips using self-made moviol. Images were  
677 acquired on a confocal laser-scanning microscope (Leica SP8, Leica, Germany) using  
678 a × 63 immersion oil objective (numeric aperture=1.4). z-Stacks were acquired with a  
679 pixel size of 141 nm and 300-nm z-steps.

680 All animal experiments were approved by the regional animal welfare committee  
681 (permit number: G132/16 Regierungspräsidium Karlsruhe).

## 682 **Western blots**

683 For western blots, we used NuPAGE Bis-Tris Gels 4–12% (Invitrogen), and the  
684 following primary antibodies: mouse anti-Fz1 (DSHB 1:500), mouse anti-Fz2 (DSHB  
685 1:500) and mouse anti-tubulin (1:10,000 Sigma), we use Tubulin as a loading control  
686 instead of actin because the tumor microtubes are Actin positive and tubulin negative  
687 as previously described <sup>19</sup>. There were 3 biological replicates and Relative Fz1

688 Average pixel intensity was measured using measurement tool from Image Studio Lite  
689 Ver 5.2 and normalized against Tubulin.

690

### 691 **Proximity ligation assay**

692 DUO92101 Duolink® In Situ Red Starter Kit Mouse/Rabbit with DUO92013 Duolink In  
693 Situ Detection Reagents FarRed (Sigma).

694 The interaction between Wg and Fz1 in Drosophila larval brains was detected *in situ*  
695 accordingly to the instructions of the manufacturer. Briefly, primary antibody incubation  
696 against Wg (mouse anti-Wg (DSHB 1:50) and Fz1 (Rabbit anti-Fz1<sup>103</sup>, 1:300)) were  
697 applied using the same conditions as immunocytochemistry staining. Duolink  
698 secondary antibodies against the primary antibodies were then added. These  
699 secondary antibodies were provided as conjugates to oligonucleotides that were able  
700 to form a closed circle via base pairing and ligation using Duolink ligation solution when  
701 the antibodies were in close proximity<sup>49</sup> at a distance estimated to be <40 nm. The  
702 detection of the signals was conducted by rolling circle amplification using DNA  
703 polymerase incorporating fluorescently labeled nucleotides into the amplification  
704 products. The resulting positive signals were visualized as bright fluorescent dots, with  
705 each dot representing one interaction event. As negative control one of the primary  
706 antibodies was not added therefore, no positive signals were obtained from that assay).  
707 The tissues were visualized using a confocal microscope system (LEICA TCS SP5).

708

### 709 **In situ hybridizations**

710 Protocol was performed according to<sup>104</sup>. Imaginal discs and brains were dissected and  
711 fixed in 4% formaldehyde for 20 min at room temperature, washed in PBS-0.1% Tween  
712 (PBT) and re-fixed for 20 min at room temperature with 4% formaldehyde and 0.1%  
713 Tween. After three washes in PBT, discs were stored at -20°C in hybridization solution  
714 (HS; 50% formamide, 5× SSC, 100 µg/ml salmon sperm DNA, 50 µg/ml heparin and  
715 0.1% Tween). Disc were pre-hybridized for 2 h at 55°C in HS and hybridized with

716 digoxigenin-labelled RNA probes at 55°C. The probes were previously denaturalized  
717 at 80°C for 10 min. After hybridization, discs were washed in HS and PBT, and  
718 incubated for 2 h at room temperature in a 1:4000 dilution of anti-DIG antibody  
719 (Roche). After incubation, the discs were washed in PBT and the detection of probes  
720 was carried out using NBT and BCIP solution (Roche). The discs were mounted in 70%  
721 glycerol. Images were acquired with a Leica DM750 microscope and Leica MC170HD  
722 camera and LASv4.8 software. The probes were generated from the cDNAs RE026007  
723 (*wg*) and LD32066 (*fz1*) from the Expression Sequence Tags (EST) collection of the  
724 Berkeley Drosophila Genome Project.

725

## 726 **TEM**

727 Transmission electron microscopy (TEM) was performed in CNS of 3rd instar larvae  
728 with horseradish peroxidase (HRP) genetically driven to glial cells. Brains were fixed in  
729 4% formaldehyde in PBS for 30 min at room temperature, and washed in PBS,  
730 followed by an amplification of HRP signal using the ABC kit (Vector Laboratories) at  
731 room temperature. After developing with DAB brains were washed with PBS and fixed  
732 with 2% glutaraldehyde, 4% formaldehyde in PBS for 2h at room temperature. After  
733 washing in phosphate buffer the samples were postfixed with OsO<sub>4</sub> 1% in 0.1 M  
734 phosphate buffer, 1% K<sub>3</sub>[Fe(CN)<sub>6</sub>] 1h at 4°C. After washing in dH<sub>2</sub>O, Brains were  
735 incubated with tannic acid in PBS for 1min at room temperature then washed in PBS  
736 for 5min and dH<sub>2</sub>O 2x5min. Then the samples were stained with 2% uranyl acetate in  
737 H<sub>2</sub>O for 1h at room temperature in darkness followed by 3 washes in H<sub>2</sub>O<sub>2</sub>d. . Brains  
738 dehydrated in ethanol series (30%, 50%, 70%, 95%, 3x100% 10 min each at 4°C).  
739 Infiltration: samples were incubated in EtOH : propylene's OXID (1:1;V.V) for 5 min,  
740 propylene's OXID 2x10min, propylene's OXID:Epon (1:1) for 45 min, Epon 100% in  
741 agitation for 1 h and Epon 100% in agitation overnight. Then change to Epon 100% for  
742 2-3 h. Finally encapsulate the samples in BEEM capsules and polymerize 48h at  
743 60°C<sup>105</sup>.

744

## 745 **Imaging**

746 Fluorescent labeled samples were mounted in Vectashield mounting media with DAPI  
747 (Vector Laboratories) and analyzed by Confocal microscopy (LEICA TCS SP5/SP8).  
748 Images were processed using Leica LAS AF Lite and Fiji (Image J 1.50e). Images were  
749 assembled using Adobe Photoshop CS5.1.

750

## 751 **Quantifications and Statistical Analysis**

752 Relative Wg, Fz1, Arm, WNT1 and  $\beta$ Catenin staining within brains was determined  
753 from images taken at the same confocal settings. Average pixel intensity was  
754 measured using measurement log tool from Fiji 1.51g and Adobe Photoshop CS5.1.  
755 Average pixel intensity was measured in the glial tissue and in the adjacent neuronal  
756 tissue (N= $\sim$ 10 for each sample) and expressed as a ratio. Total average pixel intensity  
757 of WNT1 and  $\beta$ Catenin staining within mice brains was measured in the glioma (N=6)  
758 and control samples (N=6), to quantify this, single sections were taken from similar z-  
759 positions in both control and glioma samples. Glial network volume was quantified  
760 using Imaris surface tool (Imaris 6.3.1 software). The number of Proximity ligation  
761 assay puncta, HA<sup>+</sup> puncta, Repo<sup>+</sup> cells and the number of synaptic active sites was  
762 quantified by using the Imaris 6.3.1 software.  
763 The Western Blot bands were quantified by using the Image Studio Lite 5.2 software.  
764 Data was analyzed and plotted using GraphPad Prism v7.0.0. A D'Agostino & Pearson  
765 normality test was performed and the data found to have a normal distribution were  
766 analyzed by a two-tailed t-test with Welch-correction. In the case of multiple  
767 comparisons a One-way ANOVA with bonferroni post test was used. The data that did  
768 not pass the normality test were submitted to a two-tailed Mann-Whitney U-test or in  
769 the case of multiple comparisons a Kruskal-Wallis test with Dunns post test. Error bars  
770 represent Standard Error of the Mean, significance was \*\*\* $p \leq 0.0001$ , \*\*  $p \leq 0.001$  \*  
771  $p \leq 0.01$ , ns=non-significant.

772

773

#### 774 **Viability assays**

775 Flies were crossed and progeny was raised at 25°C under standard conditions. The  
776 number of adult flies emerged from the pupae were counted for each genotype. The  
777 number of control flies was considered 100% viability and all genotypes are  
778 represented relative to controls. Experiments were performed in triplicates.

#### 779 **Survival assay**

780 Males *Tub-Gal80*; *Repo-Gal4* were crossed with males bearing a control construct  
781 (*UAS-LacZ*) or glioma (*UAS-PI3K<sup>dp110</sup>*; *UAS-EGFR<sup>Δ</sup>*) and raised at 17°C. Progeny  
782 bearing a glioma (experimental) or LacZ (control) chromosomes were put at 29°C and  
783 viability was calculated as the percentage of surviving flies with respect to the starting  
784 number of flies as follows: viability = observed (n° of flies)/starting n° of flies × 100. Six  
785 independent vials for glioma (n= 6) and control (n= 6) were analyzed, with each vial  
786 with 10 flies.

787

#### 788 **qRT-PCRs**

789 Total RNA was isolated from larvae brains (Trizol, Invitrogen) and cDNAs were  
790 synthesized with M-MLV RT (Invitrogen). The following specific probes from Applied  
791 Biosystems were used: Wingless Dm01814379\_m1 and Frizzled1 Dm01793718\_g1,  
792 RpL32 Dm02151827\_g1 was used as housekeeping.

793 qRT-PCR was performed using Taqman Gene Expression (Applied Biosystems) using  
794 a 7500 Real Time PCR System (Applied Biosystems) with cycling conditions of 95°C  
795 for 10 min and 40 cycles of 95°C for 15 s and 55°C for 1 min. Each experimental point  
796 was performed with samples from two independent crosses and three replicates per  
797 experimental point, and differences were assessed with a 2-tailed Student *t* test.

798 Results were normalized using the housekeeping RpL32 and the  $\Delta\Delta$  cycle threshold  
799 method and are expressed as the relative change (-fold) of the stimulated group over  
800 the control group, which was used as a calibrator. qRT-PCR results were analyzed with  
801 7500 v2.0.6 software (Applied Biosystems).

802

### 803 **Figure Legends**

804 **Figure 1: Co-activation of EGFR-Ras and PI3K in *Drosophila* glia causes an**  
805 **expansion of the glial network that is susceptible to Gap43 depletion.**

806 Brains from 3rd instar larvae. Glia are labeled with GFP (green) driven by *repo-Gal4*.  
807 Each brain is composed of 2 symmetrical hemispheres. (A-C) In *repo>dEGFR<sup>A</sup>*;  
808 *dp110<sup>CAAX</sup>* (*glioma*) larvae (B), both brain hemispheres and the VNC are enlarged and  
809 elongated and the number of glial cells is increased relative to *wt* control (A). The  
810 quantification of the number of glial cells is shown in (C). Arrows indicate glial nuclei.

811 (D–E) Optical sections of larval brain to visualize the glial network, glial cell bodies and  
812 membranes are labeled in red (*myrRFP*). (D) RFP signal in control brains shows glial  
813 somas and the network in *wt* brain. (E) The glioma brain shows a dramatic increase in  
814 the membrane projections and in the size of the network. Nuclei are marked with DAPI  
815 (blue). Scale bars sizes are indicated in this and all figures.

816 (F-K) Glia are labeled with *UAS-ihog-RFP* to visualize active cytoneme/TM structures  
817 in glial cells as part of an interconnecting network. (F-G) In control brains the active  
818 glial cytonemes are shown by *repo>ihog-RFP* in red. In glioma brains, the TMs grow  
819 and expand across the brain, quantification of the network volume and the network/glial  
820 cell ratio is shown in H. (I-K) Higher magnifications of control brains (I) showing the glial  
821 cytonemes (red) compared with the glioma brains where the TMs overgrow and  
822 enwrap neuronal clusters (J). Upon Gap43 downregulation the glial network does not



823 overgrow or enwrap neuronal clusters (K) and shows a pattern and size similar to the  
824 control. Nuclei are marked with DAPI. Arrows indicate glial cytonemes/TMs. (L) A  
825 viability assay shows that the lethality induced by the glioma is fully rescued upon  
826 knockdown of *Gap43*. Error bars show S.D. \*\*\*  $P < 0.0001$ . Scale bar size are indicated  
827 in this and all figures.

## 828 **Figure 2: *Drosophila* Tumor Microtubes**

829 Transmission electron microscopy (TEM) images of a 3rd instar larval brains  
830 expressing HRP in the glial cells. (A-B) HRP deposits label cell membranes, thus  
831 identifying glial cells. Coloured images from control brains showing glial cells identified  
832 by HRP staining (magenta) and HRP-negative neurons (cyan). (C) Schematic diagram,  
833 a glioma cell labeled with HRP (magenta) showing that glioma cells produce a network  
834 of TMs that grow to surround neighboring neurons (cyan). (D-G) Several magnifications  
835 of Glioma brains showing TMs that grow and enwrap neighboring neurons (cyan).  
836 Detail of several layers of a glioma membrane enwrapping a neuron (F) and a  
837 longitudinal section of a TM (G), arrows indicate glial membranes. (H-I) Control and  
838 glioma brains from 3rd instar larvae. Glia is labeled with *UAS-Ihog-RFP* driven by *repo-*  
839 *Gal4* to visualize TMs in glial cells as part of an interconnecting network (red). Glial  
840 network is marked with lifeActin-GFP reporter (green) and nuclei are marked with DAPI  
841 (blue). Imaris 3D reconstructions are shown in H''-I'').

842

## 843 **Figure 3: Wingless/Fz1 accumulate in glioma cells**

844 Larval brain sections with glial cell bodies and membranes labeled in red (myrRFP) and  
845 stained with Wg antibody show homogeneous expression in the control brains (A) in  
846 green. In the glioma brains Wg accumulates in the glial transformed cells (B),  
847 quantified in (C). Arrows indicate Wg staining in glial membranes. (D-F) Glial cells are  
848 labeled with *UAS-Ihog-RFP* to visualize the glial network, and stained with Fz1 (green).

849 (D) Fz1 is homogeneously distributed in control brains, with a slight accumulation in the  
850 Ihog<sup>+</sup> structures. (E) Fz1 accumulates in the TMs and specifically in the projections  
851 that are in contact with the neuronal clusters. (F) Upon knockdown of *fz1* in glioma  
852 brains, the tumoral glial network is still formed but Fz1 is not detectable. (G)  
853 Knockdown of *Gap43* in glioma brains restores a normal glial network and Fz1 shows a  
854 homogeneous distribution along the brain section. Arrows indicate Fz1 staining in glial  
855 membranes. (H) Quantification of Fz1 staining ratio between iHog<sup>+</sup> and iHog<sup>-</sup> domains.  
856 Nuclei are marked with DAPI. Error bars show S.D. \* P<0.01 \*\*\* P<0.0001 or ns for  
857 non-significant.

#### 858 **Figure 4: Fz1 in glia interacts with neuronal Wg**

859 GRASP technique was used and both halves of green fluorescent protein tagged with  
860 a CD4 signal to direct it to the membranes (CD4-spGFP) were expressed in neurons  
861 (*elav-lexA*) and glial (*repo-Gal4*) cells respectively. Only upon intimate contact GFP  
862 protein is reconstituted and green fluorescent signal is visible. (A-C) Control brains  
863 showed a discrete signal corresponding to the physiological interaction between glia  
864 and neurons. (D-F) In glioma brains a massive GFP signal from GRASP reporter is  
865 detected. Arrows indicate GRASP reconstitution GFP signal. (G-H) Control and Glioma  
866 brains stained with Wg (red) and Fz1 (green). Gliomas show Fz1 and Wg accumulation  
867 in glioma TMs (ihog-RFP in blue), specifically Wg protein accumulates at the border  
868 between neuron and glioma cells. Arrows indicate Wg-Fz1 co-localization at the Glia-  
869 neuron interphase. (I-K) Proximity ligation assays (PLA) were performed in control and  
870 glioma brains to quantify the interactions between Wg and Fz1. (I) Control brains  
871 showed a discrete number of puncta (green) showing the physiological interactions. (J)  
872 Glioma brains showed a five-fold increase in the number of puncta, quantified in (K).  
873 Nuclei are marked with DAPI (blue). Arrows indicate PLA<sup>+</sup> puncta. Error bars show  
874 S.D. \*\*\* P<0.0001.

875

876 **Figure 5: Wg signaling pathway is active in glioma cells, and the glioma**  
877 **inactivates it in neuronal clusters in glioma brains.**

878 Larval brain sections with glial cytonemes labeled in red and stained with Arm (green).  
879 (A) Cytoplasmic-Armadillo (Cyt-Arm) is homogeneously distributed in control sections.  
880 (B) In glioma brains Cyt-Arm accumulates in the neurons cytoplasm where it is inactive.  
881 (C) Knockdown of *Gap43* in glioma brains restores a normal glial network and Arm  
882 does not accumulate showing a homogeneous distribution similar to the control. Arrows  
883 indicate Cyt-Arm staining at the Glia-neuron interphase. (D) Quantification of Cyt-Arm  
884 staining ratio between  $lhog^+$  and  $lhog^-$  domains. Glial cell bodies and membranes are  
885 labeled with myrRFP (red). (E-H) Wg signaling pathway reporters *arm-GFP* (E-F) and  
886 *nkd-lacZ* (stained with anti-bGal (G-H) in control and glioma brains show activation of  
887 the pathway in glioma cells compared with the reporter activation mostly in neurons in  
888 the control brains. Arrows indicate cells with reporter activation. (I-N) Confocal  
889 immunofluorescence single plane images of S24 GBSC NMRI nude mice brains  
890 (glioma) and NMRI nude mice (control) brains stained with human anti- $\beta$ Catenin (I-J)  
891 and WNT1 (L-M) both show in grey (red in the merged image) an increase in the  
892 glioma samples. The corresponding quantification of the pixel intensity is shown in K  
893 and N. Green signal from tumor cell GFP expression allows specific detection of S24  
894 GBSC related structures in the mouse brain (I', L'). Arrows indicate glioma or control  
895 cells. Nuclei are marked with DAPI. Error bars show S.D. \*\*\*  $P < 0.0001$  and ns for non-  
896 significant.

897

898 **Figure 6: Glioma network is responsible for the increase in the number of glial**  
899 **cells.**

900 Larval brain sections with glial cell nuclei stained with Repo (green). The number of  
901 glial cells is quantified in the following genotypes: (A) Control, (B) Glioma showing an  
902 increase in Repo+ cells. (C) Upon knockdown of *Fz1* in glioma brains, the number of  
903 glial cells is partially restored (D) knockdown of *Gap43* in glioma brains restores the  
904 number of glial cells similar to the control. (E) Quantification of the number of Repo+  
905 cells. Nuclei are marked by DAPI (blue). (F) Viability assay showing the lethality  
906 induced by the glioma that is partially rescued upon knockdown of *fz1*. Error bars show  
907 S.D. \*\*\* P<0.0001, and ns for non-significant.

908 **Figure 7: Gliomas cause Neurodegeneration and Wg expression in glioma cells**  
909 **is dispensable for tumor progression**

910 Neurons from the larval neuromuscular junction are stained with Nc82 showing the  
911 synaptic active Zones. (A-F) Upon glioma induction (B) the number of synapses (grey)  
912 is reduced when compared with the control (A). The number of synapses is restored  
913 upon knockdown of *Fz1* (C), *Gap43* (D) or *armS10; Fz1-RNAi* (E). The quantification of  
914 synapse number in all genotypes is shown in (F). (G-L) *wg* knockdown (I) in glioma  
915 cells (*wg-RNAi*) or *armS10; Fz1-RNAi* (J) does not prevent glioma cell numbers  
916 increase nor glioma TMs volume expansion quantified in (K-L). Error bars show S.D.  
917 \*\*\* P<0.0001, \*\* P<0.001 and ns for non-significant.

918

919 **Figure 8: Knockdown of the Wg signaling pathway results in neurodegeneration**  
920 **and restoration of the glia-neuron Wg/Fz1 signaling equilibrium inhibits glioma**  
921 **progression.**

922 Neurons from the larval neuromuscular junction are stained with Nc82 showing the  
923 synaptic active Zones. (A-D) Upon knockdown of *wg* (C) or *Fz1* (B) the number of  
924 synapses (grey) is reduced when compared with the control (A). Arrows indicate  
925 synapses. The quantification of synapse number in all genotypes is shown in (D).

926 (E-H) Larval brain sections with glial network labeled with *UAS-Ihog-RFP* in red and  
927 stained with Fz1 (grey or blue in the merge). Neurons are labeled with *lexAop-CD8-*  
928 *GFP* driven by *elav-lexA*. Fz1 overexpression in neurons (green) restore homogeneous  
929 Fz1 protein distribution (blue) in the brain, rescue brain size and neuron distribution (G-  
930 H) compared to (E-F) where the *elav-lexA* is not present in the glioma brains, Nuclei  
931 are marked with DAPI in (E-F) (green). Arrows indicate Fz1 staining in the glial  
932 membranes at the Glia-neuron interphase of glioma brains and its restored localization  
933 in G-H.

934 (I-L) Neurons from the larval neuromuscular junction are stained with Nc82 showing the  
935 active Zones. Upon glioma induction the number of synapses (grey) is reduced (J)  
936 when compared with the control (I). The number of synapses is restored upon  
937 overexpression of Fz1 specifically in the neurons (K). Arrows indicate synapses. The  
938 quantification of synapse number is shown in (L). Error bars show S.D. \*\*\*  $P < 0.0001$ , \*  
939  $P < 0.01$  or ns for non-significant.

940

#### 941 **Figure 9: Glioma depletes Wg from neuronal membrane**

942

943 Larval brain sections with glial network labeled with *UAS-Ihog-RFP* in red and stained  
944 with HA (blue). (A-B, H) Control brains express  $Wg^{NRT}$  and the anti-HA (grey or blue in  
945 the merge) staining shows a positive signal in both neurons (green) and glial cells  
946 (red). (C-D) Glioma samples that do not express  $Wg^{NRT}$  in neurons do not show HA  
947 signal. (E-F, I) Glioma brains with membrane anchored Wg ( $Wg^{NRT}$  grey or blue in the  
948 merge) in neurons (green), show a homogeneous signal for HA (grey or blue in the  
949 merge) in both glioma cells and neurons, quantified in (J), and the glial network size is  
950 restored in these animals (K). Arrows indicate  $HA^+$  staining in glial or neuronal  
951 membranes. Error bars show S.D. ns for non-significant. (G) Schematic diagram of this

952 experiment: a neuron labeled with GFP (green) and a glioma cell labeled with ihog-  
953 RFP (red) showing that glioma cells produce a network of TMs that grow to reach  
954 neighboring neurons. Intimate membrane contact facilitates neuronal-Wg (blue)  
955 sequestering mediated by Fz1 receptor (black) from glioma. In this experiment neurons  
956 express a membrane anchored version of Wg (Wg<sup>NRT</sup> represented as Wg in blue with a  
957 purple anchor) which is more difficult for the glioma to retrieve from the neuron.

958

959 **Supplementary Figures and Videos Figure S1 (Related to Figure 1): TMs enwrap**  
960 **neurons in GB and cytoneme markers co-localize with glioma network**

961 Brains from 3rd instar larvae. Glia is labeled with *UAS-Ihog-RFP* or *UAS-myr-RFP*  
962 driven by *repo-Gal4* to visualize TMs in glial cells as part of an interconnecting network,  
963 nuclei are marked with DAPI (blue). (A-B) Neurons are stained in green (Hrp) and  
964 enwrapped by glial TMs in glioma brains (see magnification (B) yellow arrowheads).  
965 (C-G) Glial network is marked with several cytoneme markers: (C) lifeact-GFP reporter  
966 (green and glial nuclei are marked with Repo, magenta), (D) GMA-GFP (green), (E)  
967 GPI-YFP (green), (F) GFP-MLC (green), (G) sqh-GFP (green) in a glioma brain. (H-I)  
968 Downregulation of neuroglian (*nrg-RNAi*) in glioma brains results in defective TMs.  
969 Nuclei are marked with DAPI. Scale bar size are indicated in this and all figures.

970

971 **Figure S2 (Related to Figure 1): *Gap43* Knockdown does not show effects in the**  
972 **number of synapses in the NMJ, in the glial network or in the viability of the flies**

973 (A-B) Glial cells are stained with Repo (green) and the number of glial cells are  
974 quantified in the following genotypes: *Control*, *Glioma* showing an increase in Repo+  
975 cells, *Glioma;lacZ* and *Glioma;yellow-RNAi* showing a similar number of Repo+ cells to  
976 *Glioma* alone. (C-D) Upon *Gap43* knockdown by *RNAi* in normal brains, the glial

977 network is similar to the control. Glial cells are marked by Repo in green. Nuclei are  
978 marked by DAPI. (E-F) Neurons from the larval neuromuscular junction are stained  
979 with Nc82 showing the synaptic active sites. Upon knockdown of *Gap43* the number of  
980 synapses marked by Nc82 (green) is similar to the control. (F) Graph showing the  
981 quantification of the synapse number. (G) A viability assay shows that the knockdown  
982 of *Gap43* does not alter the viability of male and female flies. Error bars show S.D. \*\*\*  
983  $P < 0.0001$  or ns for non-significant.

984 **Figure S3 (Related to Figure 3): Cases of human GB patients with mutations in**  
985 **WNT or FZD.**

986 Complete analysis of mutations in human GB samples from COSMIC database  
987 <http://cancer.sanger.ac.uk/cosmic> (A) and Cancer Genome Atlas (TGAC) for  
988 transcriptional targets of WNT pathway (B), WNT ligands (C) and FZD receptors (D),  
989 data are represented in percentage out of 902 or 922 samples. The total number of  
990 cases with mutations in any WNT or FZD gene is shown in red. Genes from WNT and  
991 FZD family without mutations in GBs is shown in the bottom.

992

993 **Figure S4 (Related to Figure 3): Fz2 remains normal in glioma brains.**

994 (A) Wing imaginal control disc stained with Fz2 (green) showing the expected  
995 endogenous localization pattern. Brains from 3rd instar larvae displayed at the same  
996 scale. Glia is labeled with *UAS-Ihog-RFP* driven by *repo-Gal4* to visualize active  
997 filopodia/TMs in glial cells, and stained with Fz2 (green). (B) Fz2 is homogeneously  
998 distributed in control sections, (C) Fz2 is homogeneously distributed in glioma brain  
999 sections, similar to the control. Nuclei are marked by DAPI (blue). Scale bar size is  
1000 indicated in the figure. Glial cell bodies and membranes are labeled with *UAS-myrRFP*  
1001 (red) driven by *repo-Gal4* and stained with GFP antibody to visualize a tagged form of

1002 endogenous Fz1 protein. (D) Fz1-GFP accumulates specifically in glial transformed  
1003 cells that are in contact with neuronal clusters. Nuclei are marked by DAPI (blue).

1004

1005 **Figure S5 (Related to Figure 3 and 8): Validation of tools, RNAs and antibodies**

1006 (A) *UAS-Fz1-RNAi* tool was validated in epithelial tissue, wing imaginal discs. Upon  
1007 *UAS-Fz1-RNAi* expression in the posterior compartment (marked with GFP), there is a  
1008 reduction in Fz1 protein signal compared with the anterior compartment from the same  
1009 tissue. (B) *UAS-Wg-RNAi* tool was validated in epithelial tissue, wing imaginal discs.  
1010 Upon *UAS-Wg-RNAi* expression in the posterior compartment (marked with GFP),  
1011 there is a reduction in Wg protein signal compared with the anterior compartment from  
1012 the same tissue. (C) *lexAop-Fz1* tool was validated in brain tissue. Upon ectopic Fz1  
1013 expression in the neurons (driven by *ELAV-LexA* marked with GFP), there is an  
1014 increase in Fz1 protein signal compared with the rest of the brain tissue. (D) Upon  
1015 ectopic Fz1 expression in the neurons (driven by *ELAV-LexA>lexAop-Fz1* marked with  
1016 GFP), there is an increase in active Arm protein signal compared with the rest of the  
1017 brain tissue.

1018

1019 **Figure S6 (Related to Figure 4): Wg and Fz1 transcription levels are similar**  
1020 **between controls and gliomas**

1021 (A) qPCRs with RNA extracted from control and glioma larvae showing no change in  
1022 the transcription (*mRNA* levels) of *wg* or *fz1*. (B) Western blot of samples extracted from  
1023 control and glioma larvae showing no change in the amount of Fz1 or Fz2 protein.  
1024 Error bars show S.D. ns for non-significant. (C) In situ hybridization experiments for Wg  
1025 and Fz1 in controls and gliomas showing no change in the transcription (*mRNA* levels)  
1026 of *wg* or *fz1*.



1027 **Figure S7 (Related to Figure 5): Wg signaling pathway is active in glioma cells**

1028 Larval brain sections with glial network labeled in red and stained with Cyt-Arm (green).  
1029 (A) Knockdown of *Fz1* in glioma brains showing a homogeneous Cyt-Arm distribution  
1030 similar to the control. Quantification of Cyt-Arm staining ratio between Ihog<sup>+</sup> and Ihog<sup>-</sup>  
1031 domains is shown in principal Figure 5D. (B-G) Glial cell bodies and membranes are  
1032 labeled with myrRFP or ihog-RFP (red) driven by *repo-Gal4*. Wg signaling pathway  
1033 reporters *tsh-lacZ* stained with anti-bGal (B-C), *fz4-GFP* (D-E) and *dally-lacZ* stained  
1034 with anti-bGal (F-G) show activation of the pathway in glial transformed cells.

1035

1036 **Figure S8 (Related to Figure 5): Wg signaling pathway is active in human glioma**  
1037 **cells**

1038 (A-D) A series of grade II and III GB images from S24 xenografts brain sections stained  
1039 with WNT1 and  $\beta$ -Catenin show an increase of these signals in grade III when  
1040 compared with grade II brain sections, indicating that the accumulation of WNT1 and  $\beta$ -  
1041 Catenin correlates with the progression of the GB, quantified in (E-F) (G-H) Technical  
1042 immunohistofluorescence negative control in NMRI nude control mice brains stained  
1043 only with the corresponding secondary antibodies showing the background unspecific  
1044 signal. Nuclei are marked by DAPI (blue).

1045 **Figure S9 (Related to Figure 3, 5 and 7): Adult *Drosophila* gliomas**

1046 (A) Survival curve of adult control or glioma flies after a number of days of glioma  
1047 induction and progression. (B-H) Adult brain sections 7 days after glioma induction with  
1048 Glial cells are labeled with *UAS-myr-RFP* to visualize the glial network and stained with  
1049 Cyt-Arm, Fz1 and Wg antibodies. (B-C, D) Cyt-Arm staining specifically marks the  
1050 mushroom bodies and it is homogeneously distributed in the rest of the brain tissue in  
1051 control sections and accumulates in the neurons cytoplasm where it is inactive in

1052 glioma brains. Quantification of Cyt-Arm staining ratio between RFP+ and RFP-  
1053 domains (D). (B'-C', E) Fz1 staining show homogeneous localization in the control  
1054 brains (B') in blue. In the glioma brains Fz1 accumulates in the glial transformed cells  
1055 (C'), quantified in (E). (F-H) Wg is homogeneously distributed in control brains, with a  
1056 slight accumulation in the RFP+ structures. Wg accumulates in the glioma network  
1057 similar to the larval brains quantified in (H). (I) Graph showing synapse number  
1058 quantification of adult NMJs from control flies and glioma-bearing flies.

1059

1060 **Figure S10 (Related to Figure 8): Restoration of the glia-neuron Wg/Fz1 signaling**  
1061 **equilibrium inhibits glioma progression**

1062 (A-D) Brains from 3rd instar larvae displayed at the same scale. Glia is labeled with  
1063 *UAS-Ihog-RFP* driven by *repo-Gal4* to visualize active filopodia in glial cells, and  
1064 stained with Wg or Arm (green). Neurons are labeled with *lexAop-CD8-GFP* driven by  
1065 *elav-lexA* (blue). Fz1 overexpression in neurons (blue) restore homogeneous Wg (grey  
1066 or green in the merge) (B) and Cyt-Arm (D) protein distribution (green) in the brain,  
1067 compared to (A, C) where the *elav-lexA* is not present in the glioma brains, Nuclei are  
1068 marked by DAPI (blue) in (A, C).

1069 **Video S1: Control Network**

1070 3D video reconstruction of control brains with glia labeled with *ihog-RFP* (*repo>ihog-*  
1071 *RFP*) in red (grey in the 3D reconstruction) to visualize cytoneme structures in glial  
1072 cells as part of an interconnecting network.

1073

1074 **Video S2: Glioma TMs**

1075 3D video reconstruction of Glioma brains with glia labeled with *ihog-RFP* (*repo>ihog-*  
1076 *RFP*) in red (grey in the 3D reconstruction) to visualize TMs structures in glial cells as

1077 part of an interconnecting network. In glioma brains, the TMs expand across the brain  
1078 and form perineuronal nests.

1079

1080 **Video S3: Glioma Gap43-RNAi Network**

1081 3D video reconstruction of Glioma; Gap43-RNAi brains with glia labeled with *ihog-RFP*  
1082 (*repo>ihog-RFP*) in red (grey in the 3D reconstruction) to visualize TM structures in  
1083 glial cells as part of an interconnecting network. Upon Gap43 downregulation the glial  
1084 network does not overgrow or enwrap neuronal clusters and shows a pattern and size  
1085 similar to the control.

1086

1087 **Video S4: Control LifeActin**

1088 3D video reconstruction of control brains from 3rd instar larvae. Glia is labeled with  
1089 *UAS-Ihog-RFP* driven by *repo-Gal4* to visualize cytonemes in glial cells as part of an  
1090 interconnecting network (red). Glial network is marked with lifeActin-GFP reporter  
1091 (green) and nuclei are marked with DAPI (blue).

1092

1093 **Video S5: Glioma LifeActin**

1094 3D video reconstruction of gliomal brains from 3rd instar larvae. Glia is labeled with  
1095 *UAS-Ihog-RFP* driven by *repo-Gal4* to visualize TMs in glial cells as part of an  
1096 interconnecting network (red). Glial network is marked with lifeActin-GFP reporter  
1097 (green) and nuclei are marked with DAPI (blue). Glial TMs enwrap clusters of neurons  
1098 in individual GB perineuronal nests.

1099

1100 **Video S6: Climbing assay**

1101 Video of *Drosophila* adult negative geotaxis behavior analysis (climbing assay), as an  
1102 indication for possible motor defects associated with neurodegeneration. The results  
1103 showed symptoms of neurodegeneration in glioma flies (right tube) compared to  
1104 controls (left tube).

1105

1106

- 1107 1 Bi, W. L. & Beroukhi, R. Beating the odds: extreme long-term survival with  
1108 glioblastoma. *Neuro Oncol* **16**, 1159-1160, doi:nou166 [pii]  
1109 10.1093/neuonc/nou166 (2014).
- 1110 2 Messaoudi, K., Clavreul, A. & Lagarce, F. Toward an effective strategy in glioblastoma  
1111 treatment. Part I: resistance mechanisms and strategies to overcome resistance of  
1112 glioblastoma to temozolomide. *Drug Discov Today* **20**, 899-905, doi:S1359-  
1113 6446(15)00080-X [pii]  
1114 10.1016/j.drudis.2015.02.011 (2015).
- 1115 3 Belhadj, Z. *et al.* Multifunctional targeted liposomal drug delivery for efficient  
1116 glioblastoma treatment. *Oncotarget*, doi:17976 [pii]  
1117 10.18632/oncotarget.17976 (2017).
- 1118 4 Xu, Y. Y., Gao, P., Sun, Y. & Duan, Y. R. Development of targeted therapies in treatment  
1119 of glioblastoma. *Cancer Biol Med* **12**, 223-237, doi:10.7497/j.issn.2095-3941.2015.0020  
1120 cbm-12-03-223 [pii] (2015).
- 1121 5 Zhu, Y. *et al.* Bi-specific molecule against EGFR and death receptors simultaneously  
1122 targets proliferation and death pathways in tumors. *Sci Rep* **7**, 2602,  
1123 doi:10.1038/s41598-017-02483-9  
1124 10.1038/s41598-017-02483-9 [pii] (2017).
- 1125 6 Osuka, S. & Van Meir, E. G. Overcoming therapeutic resistance in glioblastoma: the  
1126 way forward. *J Clin Invest* **127**, 415-426, doi:89587 [pii]  
1127 10.1172/JCI89587 (2017).
- 1128 7 Shtutman, M. *et al.* The cyclin D1 gene is a target of the beta-catenin/LEF-1 pathway.  
1129 *Proc Natl Acad Sci U S A* **96**, 5522-5527 (1999).
- 1130 8 He, T. C. *et al.* Identification of c-MYC as a target of the APC pathway. *Science* **281**,  
1131 1509-1512 (1998).
- 1132 9 Loh, K. M., van Amerongen, R. & Nusse, R. Generating Cellular Diversity and Spatial  
1133 Form: Wnt Signaling and the Evolution of Multicellular Animals. *Dev Cell* **38**, 643-655,  
1134 doi:10.1016/j.devcel.2016.08.011 (2016).
- 1135 10 Oliva, C. A., Vargas, J. Y. & Inestrosa, N. C. Wnts in adult brain: from synaptic plasticity  
1136 to cognitive deficiencies. *Front Cell Neurosci* **7**, 224, doi:10.3389/fncel.2013.00224  
1137 (2013).
- 1138 11 Inestrosa, N. C. & Varela-Nallar, L. Wnt signaling in the nervous system and in  
1139 Alzheimer's disease. *J Mol Cell Biol* **6**, 64-74, doi:10.1093/jmcb/mjt051 (2014).
- 1140 12 Arnes, M. & Casas Tinto, S. Aberrant Wnt signaling: a special focus in CNS diseases. *J*  
1141 *Neurogenet*, 1-7, doi:10.1080/01677063.2017.1338696 (2017).

- 1142 13 Paul, I., Bhattacharya, S., Chatterjee, A. & Ghosh, M. K. Current Understanding on  
1143 EGFR and Wnt/beta-Catenin Signaling in Glioma and Their Possible Crosstalk. *Genes*  
1144 *Cancer* **4**, 427-446, doi:10.1177/1947601913503341  
1145 10.1177\_1947601913503341 [pii] (2013).
- 1146 14 Qiu, X., Jiao, J., Li, Y. & Tian, T. Overexpression of FZD7 promotes glioma cell  
1147 proliferation by upregulating TAZ. *Oncotarget* **7**, 85987-85999, doi:13292 [pii]  
1148 10.18632/oncotarget.13292 (2016).
- 1149 15 Suwala, A. K., Hanaford, A., Kahlert, U. D. & Maciaczyk, J. Clipping the Wings of  
1150 Glioblastoma: Modulation of WNT as a Novel Therapeutic Strategy. *J Neuropathol Exp*  
1151 *Neurol* **75**, 388-396, doi:nlw013 [pii]  
1152 10.1093/jnen/nlw013 (2016).
- 1153 16 Liu, C. *et al.* Wnt/beta-Catenin pathway in human glioma: expression pattern and  
1154 clinical/prognostic correlations. *Clin Exp Med* **11**, 105-112, doi:10.1007/s10238-010-  
1155 0110-9 (2011).
- 1156 17 Sareddy, G. R., Panigrahi, M., Challa, S., Mahadevan, A. & Babu, P. P. Activation of  
1157 Wnt/beta-catenin/Tcf signaling pathway in human astrocytomas. *Neurochem Int* **55**,  
1158 307-317, doi:S0197-0186(09)00123-5 [pii]  
1159 10.1016/j.neuint.2009.03.016 (2009).
- 1160 18 Rheinbay, E. *et al.* An aberrant transcription factor network essential for Wnt signaling  
1161 and stem cell maintenance in glioblastoma. *Cell Rep* **3**, 1567-1579, doi:S2211-  
1162 1247(13)00203-9 [pii]  
1163 10.1016/j.celrep.2013.04.021 (2013).
- 1164 19 Osswald, M. *et al.* Brain tumour cells interconnect to a functional and resistant  
1165 network. *Nature* **528**, 93-98, doi:nature16071 [pii]  
1166 10.1038/nature16071 (2015).
- 1167 20 Weil, S. *et al.* Tumor microtubules convey resistance to surgical lesions and  
1168 chemotherapy in gliomas. *Neuro Oncol* **19**, 1316-1326, doi:3738031 [pii]  
1169 10.1093/neuonc/nox070 (2017).
- 1170 21 Lou, E. *et al.* Imaging Tunneling Membrane Tubes Elucidates Cell Communication in  
1171 Tumors. *Trends Cancer* **3**, 678-685, doi:S2405-8033(17)30158-9 [pii]  
1172 10.1016/j.trecan.2017.08.001 (2017).
- 1173 22 Ramirez-Weber, F. A. & Kornberg, T. B. Cytonemes: cellular processes that project to  
1174 the principal signaling center in *Drosophila* imaginal discs. *Cell* **97**, 599-607, doi:S0092-  
1175 8674(00)80771-0 [pii] (1999).
- 1176 23 Kornberg, T. B. Distributing signaling proteins in space and time: the province of  
1177 cytonemes. *Curr Opin Genet Dev* **45**, 22-27, doi:S0959-437X(16)30219-2 [pii]  
1178 10.1016/j.gde.2017.02.010 (2017).
- 1179 24 Read, R. D., Cavenee, W. K., Furnari, F. B. & Thomas, J. B. A *drosophila* model for EGFR-  
1180 Ras and PI3K-dependent human glioma. *PLoS Genet* **5**, e1000374,  
1181 doi:10.1371/journal.pgen.1000374 (2009).
- 1182 25 Read, R. D. *et al.* A kinome-wide RNAi screen in *Drosophila* Glia reveals that the RIO  
1183 kinases mediate cell proliferation and survival through TORC2-Akt signaling in  
1184 glioblastoma. *PLoS Genet* **9**, e1003253, doi:10.1371/journal.pgen.1003253  
1185 PGENETICS-D-12-01408 [pii] (2013).
- 1186 26 Yao, S., Lum, L. & Beachy, P. The ihog cell-surface proteins bind Hedgehog and mediate  
1187 pathway activation. *Cell* **125**, 343-357, doi:10.1016/j.cell.2006.02.040 (2006).
- 1188 27 Callejo, A. *et al.* Dispatched mediates Hedgehog basolateral release to form the long-  
1189 range morphogenetic gradient in the *Drosophila* wing disk epithelium. *Proc Natl Acad*  
1190 *Sci U S A* **108**, 12591-12598, doi:1106881108 [pii]  
1191 10.1073/pnas.1106881108 (2011).

- 1192 28 Bischoff, M. *et al.* Cytonemes are required for the establishment of a normal  
1193 Hedgehog morphogen gradient in *Drosophila* epithelia. *Nat Cell Biol* **15**, 1269-1281,  
1194 doi:ncb2856 [pii]  
1195 10.1038/ncb2856 (2013).
- 1196 29 Holland, E. C. Glioblastoma multiforme: the terminator. *Proc Natl Acad Sci U S A* **97**,  
1197 6242-6244, doi:97/12/6242 [pii] (2000).
- 1198 30 Roy, S., Huang, H., Liu, S. & Kornberg, T. B. Cytoneme-mediated contact-dependent  
1199 transport of the *Drosophila* decapentaplegic signaling protein. *Science* **343**, 1244624,  
1200 doi:science.1244624 [pii]  
1201 10.1126/science.1244624 (2014).
- 1202 31 Neel, V. A. & Young, M. W. Igloo, a GAP-43-related gene expressed in the developing  
1203 nervous system of *Drosophila*. *Development* **120**, 2235-2243 (1994).
- 1204 32 Campos, B., Olsen, L. R., Urup, T. & Poulsen, H. S. A comprehensive profile of recurrent  
1205 glioblastoma. *Oncogene* **35**, 5819-5825, doi:onc201685 [pii]  
1206 10.1038/onc.2016.85 (2016).
- 1207 33 Venkatesan, S., Lamfers, M. L., Dirven, C. M. & Leenstra, S. Genetic biomarkers of drug  
1208 response for small-molecule therapeutics targeting the RTK/Ras/PI3K, p53 or Rb  
1209 pathway in glioblastoma. *CNS Oncol* **5**, 77-90, doi:10.2217/cns-2015-0005 (2016).
- 1210 34 Kahlert, U. D. *et al.* Pharmacologic Wnt Inhibition Reduces Proliferation, Survival, and  
1211 Clonogenicity of Glioblastoma Cells. *J Neuropathol Exp Neurol* **74**, 889-900,  
1212 doi:10.1097/NEN.0000000000000227 (2015).
- 1213 35 Paw, I., Carpenter, R. C., Watabe, K., Debinski, W. & Lo, H. W. Mechanisms regulating  
1214 glioma invasion. *Cancer Lett* **362**, 1-7, doi:S0304-3835(15)00195-0 [pii]  
1215 10.1016/j.canlet.2015.03.015 (2015).
- 1216 36 Zheng, H. *et al.* PLAGL2 regulates Wnt signaling to impede differentiation in neural  
1217 stem cells and gliomas. *Cancer Cell* **17**, 497-509, doi:S1535-6108(10)00147-9 [pii]  
1218 10.1016/j.ccr.2010.03.020 (2010).
- 1219 37 Kim, Y. *et al.* Wnt activation is implicated in glioblastoma radioresistance. *Lab Invest*  
1220 **92**, 466-473, doi:labinvest2011161 [pii]  
1221 10.1038/labinvest.2011.161 (2012).
- 1222 38 Kamino, M. *et al.* Wnt-5a signaling is correlated with infiltrative activity in human  
1223 glioma by inducing cellular migration and MMP-2. *Cancer Sci* **102**, 540-548,  
1224 doi:10.1111/j.1349-7006.2010.01815.x (2011).
- 1225 39 Pu, P. *et al.* Downregulation of Wnt2 and beta-catenin by siRNA suppresses malignant  
1226 glioma cell growth. *Cancer Gene Ther* **16**, 351-361, doi:cgt200878 [pii]  
1227 10.1038/cgt.2008.78 (2009).
- 1228 40 Lee, Y., Lee, J. K., Ahn, S. H., Lee, J. & Nam, D. H. WNT signaling in glioblastoma and  
1229 therapeutic opportunities. *Lab Invest* **96**, 137-150, doi:labinvest2015140 [pii]  
1230 10.1038/labinvest.2015.140 (2016).
- 1231 41 Jin, X. *et al.* Frizzled 4 regulates stemness and invasiveness of migrating glioma cells  
1232 established by serial intracranial transplantation. *Cancer Res* **71**, 3066-3075, doi:0008-  
1233 5472.CAN-10-1495 [pii]  
1234 10.1158/0008-5472.CAN-10-1495 (2011).
- 1235 42 Lee, Y. *et al.* FoxM1 Promotes Stemness and Radio-Resistance of Glioblastoma by  
1236 Regulating the Master Stem Cell Regulator Sox2. *PLoS One* **10**, e0137703,  
1237 doi:10.1371/journal.pone.0137703  
1238 PONE-D-15-20790 [pii] (2015).
- 1239 43 Nager, M. *et al.* beta-Catenin Signalling in Glioblastoma Multiforme and Glioma-  
1240 Initiating Cells. *Chemother Res Pract* **2012**, 192362, doi:10.1155/2012/192362 (2012).
- 1241 44 Wang, Z., Zhang, S., Siu, T. L. & Huang, S. Glioblastoma multiforme formation and EMT:  
1242 role of FoxM1 transcription factor. *Curr Pharm Des* **21**, 1268-1271, doi:CPD-EPUB-  
1243 63931 [pii] (2015).

- 1244 45 Zhang, N. *et al.* FoxM1 promotes beta-catenin nuclear localization and controls Wnt  
1245 target-gene expression and glioma tumorigenesis. *Cancer Cell* **20**, 427-442, doi:S1535-  
1246 6108(11)00312-6 [pii]  
1247 10.1016/j.ccr.2011.08.016 (2011).
- 1248 46 Denysenko, T. *et al.* WNT/beta-catenin Signaling Pathway and Downstream  
1249 Modulators in Low- and High-grade Glioma. *Cancer Genomics Proteomics* **13**, 31-45,  
1250 doi:13/1/31 [pii] (2016).
- 1251 47 Schilling, S., Steiner, S., Zimmerli, D. & Basler, K. A regulatory receptor network directs  
1252 the range and output of the Wingless signal. *Development* **141**, 2483-2493,  
1253 doi:10.1242/dev.108662 (2014).
- 1254 48 Feinberg, E. H. *et al.* GFP Reconstitution Across Synaptic Partners (GRASP) defines cell  
1255 contacts and synapses in living nervous systems. *Neuron* **57**, 353-363, doi:S0896-  
1256 6273(07)01020-3 [pii]  
1257 10.1016/j.neuron.2007.11.030 (2008).
- 1258 49 Soderberg, O. *et al.* Direct observation of individual endogenous protein complexes in  
1259 situ by proximity ligation. *Nat Methods* **3**, 995-1000, doi:nmeth947 [pii]  
1260 10.1038/nmeth947 (2006).
- 1261 50 Koos, B. *et al.* Analysis of protein interactions in situ by proximity ligation assays. *Curr*  
1262 *Top Microbiol Immunol* **377**, 111-126, doi:10.1007/82\_2013\_334 (2014).
- 1263 51 Klaus, A. & Birchmeier, W. Wnt signalling and its impact on development and cancer.  
1264 *Nat Rev Cancer* **8**, 387-398, doi:nrc2389 [pii]  
1265 10.1038/nrc2389 (2008).
- 1266 52 Riggleman, B., Schedl, P. & Wieschaus, E. Spatial expression of the Drosophila segment  
1267 polarity gene armadillo is posttranscriptionally regulated by wingless. *Cell* **63**, 549-560,  
1268 doi:0092-8674(90)90451-J [pii] (1990).
- 1269 53 Singh, A., Kango-Singh, M. & Sun, Y. H. Eye suppression, a novel function of teashirt,  
1270 requires Wingless signaling. *Development* **129**, 4271-4280 (2002).
- 1271 54 DasGupta, R., Kaykas, A., Moon, R. T. & Perrimon, N. Functional genomic analysis of  
1272 the Wnt-wingless signaling pathway. *Science* **308**, 826-833, doi:1109374 [pii]  
1273 10.1126/science.1109374 (2005).
- 1274 55 Franz, A., Shlyueva, D., Brunner, E., Stark, A. & Basler, K. Probing the canonicity of the  
1275 Wnt/Wingless signaling pathway. *PLoS Genet* **13**, e1006700,  
1276 doi:10.1371/journal.pgen.1006700  
1277 PGENETICS-D-17-00130 [pii] (2017).
- 1278 56 Scherer, H. J. A Critical Review: The Pathology of Cerebral Gliomas. *J Neurol Psychiatry*  
1279 **3**, 147-177 (1940).
- 1280 57 Peng, F. *et al.* Loss of Polo ameliorates APP-induced Alzheimer's disease-like symptoms  
1281 in Drosophila. *Sci Rep* **5**, 16816, doi:srep16816 [pii]  
1282 10.1038/srep16816 (2015).
- 1283 58 Keshishian, H., Broadie, K., Chiba, A. & Bate, M. The drosophila neuromuscular  
1284 junction: a model system for studying synaptic development and function. *Annu Rev*  
1285 *Neurosci* **19**, 545-575, doi:10.1146/annurev.ne.19.030196.002553 (1996).
- 1286 59 Mhatre, S. D. *et al.* Synaptic abnormalities in a Drosophila model of Alzheimer's  
1287 disease. *Dis Model Mech* **7**, 373-385, doi:dmm.012104 [pii]  
1288 10.1242/dmm.012104 (2014).
- 1289 60 Penney, J. *et al.* LRRK2 regulates retrograde synaptic compensation at the Drosophila  
1290 neuromuscular junction. *Nat Commun* **7**, 12188, doi:ncomms12188 [pii]  
1291 10.1038/ncomms12188 (2016).
- 1292 61 Boyle, M., Bonini, N. & DiNardo, S. Expression and function of clift in the development  
1293 of somatic gonadal precursors within the Drosophila mesoderm. *Development* **124**,  
1294 971-982 (1997).

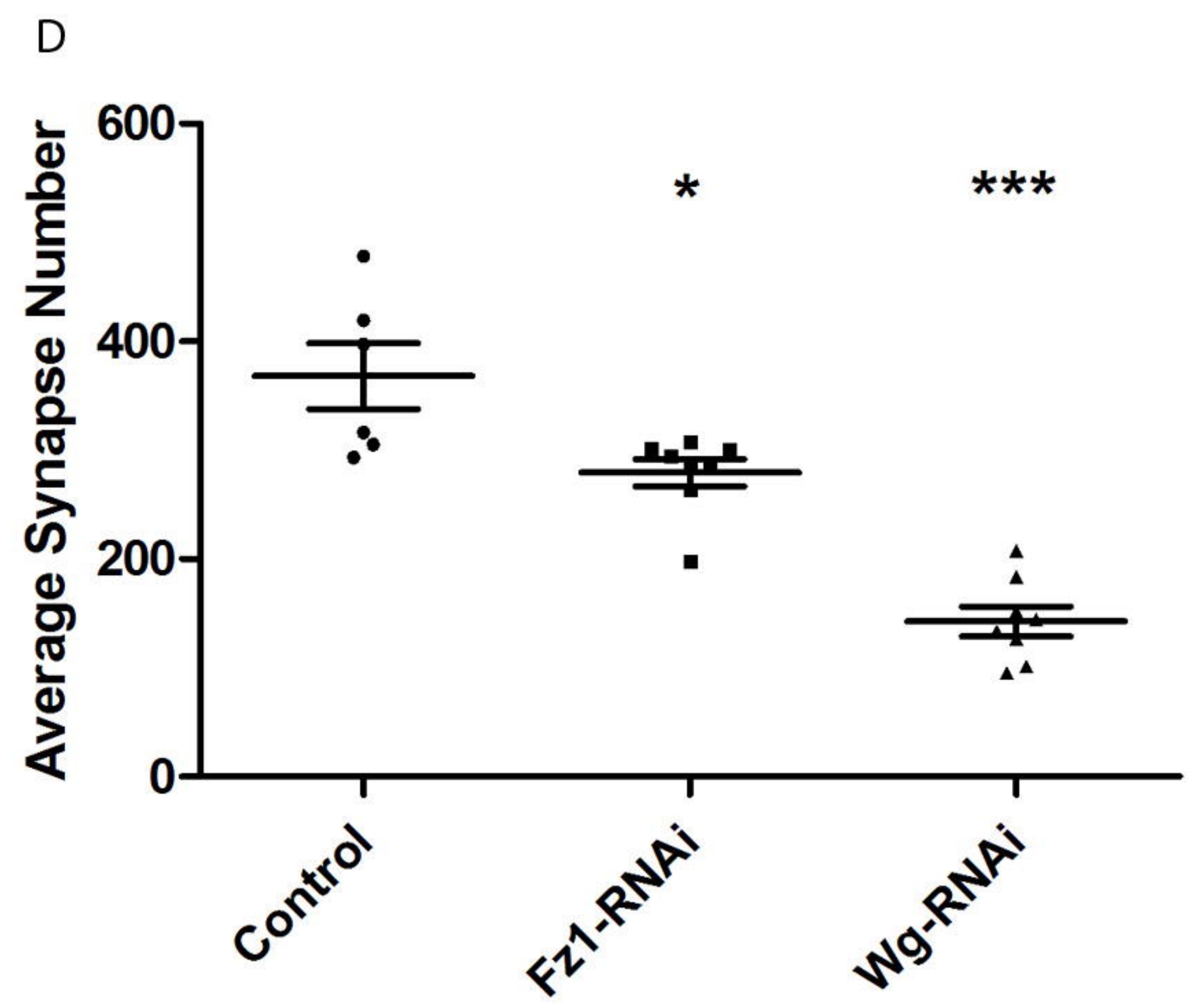
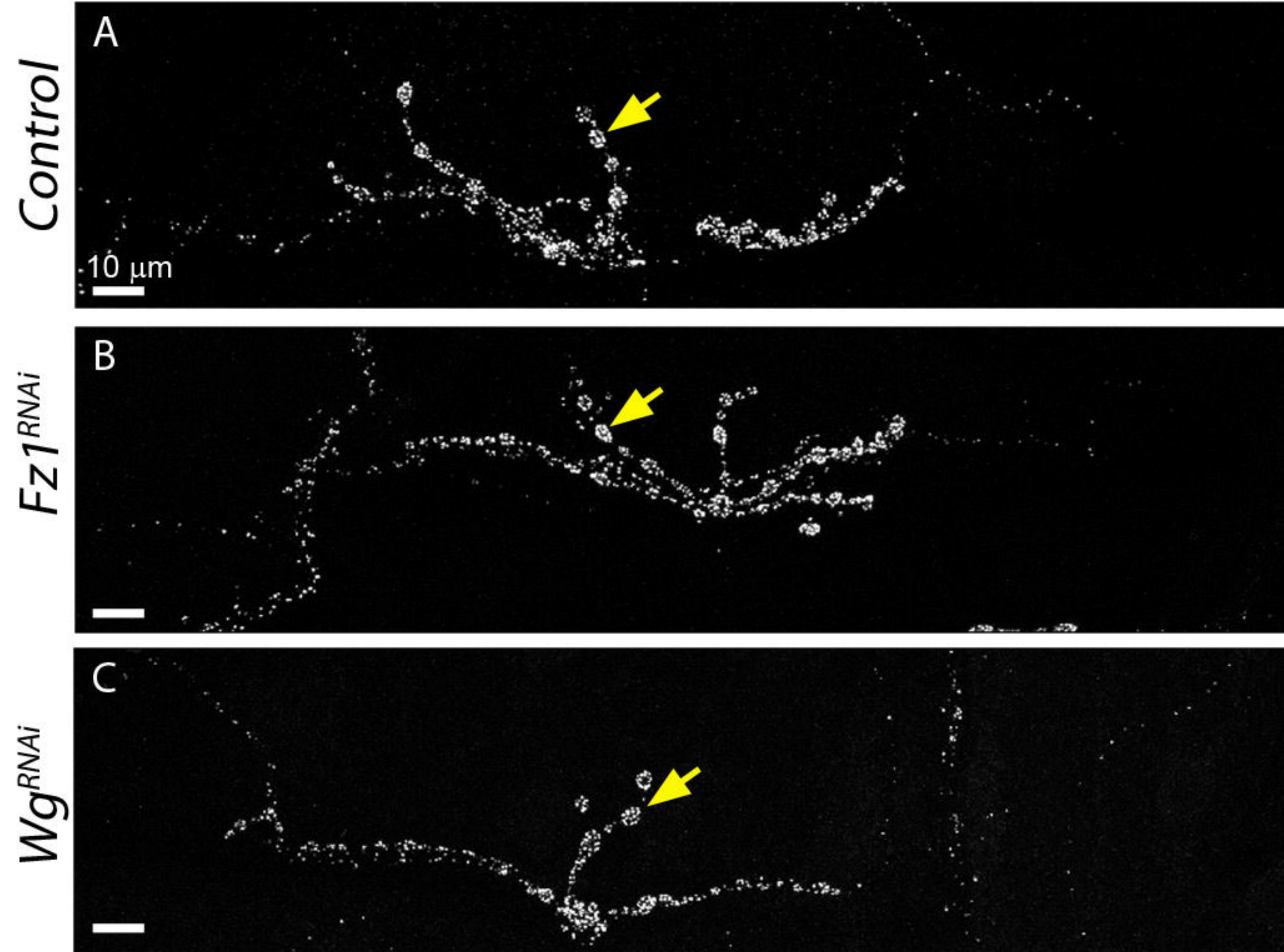
- 1295 62 Arrazola, M. S., Silva-Alvarez, C. & Inestrosa, N. C. How the Wnt signaling pathway  
1296 protects from neurodegeneration: the mitochondrial scenario. *Front Cell Neurosci* **9**,  
1297 166, doi:10.3389/fncel.2015.00166 (2015).
- 1298 63 Garcia-Velazquez, L. & Arias, C. The emerging role of Wnt signaling dysregulation in the  
1299 understanding and modification of age-associated diseases. *Ageing Res Rev* **37**, 135-  
1300 145, doi:S1568-1637(17)30090-9 [pii]  
1301 10.1016/j.arr.2017.06.001 (2017).
- 1302 64 Kahn, M. Can we safely target the WNT pathway? *Nat Rev Drug Discov* **13**, 513-532,  
1303 doi:nrd4233 [pii]  
1304 10.1038/nrd4233 (2014).
- 1305 65 Libro, R., Bramanti, P. & Mazzon, E. The role of the Wnt canonical signaling in  
1306 neurodegenerative diseases. *Life Sci* **158**, 78-88, doi:S0024-3205(16)30380-0 [pii]  
1307 10.1016/j.lfs.2016.06.024 (2016).
- 1308 66 Casas-Tinto, S., Arnes, M. & Ferrus, A. Drosophila enhancer-Gal4 lines show ectopic  
1309 expression during development. *R Soc Open Sci* **4**, 170039, doi:10.1098/rsos.170039  
1310 rsos170039 [pii] (2017).
- 1311 67 Lai, S. L. & Lee, T. Genetic mosaic with dual binary transcriptional systems in  
1312 Drosophila. *Nat Neurosci* **9**, 703-709, doi:10.1038/nn1681 (2006).
- 1313 68 Bejsovec, A. & Martinez Arias, A. Roles of wingless in patterning the larval epidermis of  
1314 Drosophila. *Development* **113**, 471-485 (1991).
- 1315 69 Alexandre, C., Baena-Lopez, A. & Vincent, J. P. Patterning and growth control by  
1316 membrane-tethered Wingless. *Nature* **505**, 180-185, doi:10.1038/nature12879 (2014).
- 1317 70 Zecca, M., Basler, K. & Struhl, G. Direct and long-range action of a wingless morphogen  
1318 gradient. *Cell* **87**, 833-844 (1996).
- 1319 71 Venkatesh, H. S. *et al.* Neuronal Activity Promotes Glioma Growth through Neuroigin-  
1320 3 Secretion. *Cell* **161**, 803-816, doi:S0092-8674(15)00429-8 [pii]  
1321 10.1016/j.cell.2015.04.012 (2015).
- 1322 72 Johung, T. & Monje, M. Neuronal activity in the glioma microenvironment. *Curr Opin*  
1323 *Neurobiol* **47**, 156-161, doi:S0959-4388(17)30058-2 [pii]  
1324 10.1016/j.conb.2017.10.009 (2017).
- 1325 73 Qin, E. Y. *et al.* Neural Precursor-Derived Pleiotrophin Mediates Subventricular Zone  
1326 Invasion by Glioma. *Cell* **170**, 845-859 e819, doi:10.1016/j.cell.2017.07.016 (2017).
- 1327 74 Jung, E. *et al.* Tweety-Homolog 1 Drives Brain Colonization of Gliomas. *J Neurosci* **37**,  
1328 6837-6850, doi:JNEUROSCI.3532-16.2017 [pii]  
1329 10.1523/JNEUROSCI.3532-16.2017 (2017).
- 1330 75 Bergo, E. *et al.* Cognitive Rehabilitation in Patients with Gliomas and Other Brain  
1331 Tumors: State of the Art. *Biomed Res Int* **2016**, 3041824, doi:10.1155/2016/3041824  
1332 (2016).
- 1333 76 Bosma, I. *et al.* The course of neurocognitive functioning in high-grade glioma patients.  
1334 *Neuro Oncol* **9**, 53-62, doi:10.1215/15228517-2006-012 (2007).
- 1335 77 Brown, P. D. *et al.* Detrimental effects of tumor progression on cognitive function of  
1336 patients with high-grade glioma. *J Clin Oncol* **24**, 5427-5433,  
1337 doi:10.1200/JCO.2006.08.5605 (2006).
- 1338 78 Wefel, J. S. *et al.* Neurocognitive function in patients with recurrent glioblastoma  
1339 treated with bevacizumab. *Neuro Oncol* **13**, 660-668, doi:10.1093/neuonc/nor024  
1340 (2011).
- 1341 79 Gehrke, A. K., Baisley, M. C., Sonck, A. L., Wronski, S. L. & Feuerstein, M.  
1342 Neurocognitive deficits following primary brain tumor treatment: systematic review of  
1343 a decade of comparative studies. *J Neurooncol* **115**, 135-142, doi:10.1007/s11060-013-  
1344 1215-2 (2013).



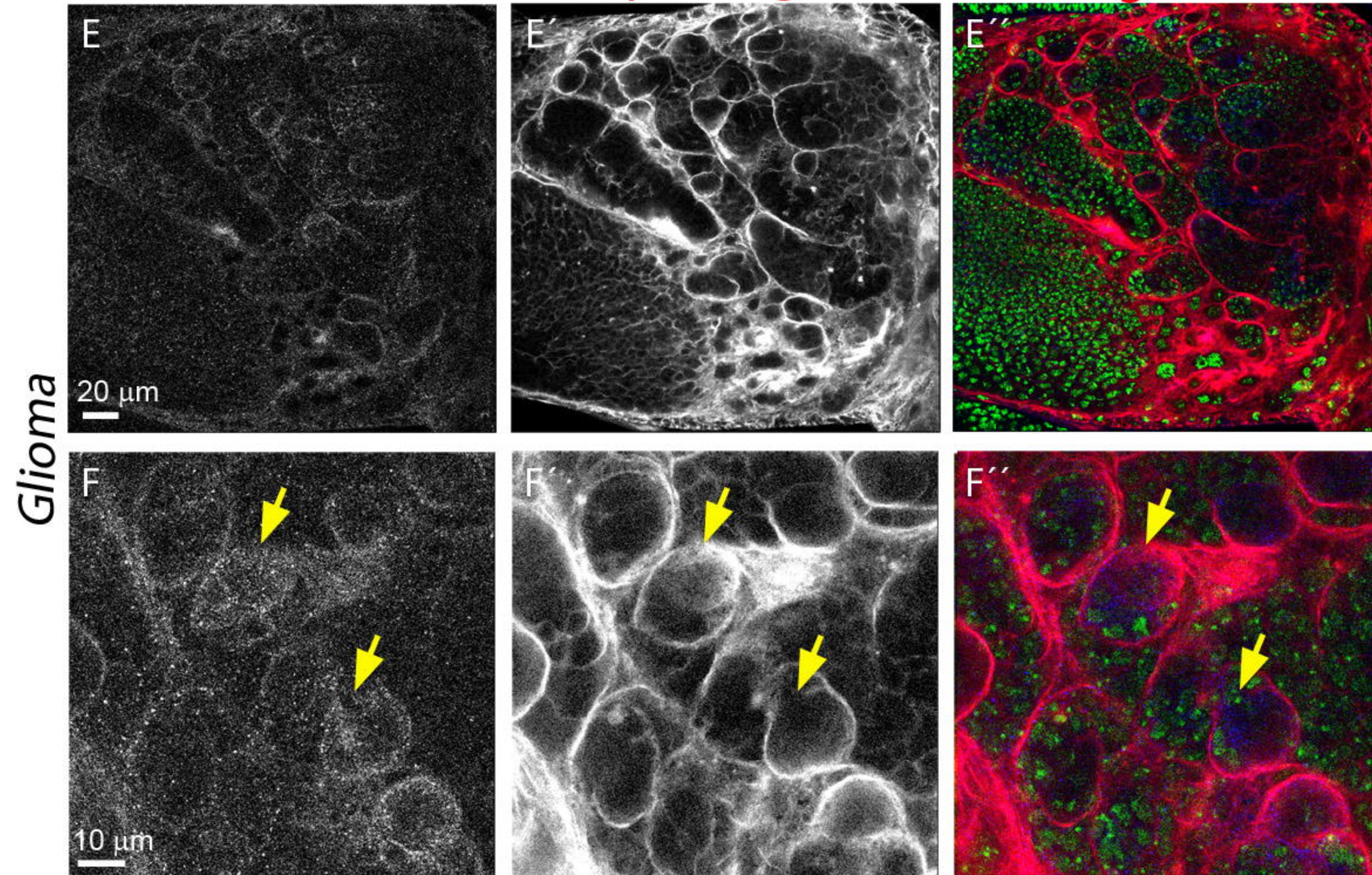
- 1345 80 Henstridge, C. M., Pickett, E. & Spires-Jones, T. L. Synaptic pathology: A shared  
1346 mechanism in neurological disease. *Ageing Res Rev* **28**, 72-84,  
1347 doi:10.1016/j.arr.2016.04.005 (2016).
- 1348 81 Hong, S. *et al.* Complement and microglia mediate early synapse loss in Alzheimer  
1349 mouse models. *Science* **352**, 712-716, doi:10.1126/science.aad8373 (2016).
- 1350 82 Sephton, C. F. & Yu, G. The function of RNA-binding proteins at the synapse:  
1351 implications for neurodegeneration. *Cell Mol Life Sci* **72**, 3621-3635,  
1352 doi:10.1007/s00018-015-1943-x (2015).
- 1353 83 Mansilla, A. *et al.* Interference of the complex between NCS-1 and Ric8a with  
1354 phenothiazines regulates synaptic function and is an approach for fragile X syndrome.  
1355 *Proc Natl Acad Sci U S A* **114**, E999-E1008, doi:10.1073/pnas.1611089114 (2017).
- 1356 84 Romero-Pozuelo, J. *et al.* The guanine-exchange factor Ric8a binds to the Ca<sup>2</sup>(+)  
1357 sensor NCS-1 to regulate synapse number and neurotransmitter release. *J Cell Sci* **127**,  
1358 4246-4259, doi:10.1242/jcs.152603 (2014).
- 1359 85 John Lin, C. C. *et al.* Identification of diverse astrocyte populations and their malignant  
1360 analogs. *Nat Neurosci* **20**, 396-405, doi:10.1038/nn.4493 (2017).
- 1361 86 Salter, M. W. & Stevens, B. Microglia emerge as central players in brain disease. *Nat*  
1362 *Med* **23**, 1018-1027, doi:nm.4397 [pii]  
1363 10.1038/nm.4397 (2017).
- 1364 87 Niikura, T., Tajima, H. & Kita, Y. Neuronal cell death in Alzheimer's disease and a  
1365 neuroprotective factor, humanin. *Curr Neuropharmacol* **4**, 139-147 (2006).
- 1366 88 Ye, Z. C., Rothstein, J. D. & Sontheimer, H. Compromised glutamate transport in human  
1367 glioma cells: reduction-mislocalization of sodium-dependent glutamate transporters  
1368 and enhanced activity of cystine-glutamate exchange. *J Neurosci* **19**, 10767-10777  
1369 (1999).
- 1370 89 Lee, S. G. *et al.* Oncogene AEG-1 promotes glioma-induced neurodegeneration by  
1371 increasing glutamate excitotoxicity. *Cancer Res* **71**, 6514-6523, doi:0008-5472.CAN-11-  
1372 0782 [pii]  
1373 10.1158/0008-5472.CAN-11-0782 (2011).
- 1374 90 Robert, S. M. *et al.* SLC7A11 expression is associated with seizures and predicts poor  
1375 survival in patients with malignant glioma. *Sci Transl Med* **7**, 289ra286,  
1376 doi:7/289/289ra86 [pii]  
1377 10.1126/scitranslmed.aaa8103 (2015).
- 1378 91 Kornberg, T. B. Cytonemes extend their reach. *EMBO J* **32**, 1658-1659,  
1379 doi:emboj2013115 [pii]  
1380 10.1038/emboj.2013.115 (2013).
- 1381 92 Kornberg, T. B. & Roy, S. Cytonemes as specialized signaling filopodia. *Development*  
1382 **141**, 729-736, doi:141/4/729 [pii]  
1383 10.1242/dev.086223 (2014).
- 1384 93 Sherer, N. M. & Mothes, W. Cytonemes and tunneling nanotubules in cell-cell  
1385 communication and viral pathogenesis. *Trends Cell Biol* **18**, 414-420, doi:S0962-  
1386 8924(08)00190-6 [pii]  
1387 10.1016/j.tcb.2008.07.003 (2008).
- 1388 94 Neumann-Giesen, C. *et al.* Membrane and raft association of reggie-1/flotillin-2: role of  
1389 myristoylation, palmitoylation and oligomerization and induction of filopodia by  
1390 overexpression. *Biochem J* **378**, 509-518, doi:10.1042/BJ20031100 (2004).
- 1391 95 Watts, R. J., Schuldiner, O., Perrino, J., Larsen, C. & Luo, L. Glia engulf degenerating  
1392 axons during developmental axon pruning. *Curr Biol* **14**, 678-684,  
1393 doi:10.1016/j.cub.2004.03.035  
1394 S0960-9822(04)00214-3 [pii] (2004).

- 1395 96 Greco, V., Hannus, M. & Eaton, S. Argosomes: a potential vehicle for the spread of  
1396 morphogens through epithelia. *Cell* **106**, 633-645, doi:S0092-8674(01)00484-6 [pii]  
1397 (2001).
- 1398 97 Bloor, J. W. & Kiehart, D. P. zipper Nonmuscle myosin-II functions downstream of PS2  
1399 integrin in *Drosophila* myogenesis and is necessary for myofibril formation. *Dev Biol*  
1400 **239**, 215-228, doi:10.1006/dbio.2001.0452  
1401 S0012-1606(01)90452-X [pii] (2001).
- 1402 98 Furnari, F. B. *et al.* Malignant astrocytic glioma: genetics, biology, and paths to  
1403 treatment. *Genes Dev* **21**, 2683-2710, doi:21/21/2683 [pii]  
1404 10.1101/gad.1596707 (2007).
- 1405 99 Maher, E. A. *et al.* Malignant glioma: genetics and biology of a grave matter. *Genes Dev*  
1406 **15**, 1311-1333, doi:10.1101/gad.891601 (2001).
- 1407 100 Kegelman, T. P. *et al.* In vivo modeling of malignant glioma: the road to effective  
1408 therapy. *Adv Cancer Res* **121**, 261-330, doi:B978-0-12-800249-0.00007-X [pii]  
1409 10.1016/B978-0-12-800249-0.00007-X (2014).
- 1410 101 Read, R. D. *Drosophila melanogaster* as a model system for human brain cancers. *Glia*  
1411 **59**, 1364-1376, doi:10.1002/glia.21148 (2011).
- 1412 102 Brand, A. H. & Perrimon, N. Targeted gene expression as a means of altering cell fates  
1413 and generating dominant phenotypes. *Development* **118**, 401-415 (1993).
- 1414 103 Bastock, R. & Strutt, D. The planar polarity pathway promotes coordinated cell  
1415 migration during *Drosophila* oogenesis. *Development* **134**, 3055-3064,  
1416 doi:10.1242/dev.010447 (2007).
- 1417 104 Martin, M., Ostale, C. M. & de Celis, J. F. Patterning of the *Drosophila* L2 vein is driven  
1418 by regulatory interactions between region-specific transcription factors expressed in  
1419 response to Dpp signalling. *Development* **144**, 3168-3176, doi:dev.143461 [pii]  
1420 10.1242/dev.143461 (2017).
- 1421 105 Martin-Pena, A. *et al.* Cell types and coincident synapses in the ellipsoid body of  
1422 *Drosophila*. *Eur J Neurosci* **39**, 1586-1601, doi:10.1111/ejn.12537 (2014).  
1423  
1424

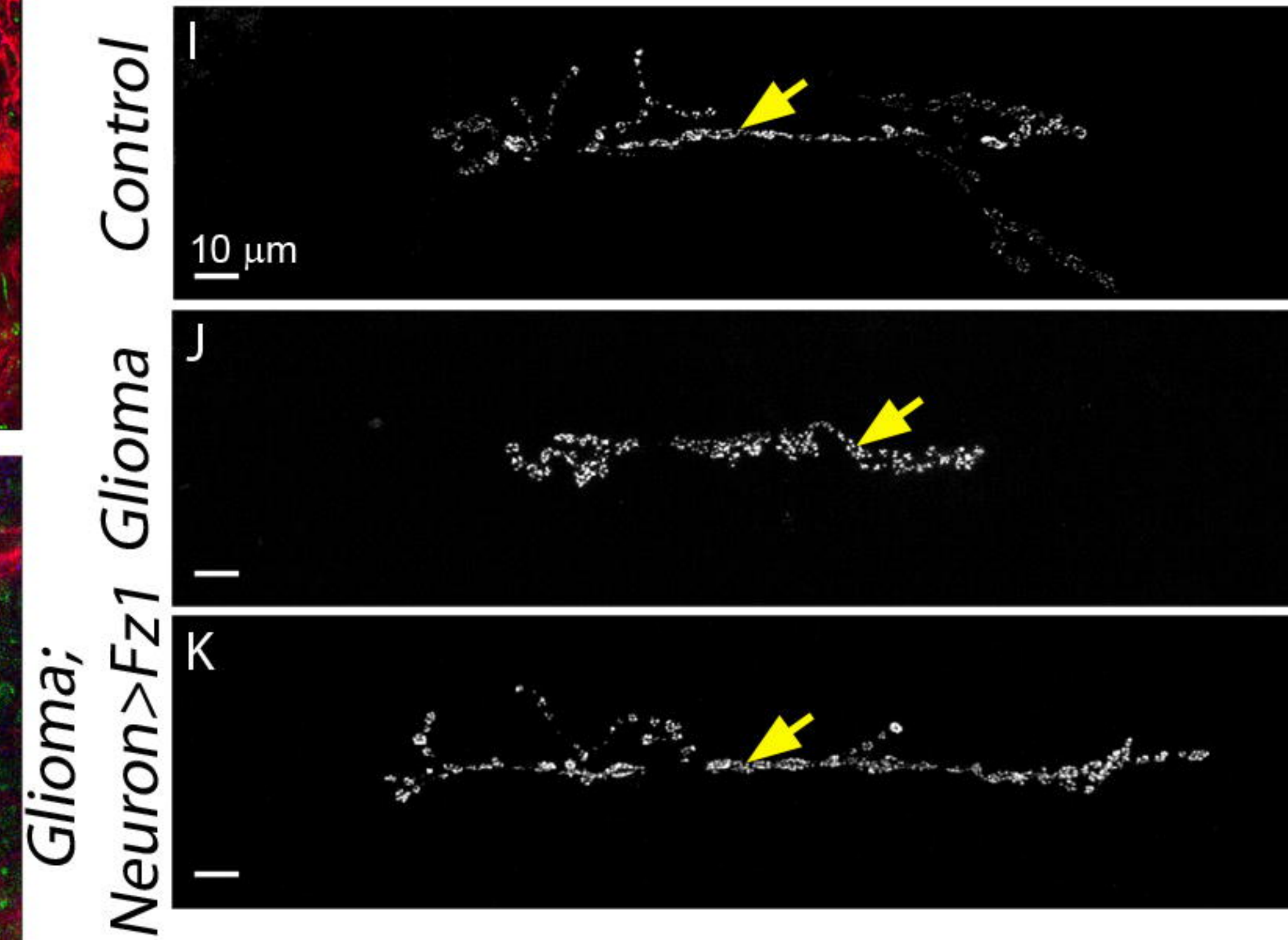
Active Zones Nc82



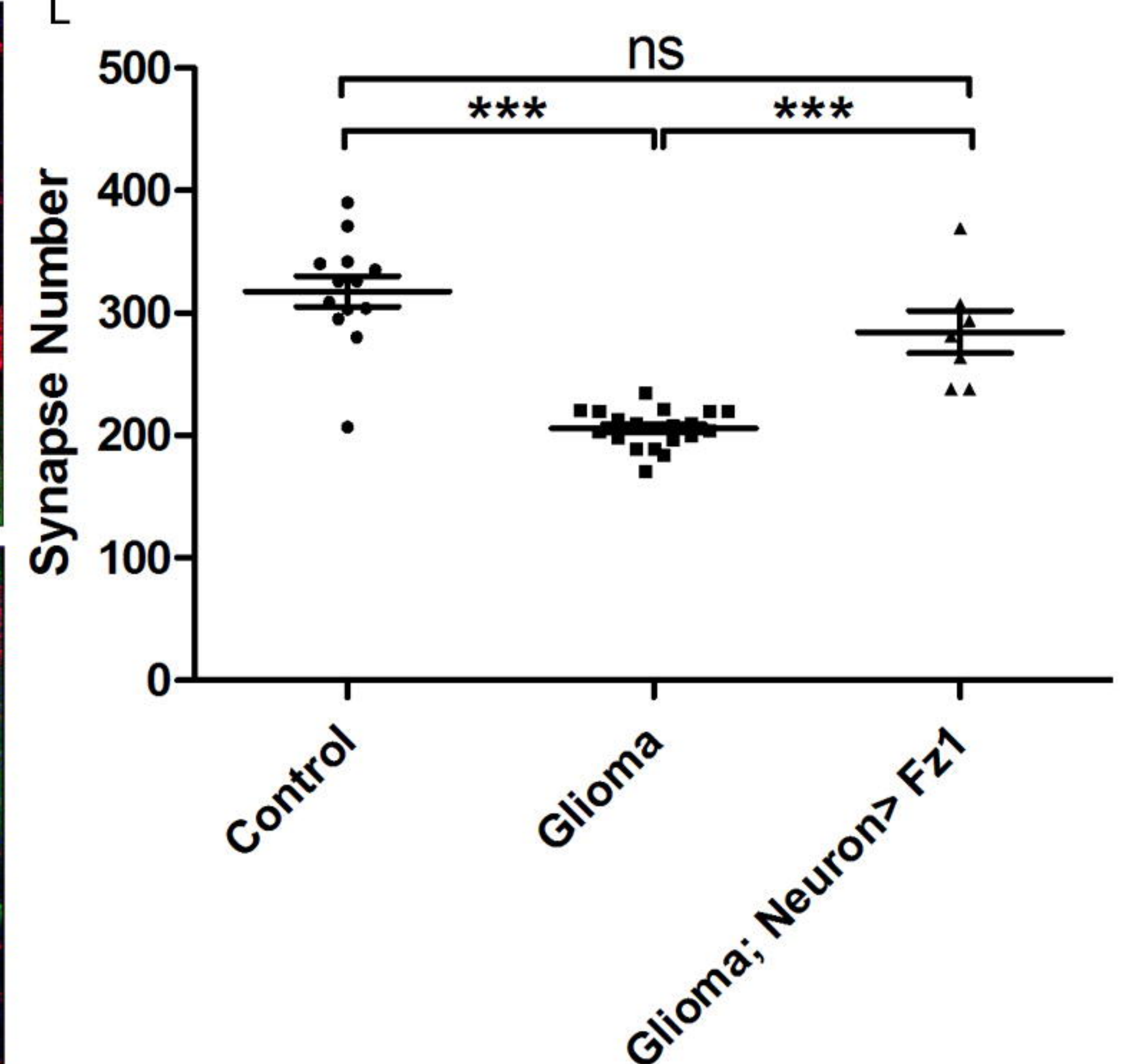
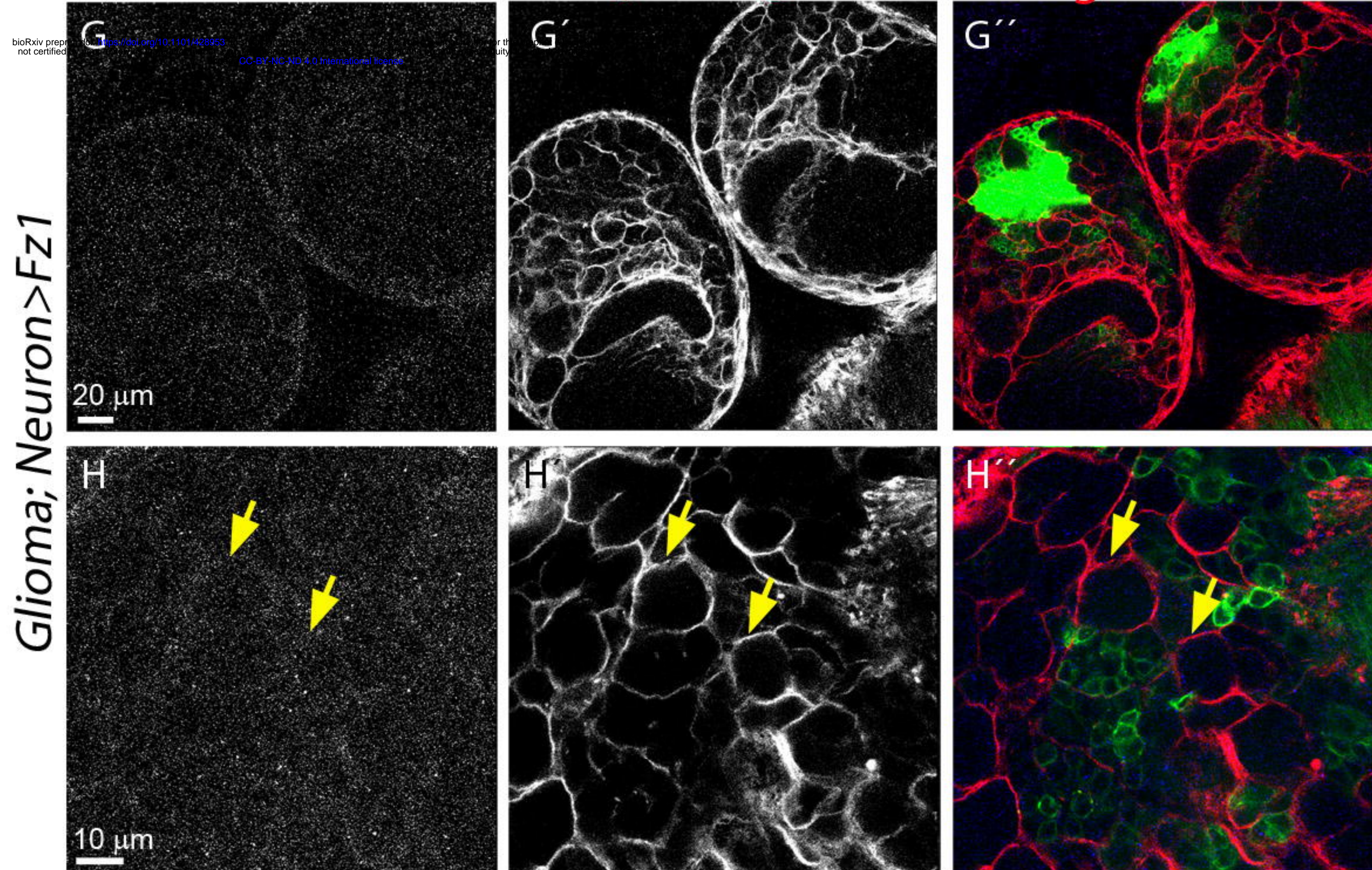
Fz1 Repo-ihog-RFP Fz1 ihog-RFP DAPI



Active Zones Nc82



Fz1 Repo-ihog-RFP Fz1 ihog-RFP ELAV-GFP



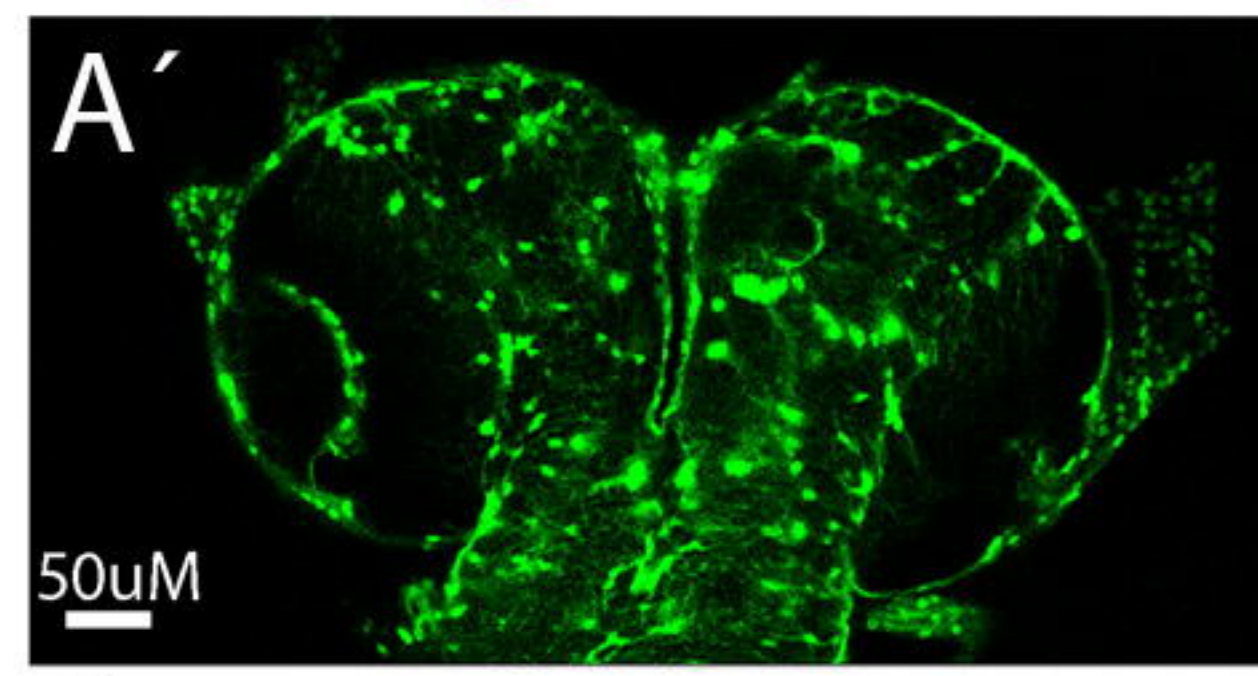
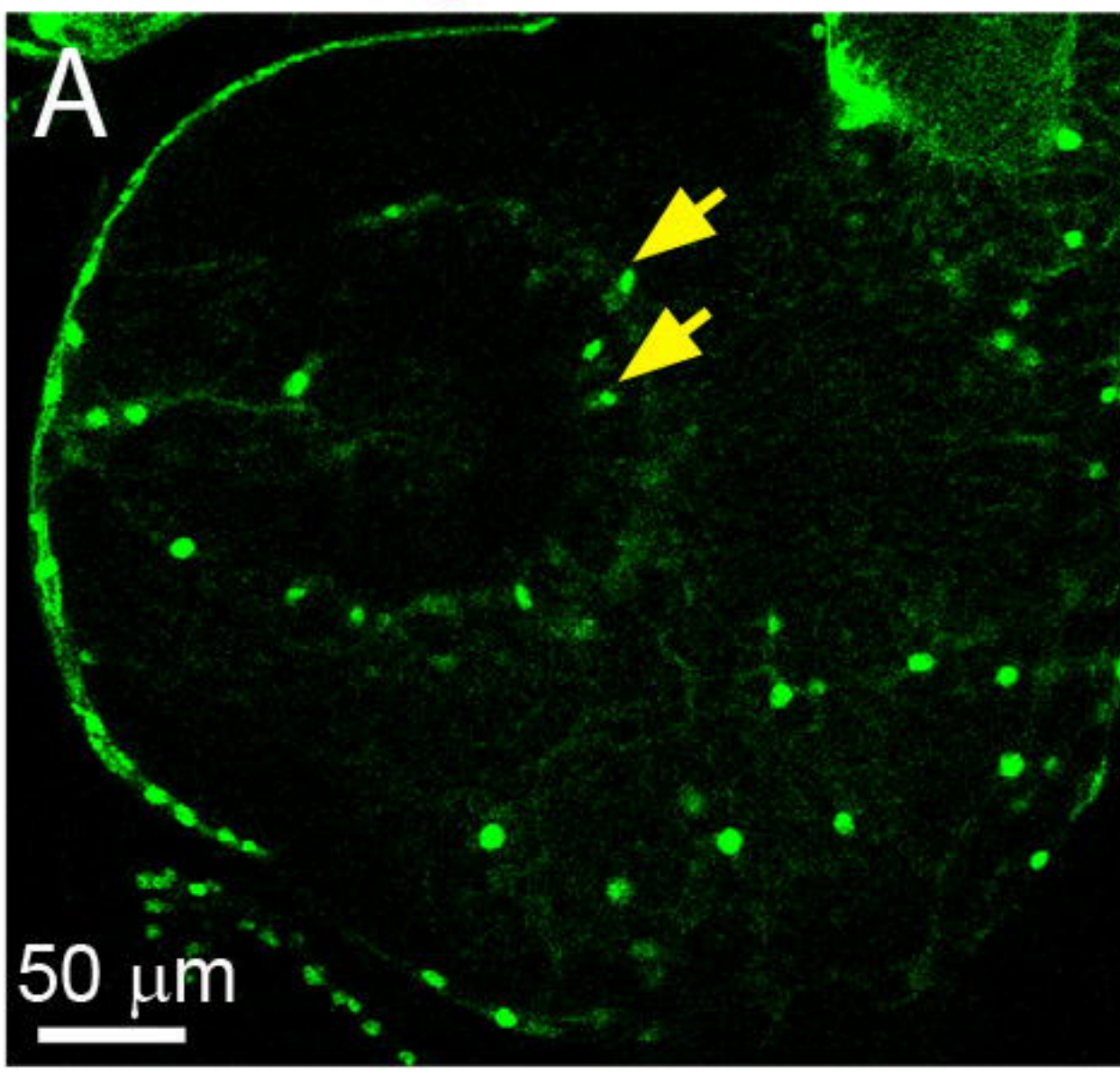
Repo-GFP

Repo-GFP

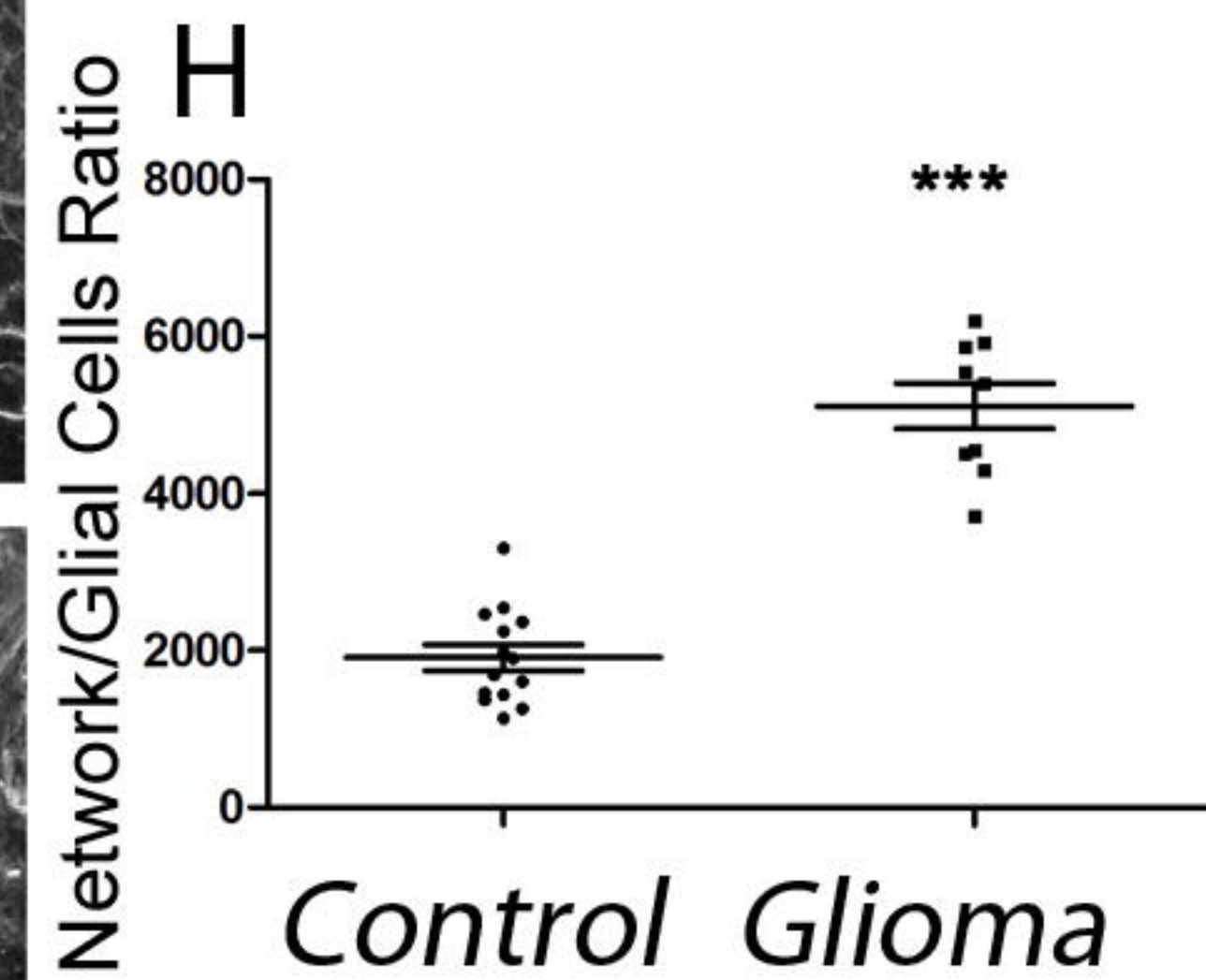
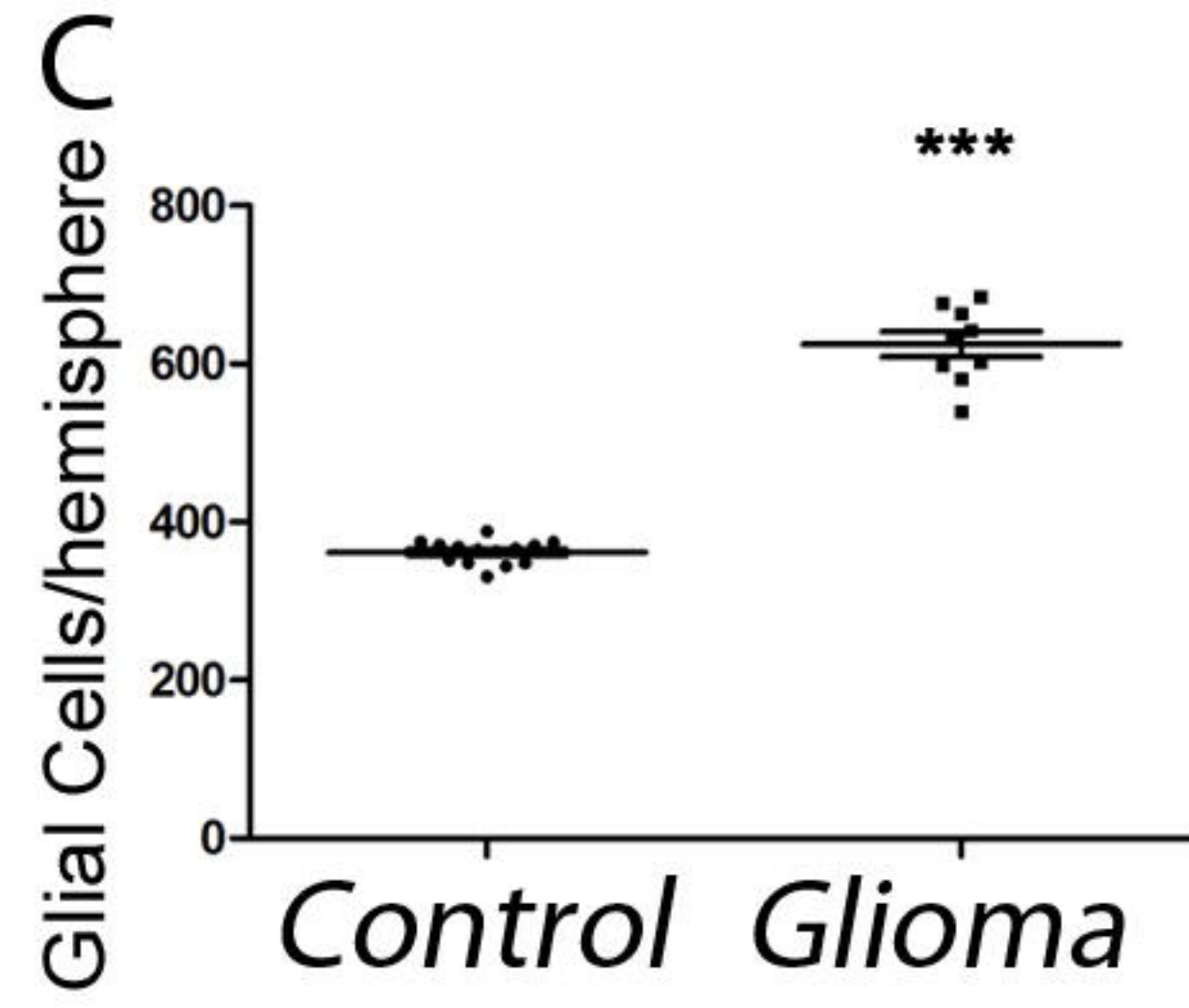
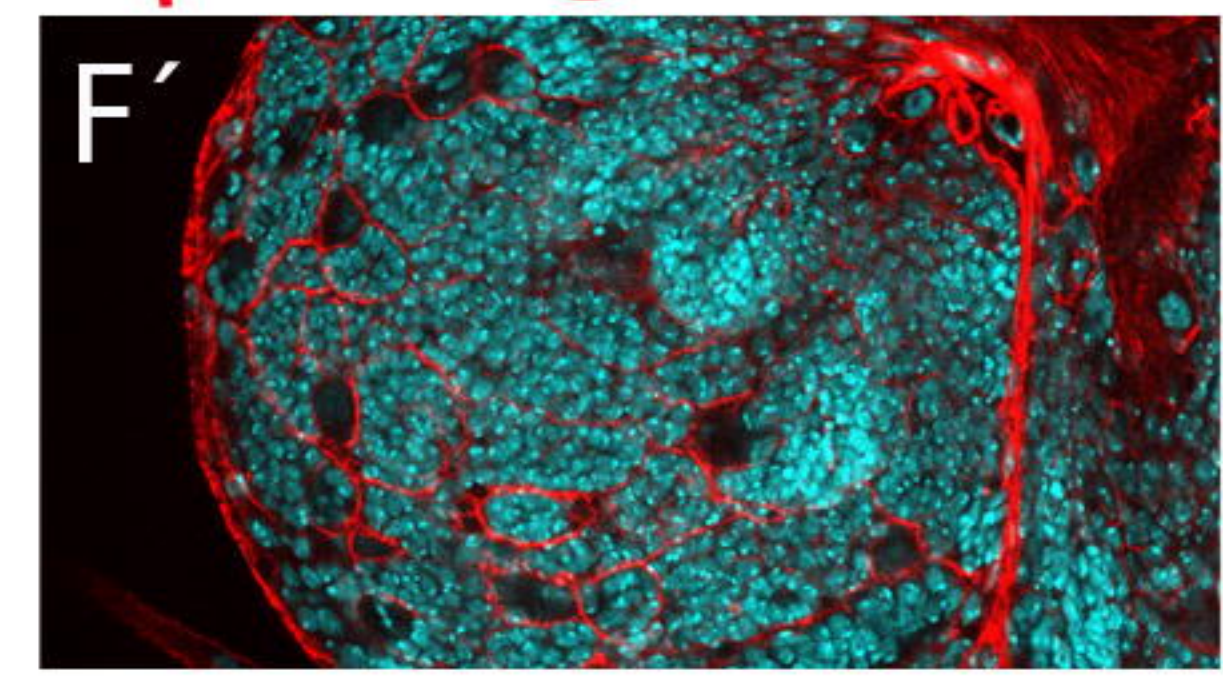
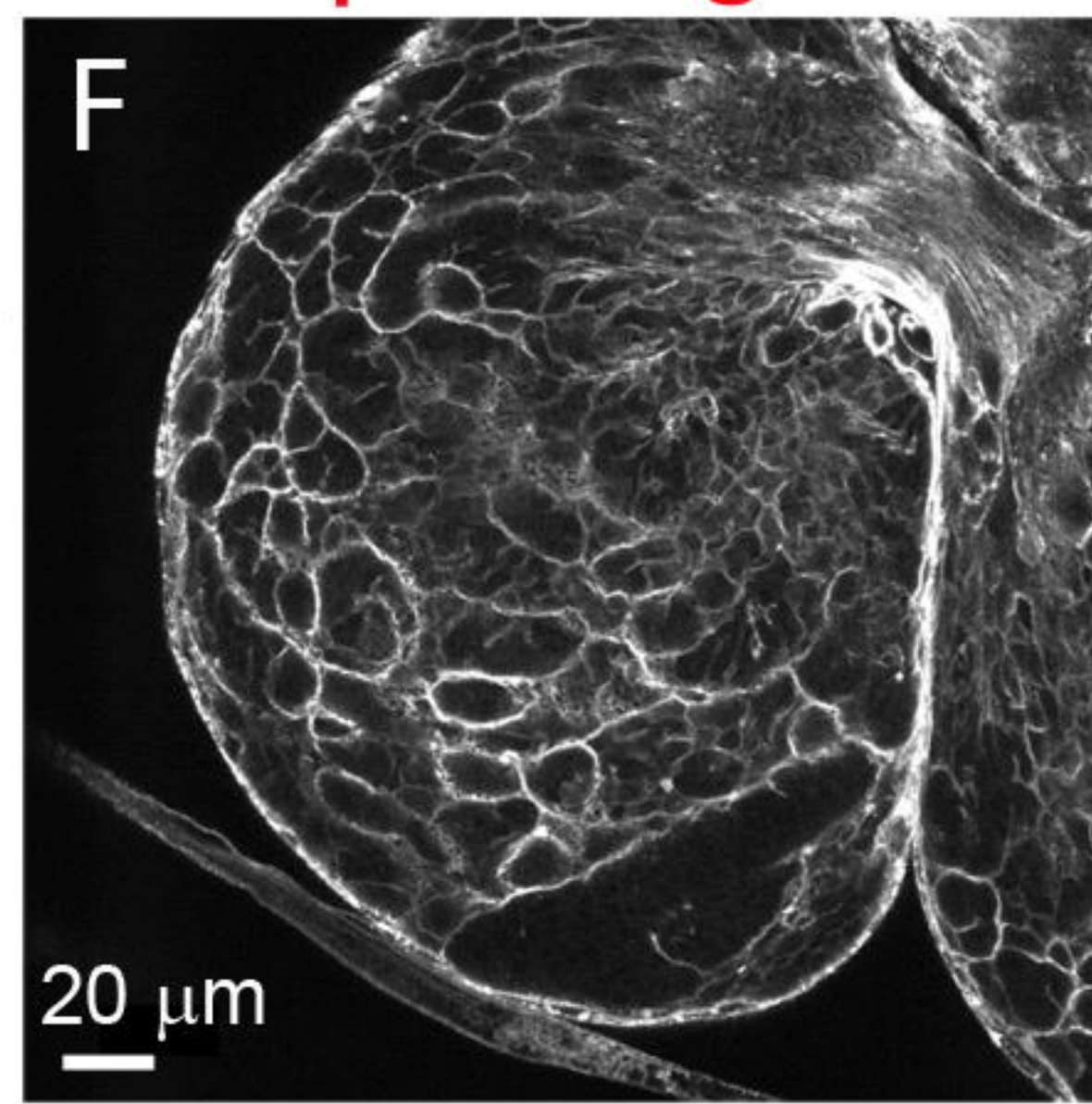
Repo-ihog-RFP

Repo-ihog-RFP DAPI

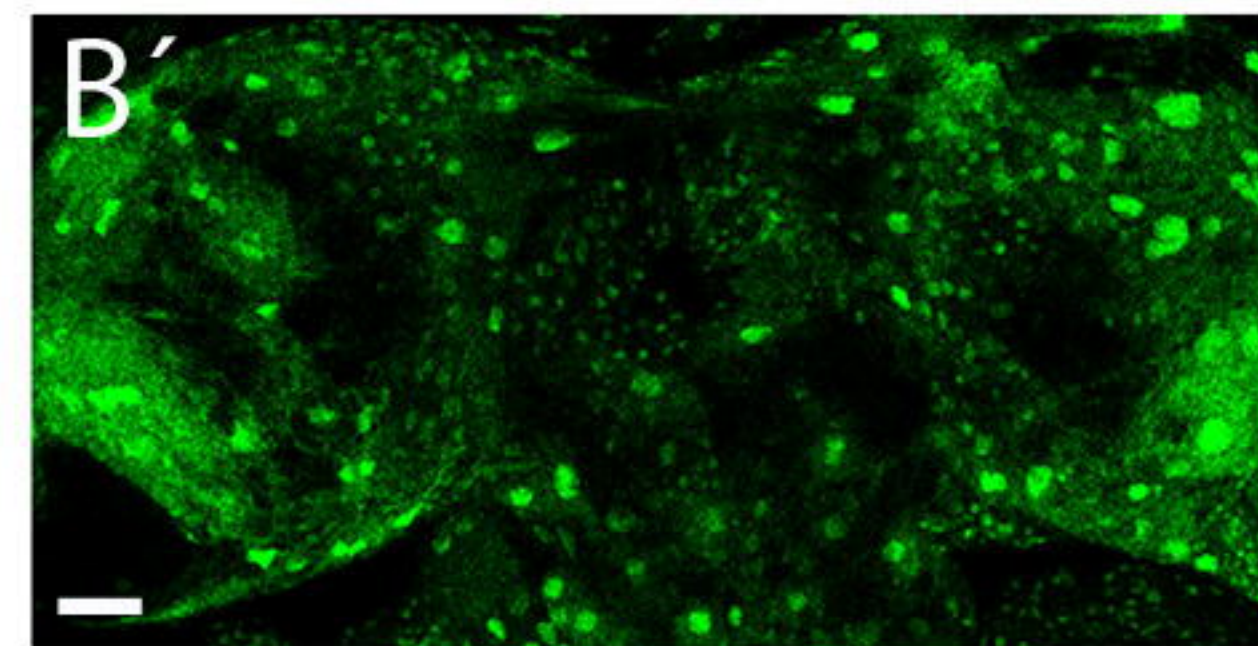
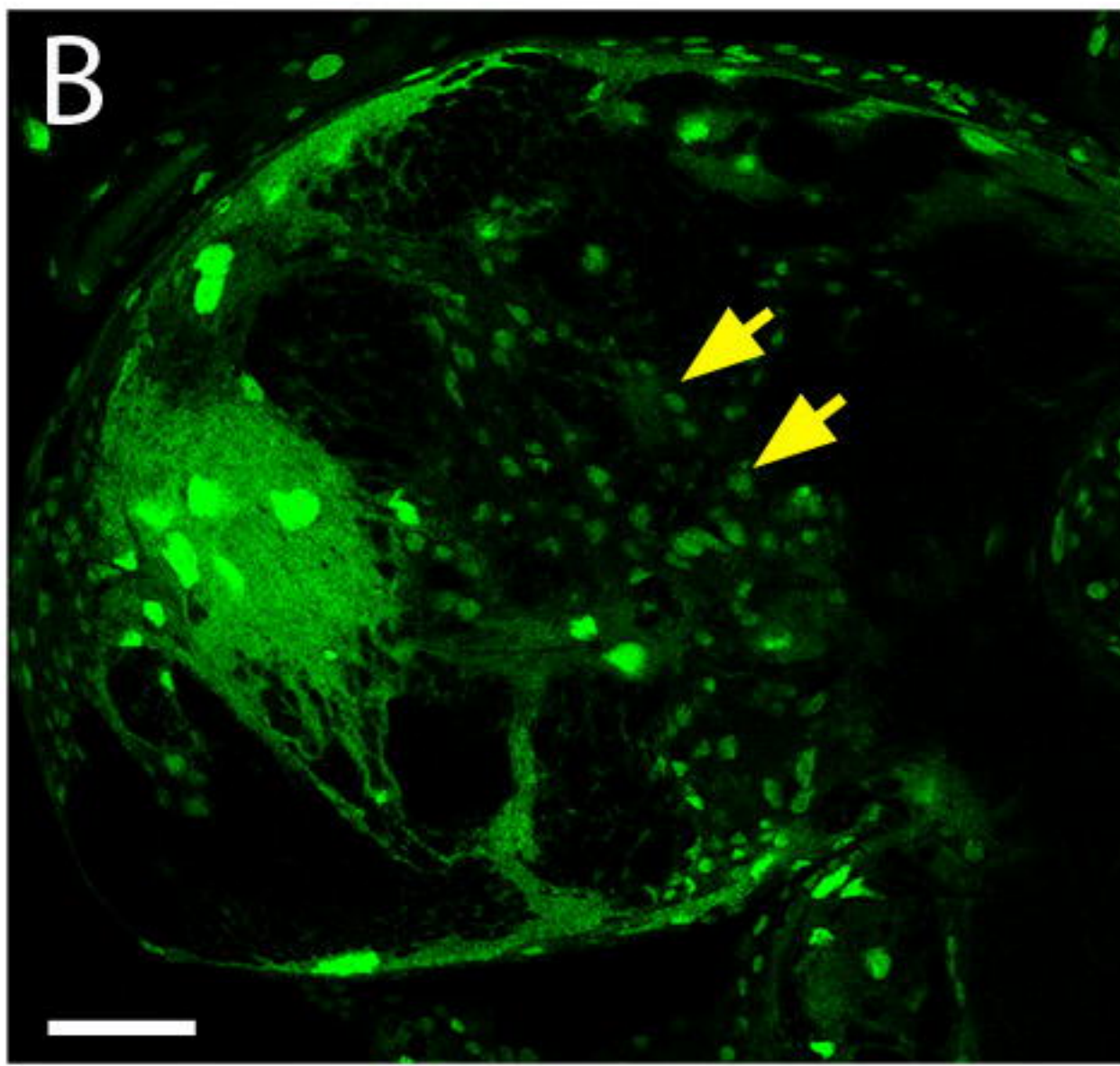
Control



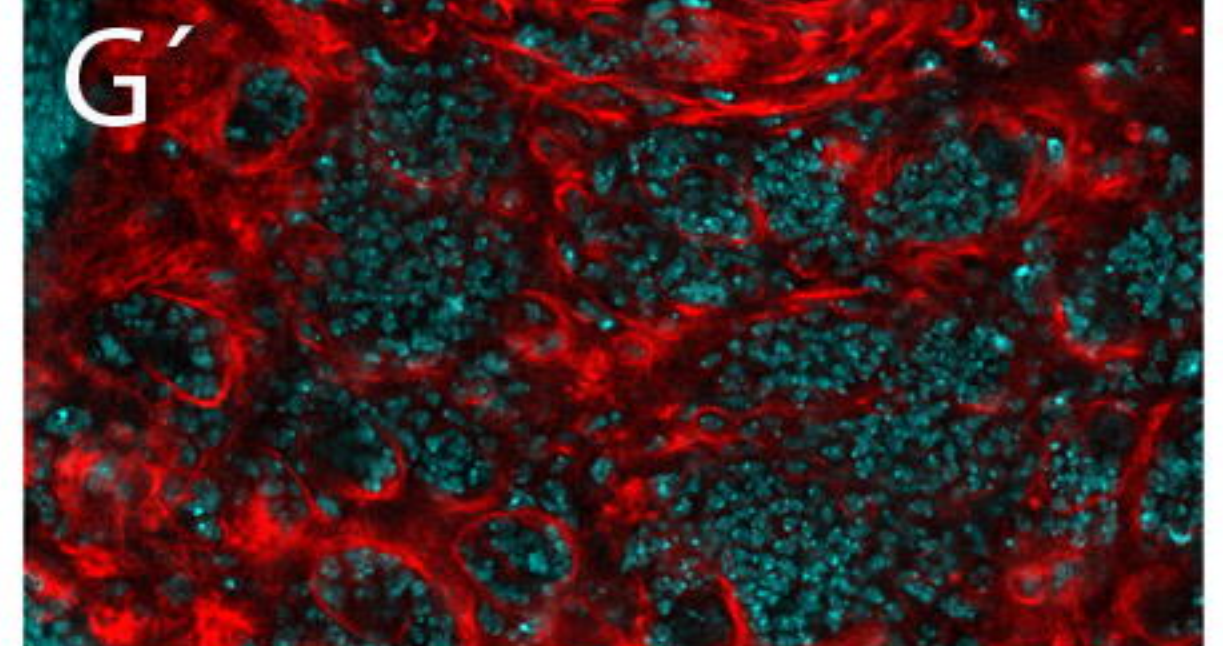
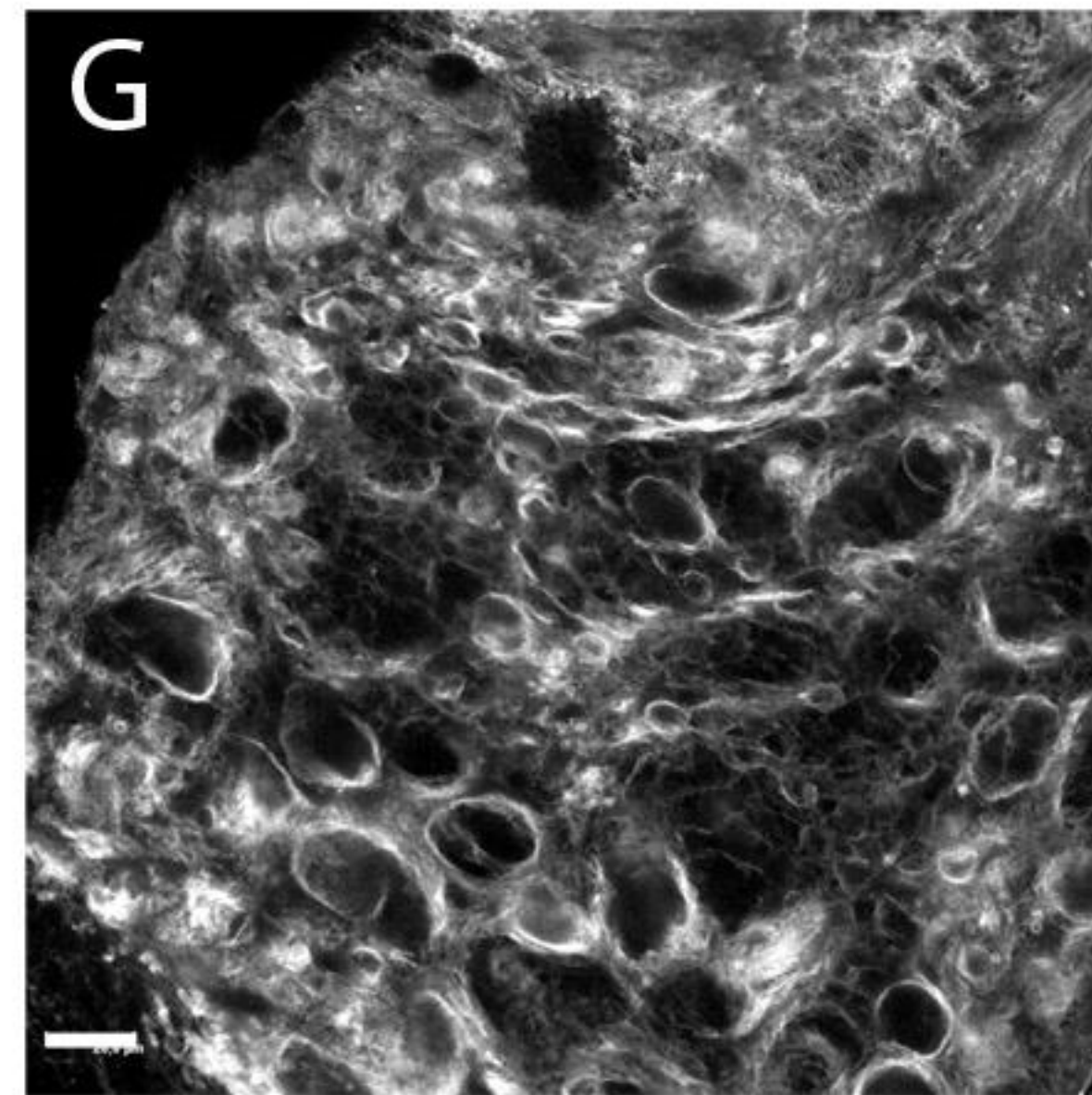
Control



Glioma



Glioma



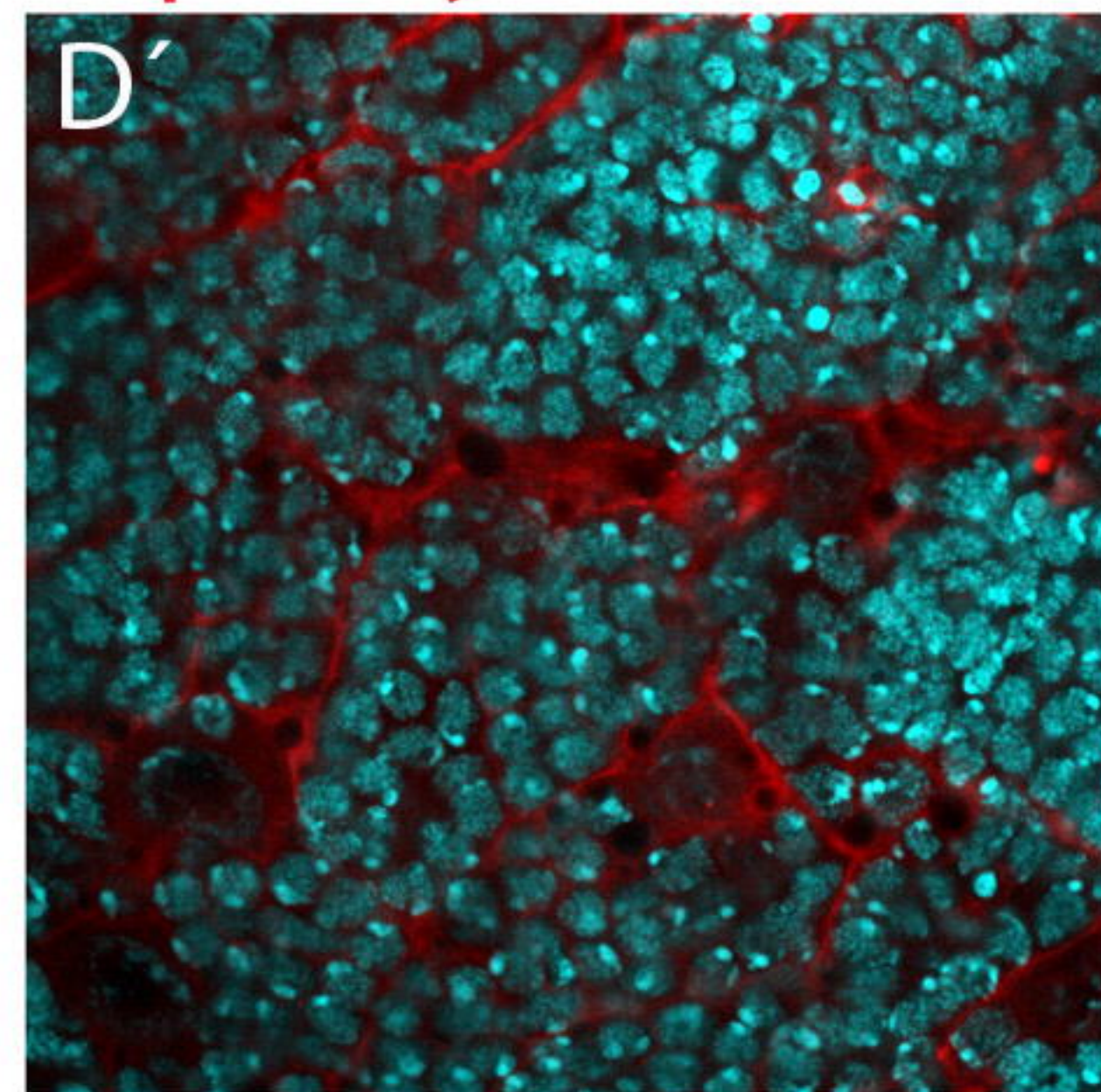
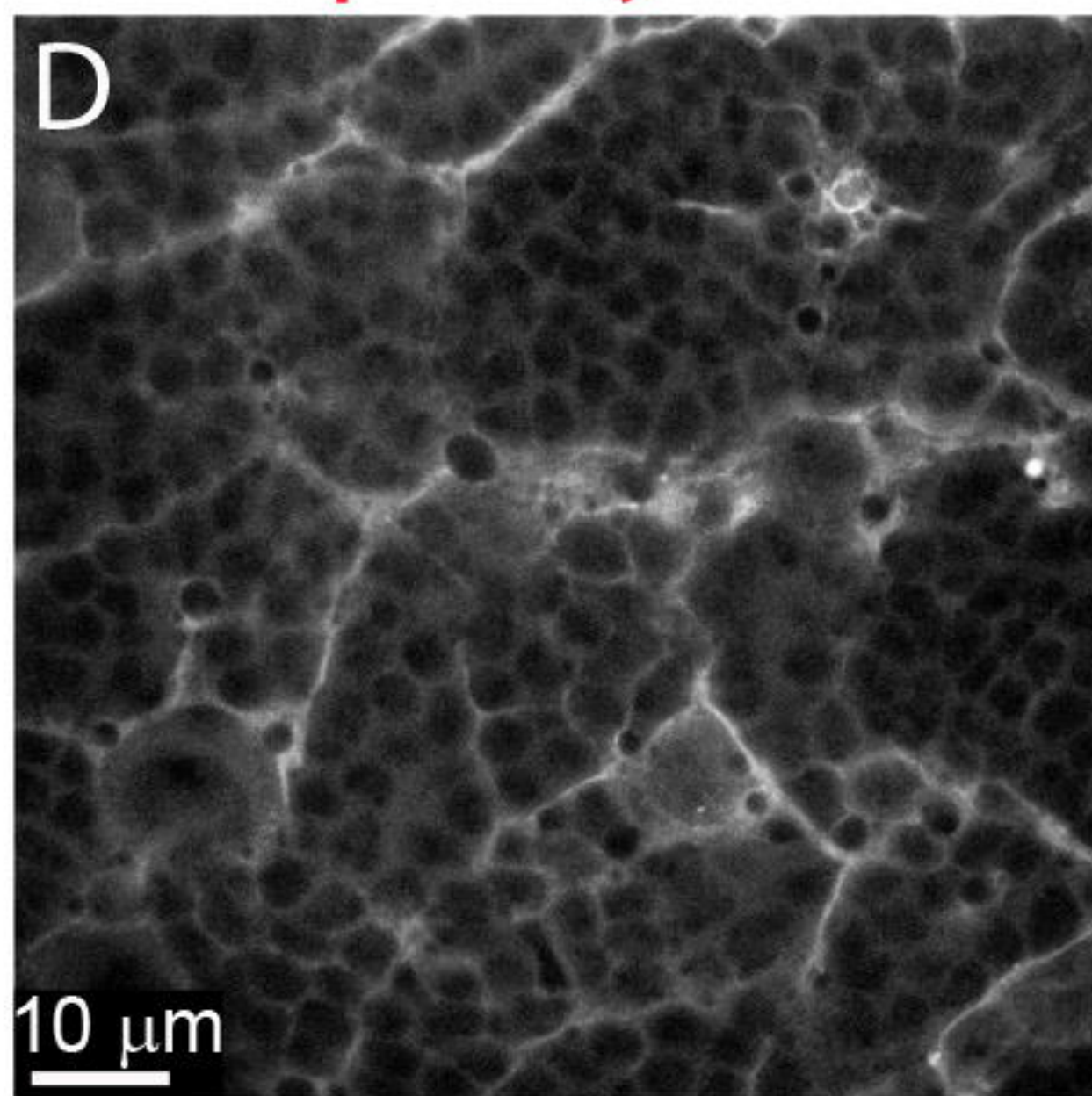
Repo-myr-RFP

Repo-myr-RFP DAPI

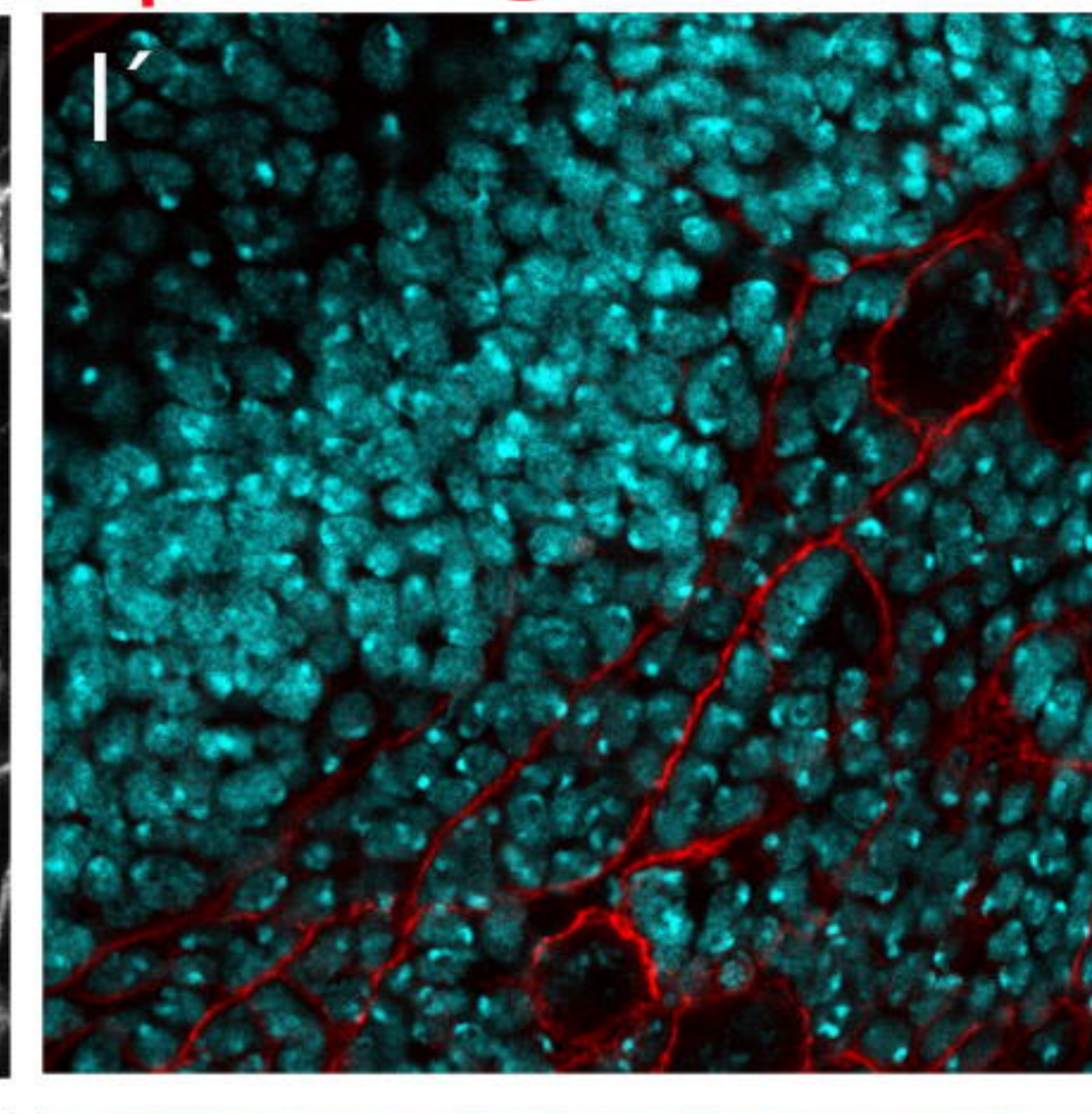
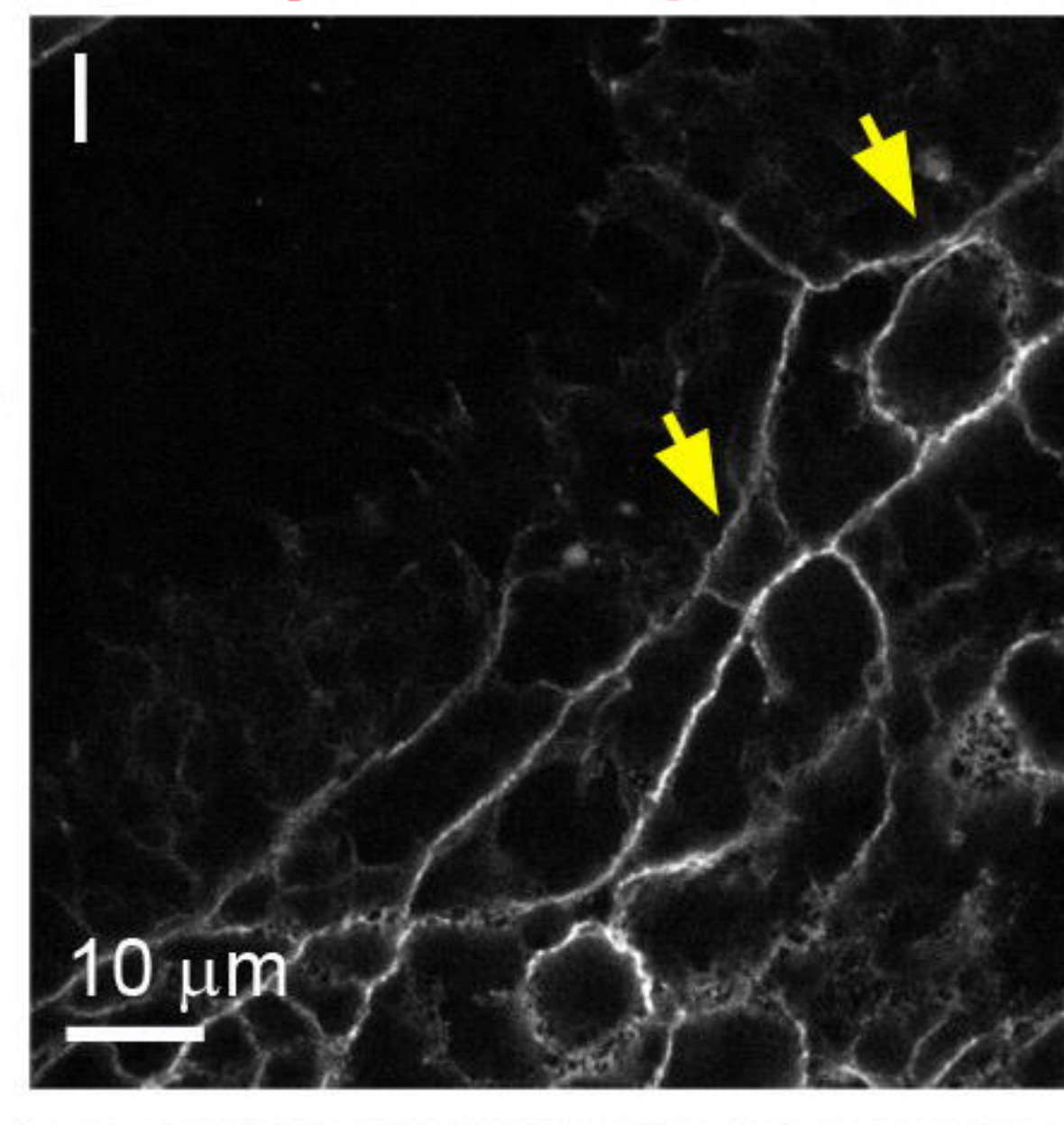
Repo-ihog-RFP

Repo-ihog-RFP DAPI

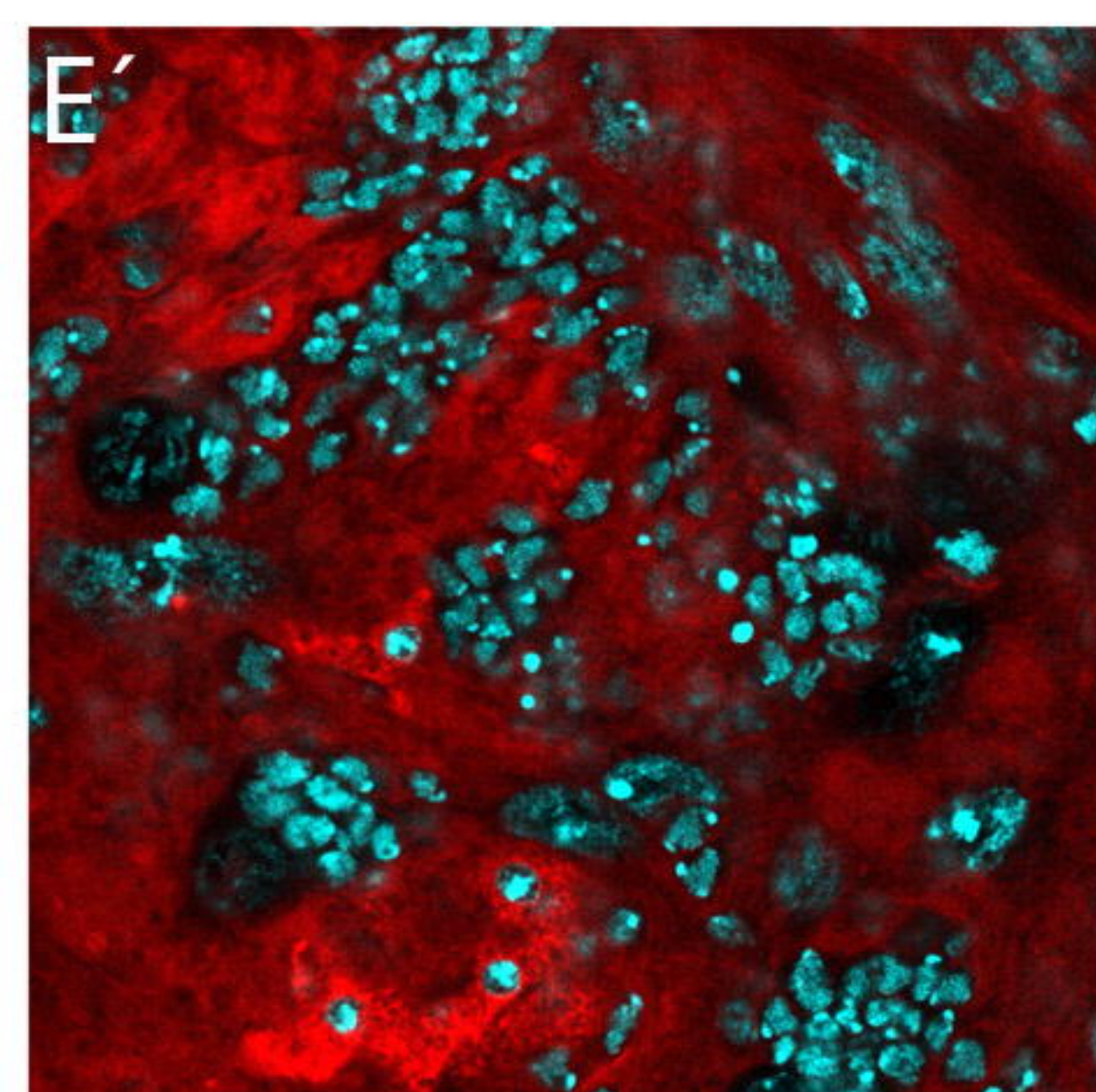
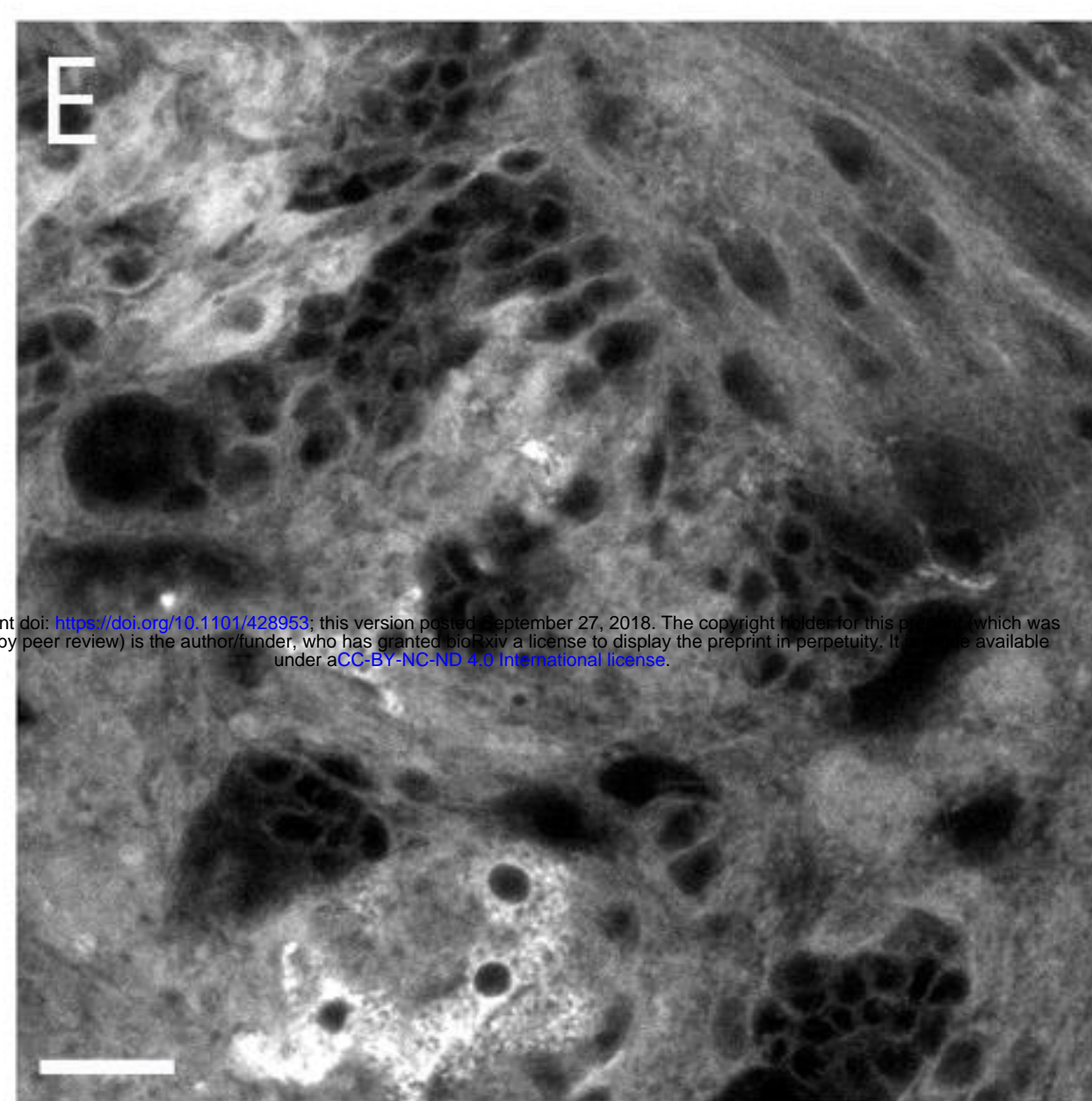
Control



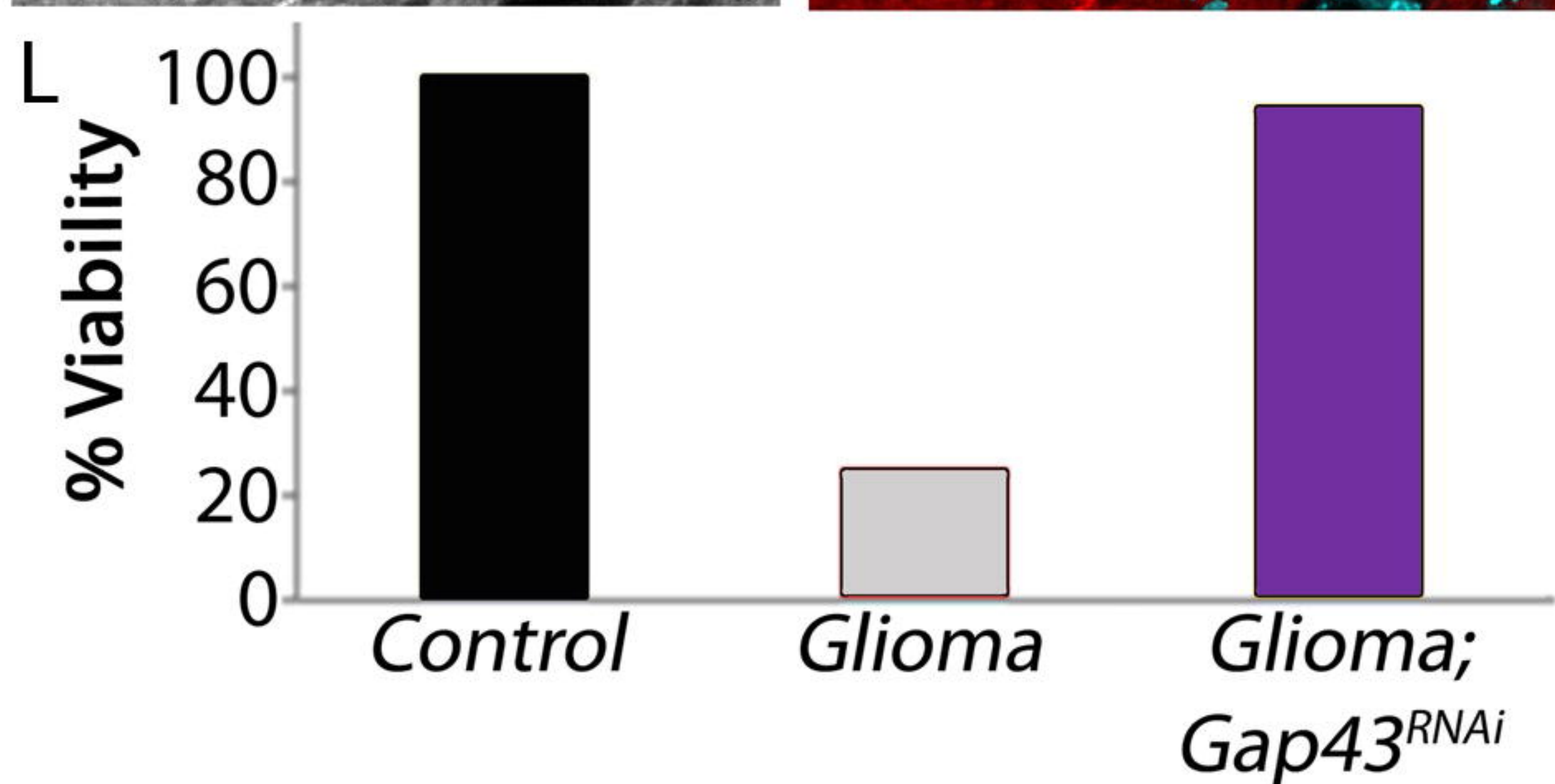
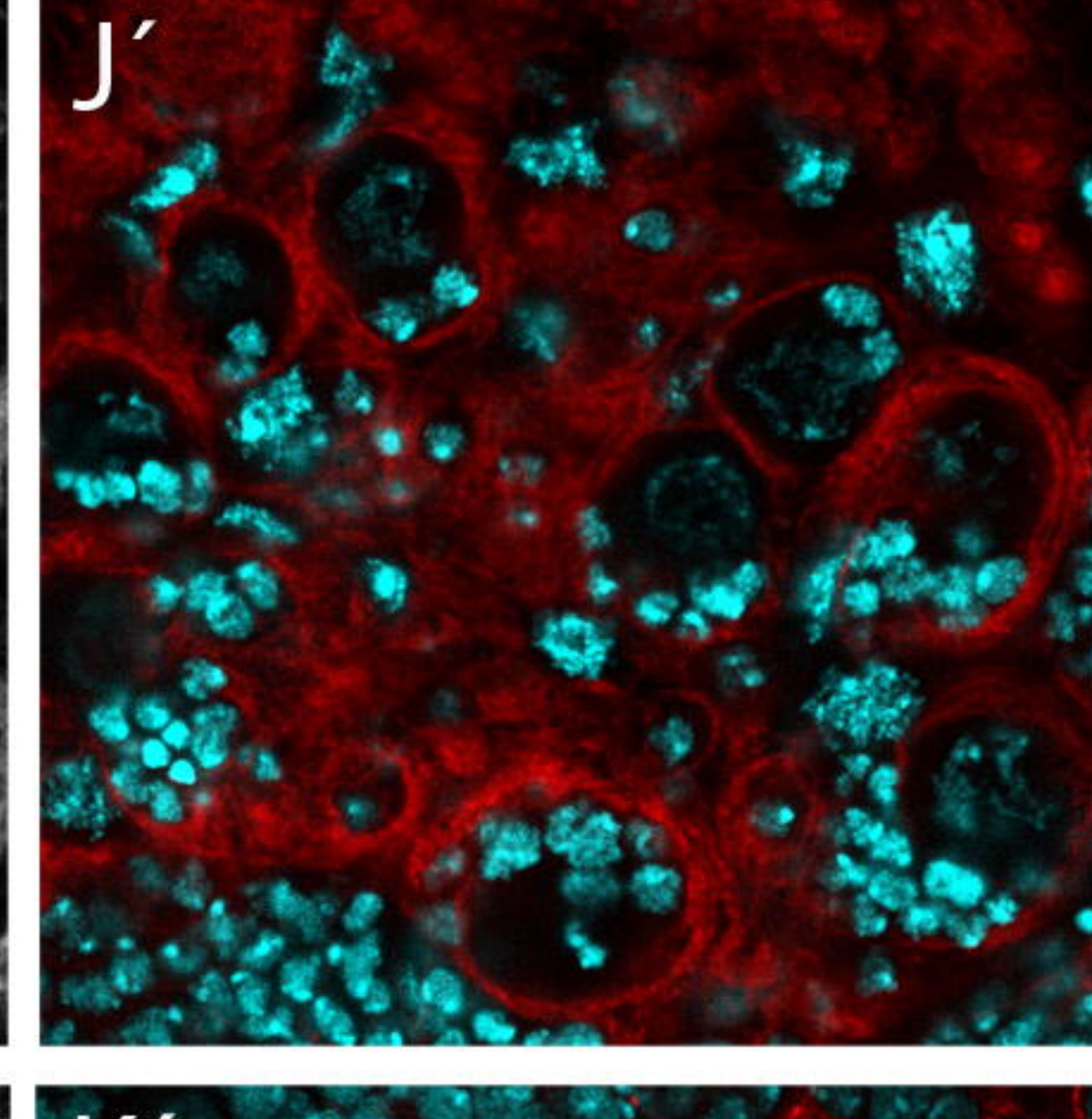
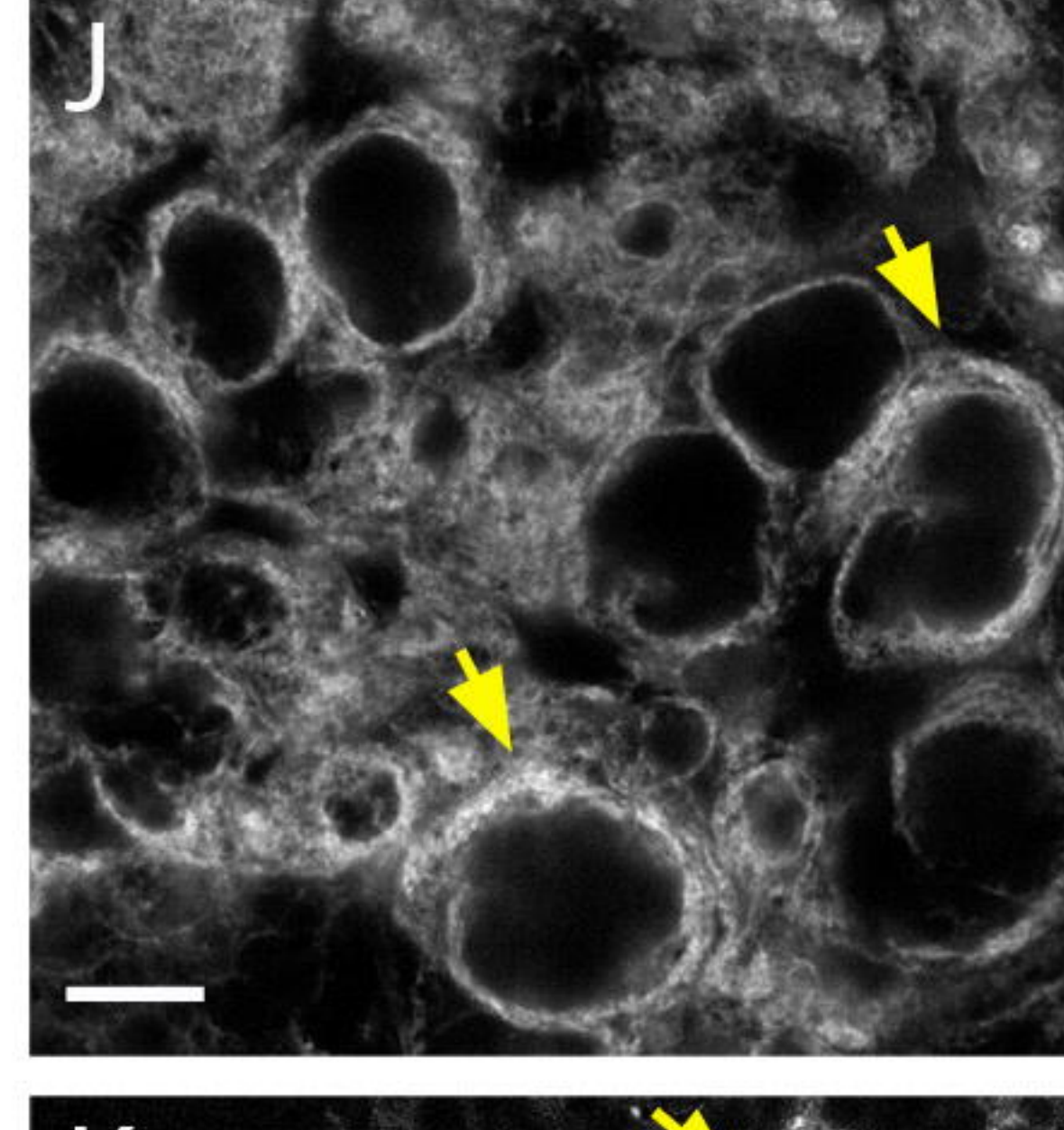
Control



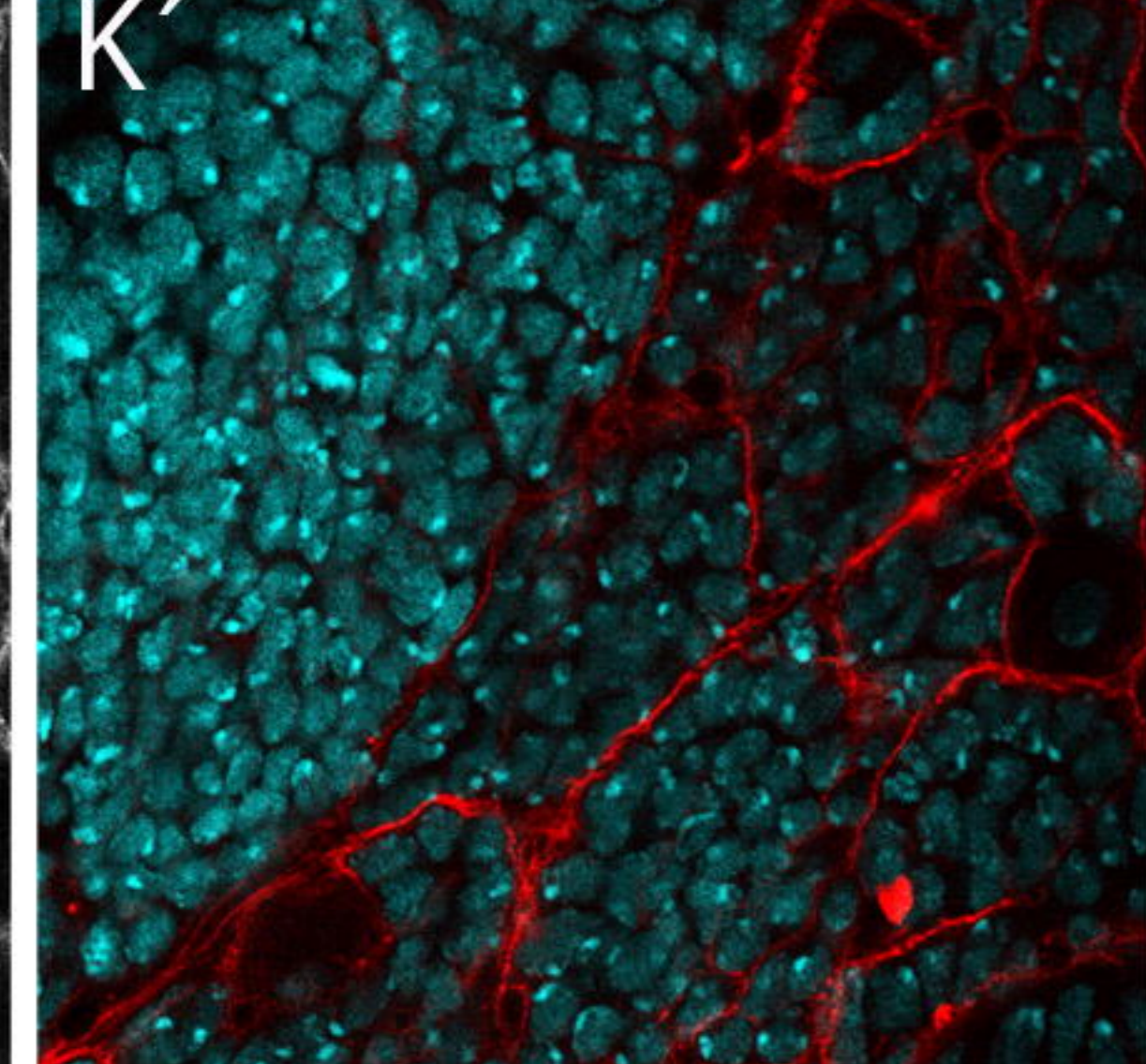
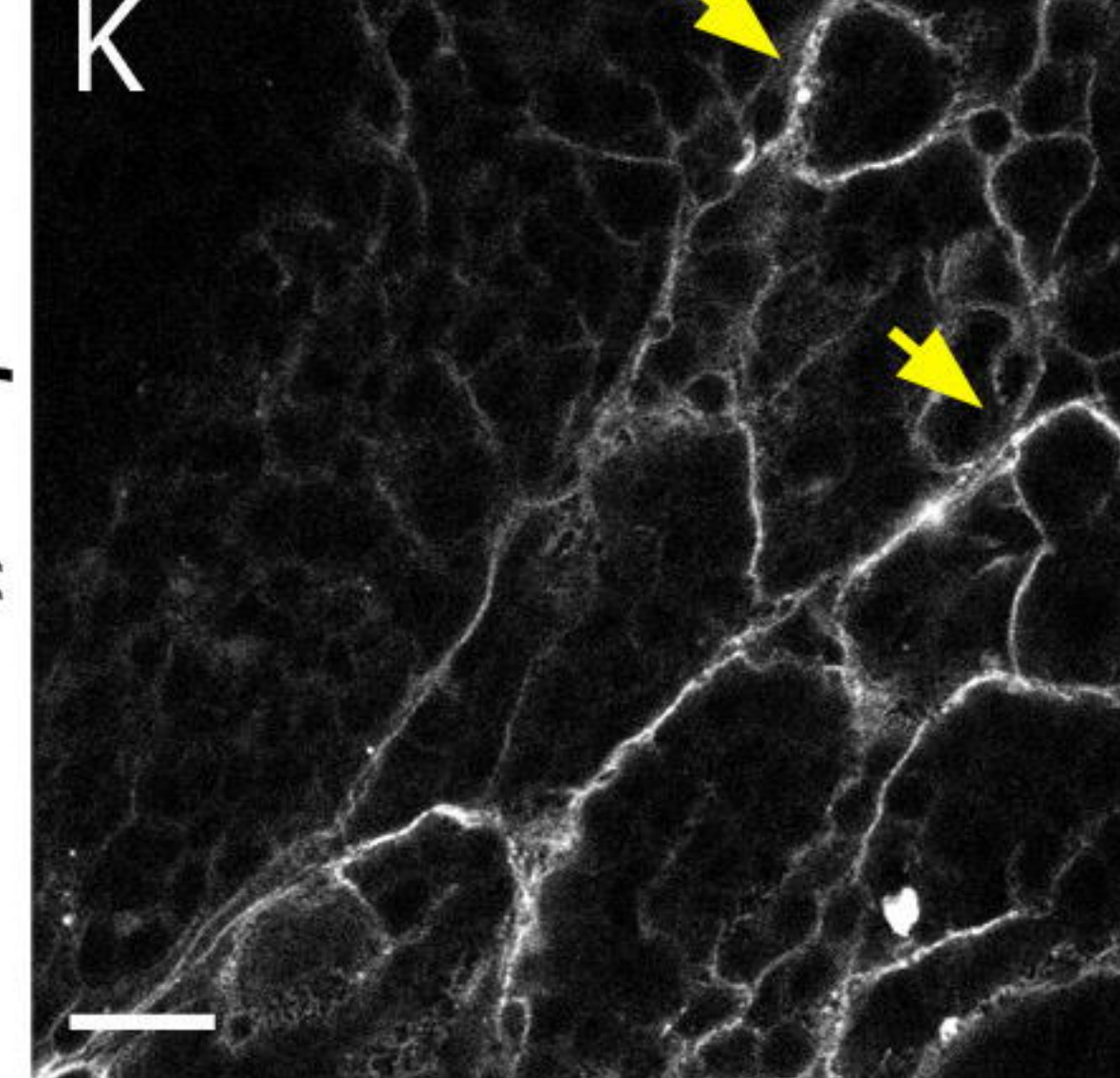
Glioma



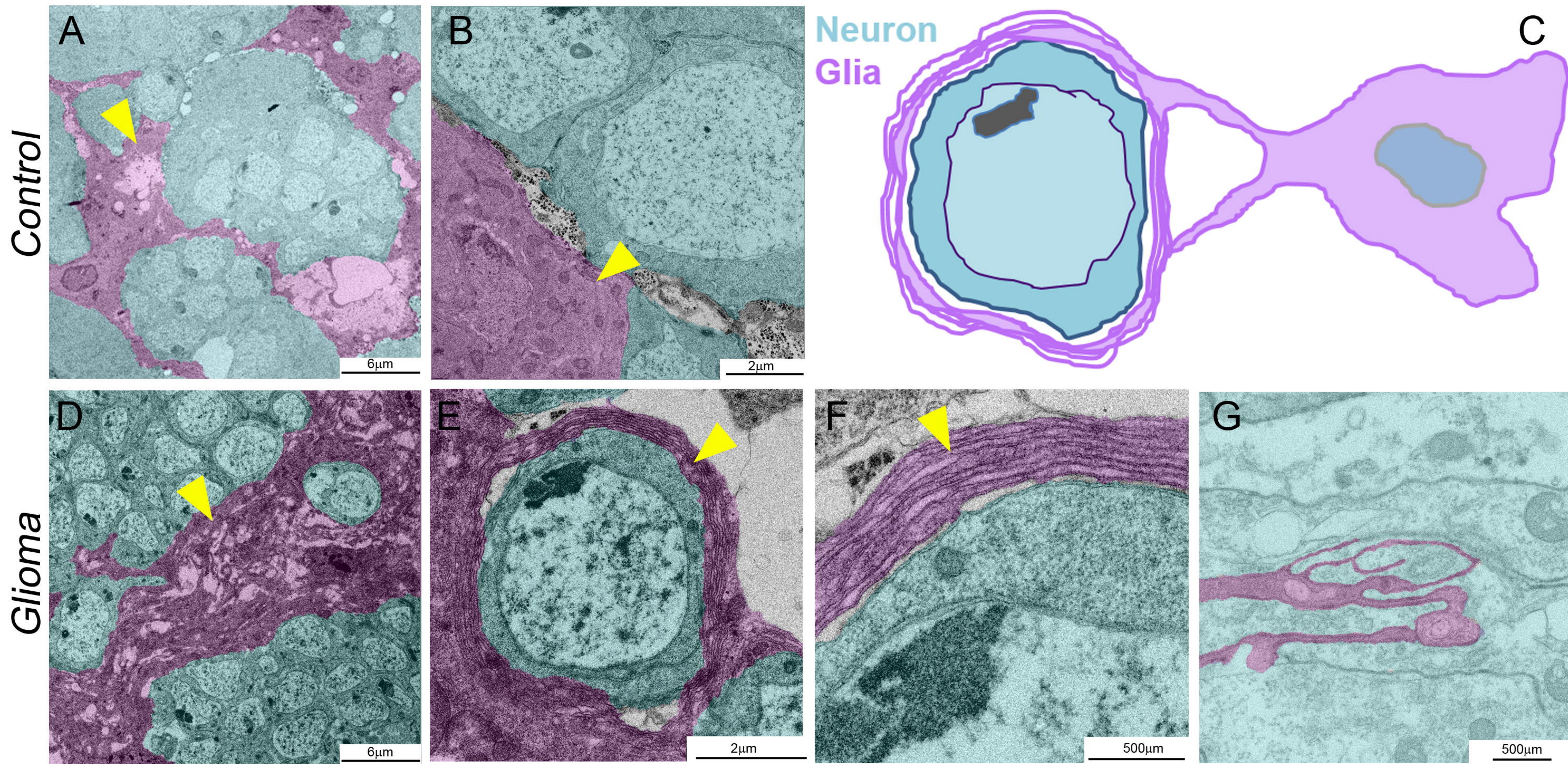
Glioma



Glioma; Gap43<sup>RNAi</sup>



bioRxiv preprint doi: <https://doi.org/10.1101/020333>; this version posted November 27, 2015. The copyright holder for this preprint (which was not certified by peer review) is the author/funder, who has granted bioRxiv a license to display the preprint in perpetuity. It is made available under aCC-BY-NC-ND 4.0 International license.

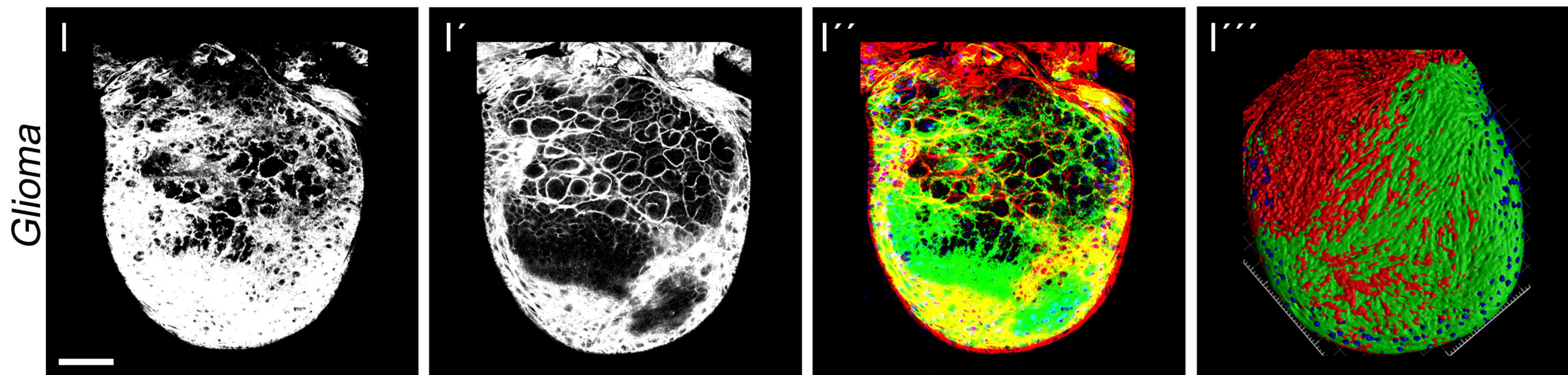
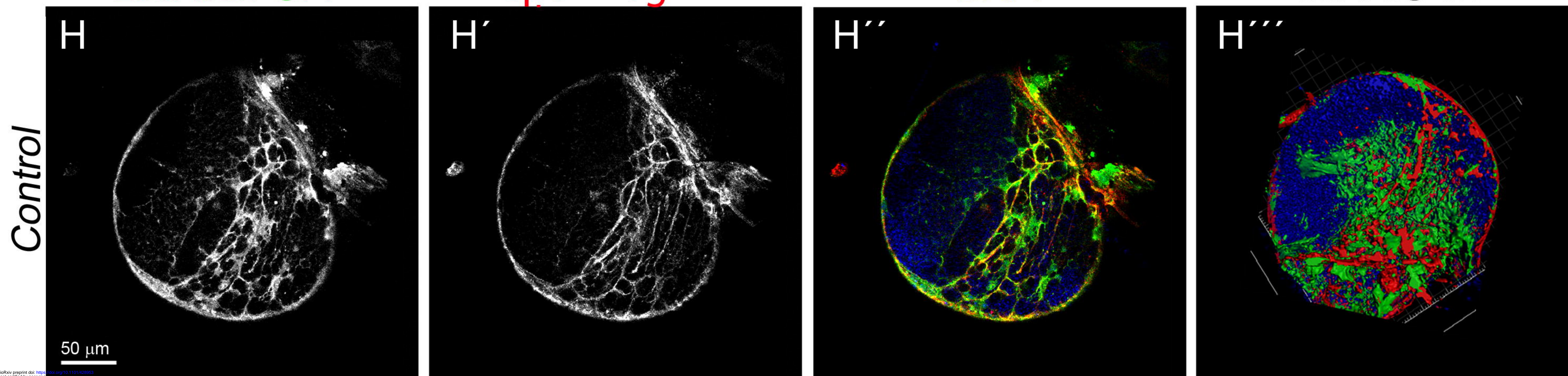


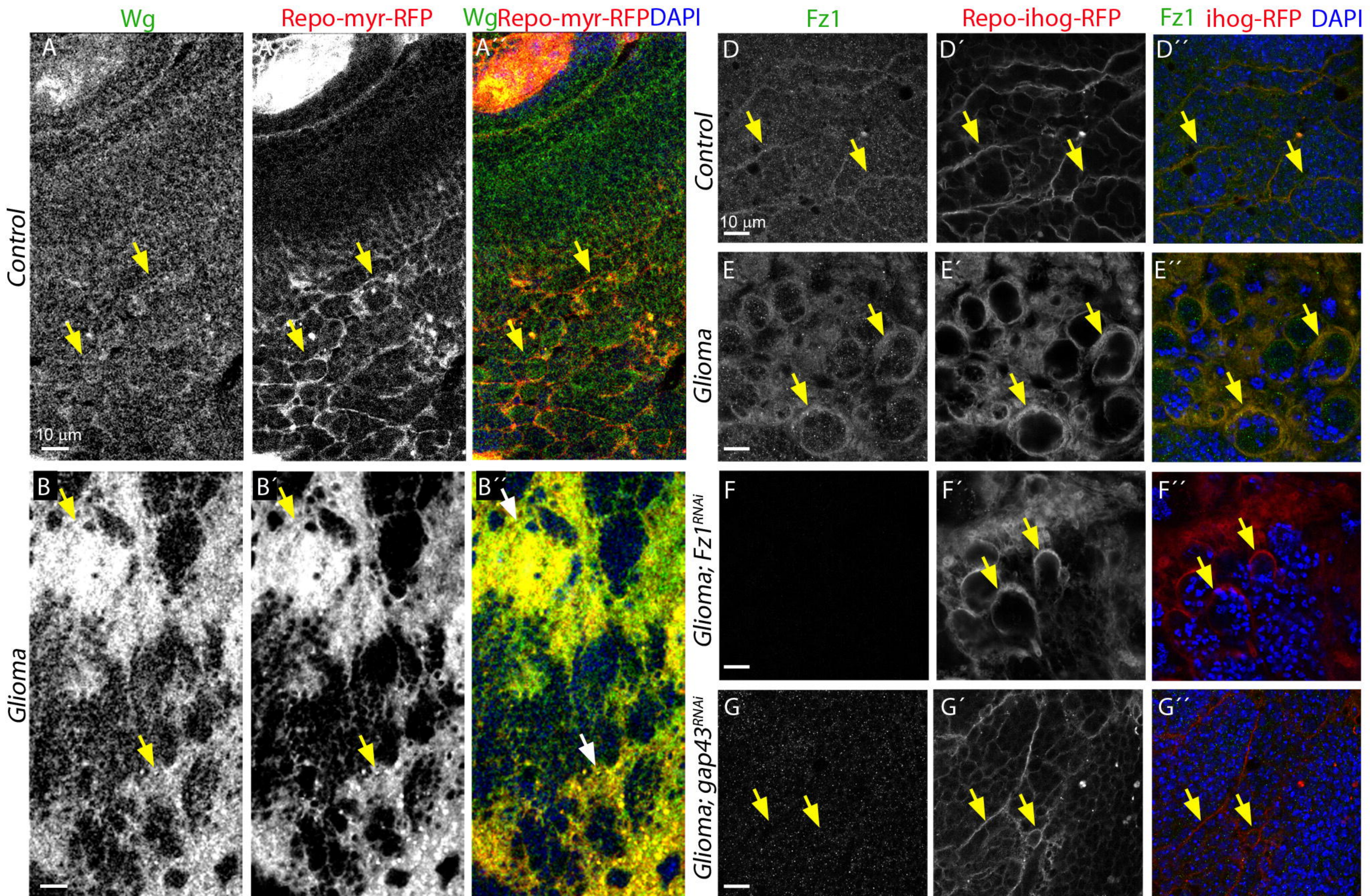
LifeActin-GFP

Repo-ihog-RFP

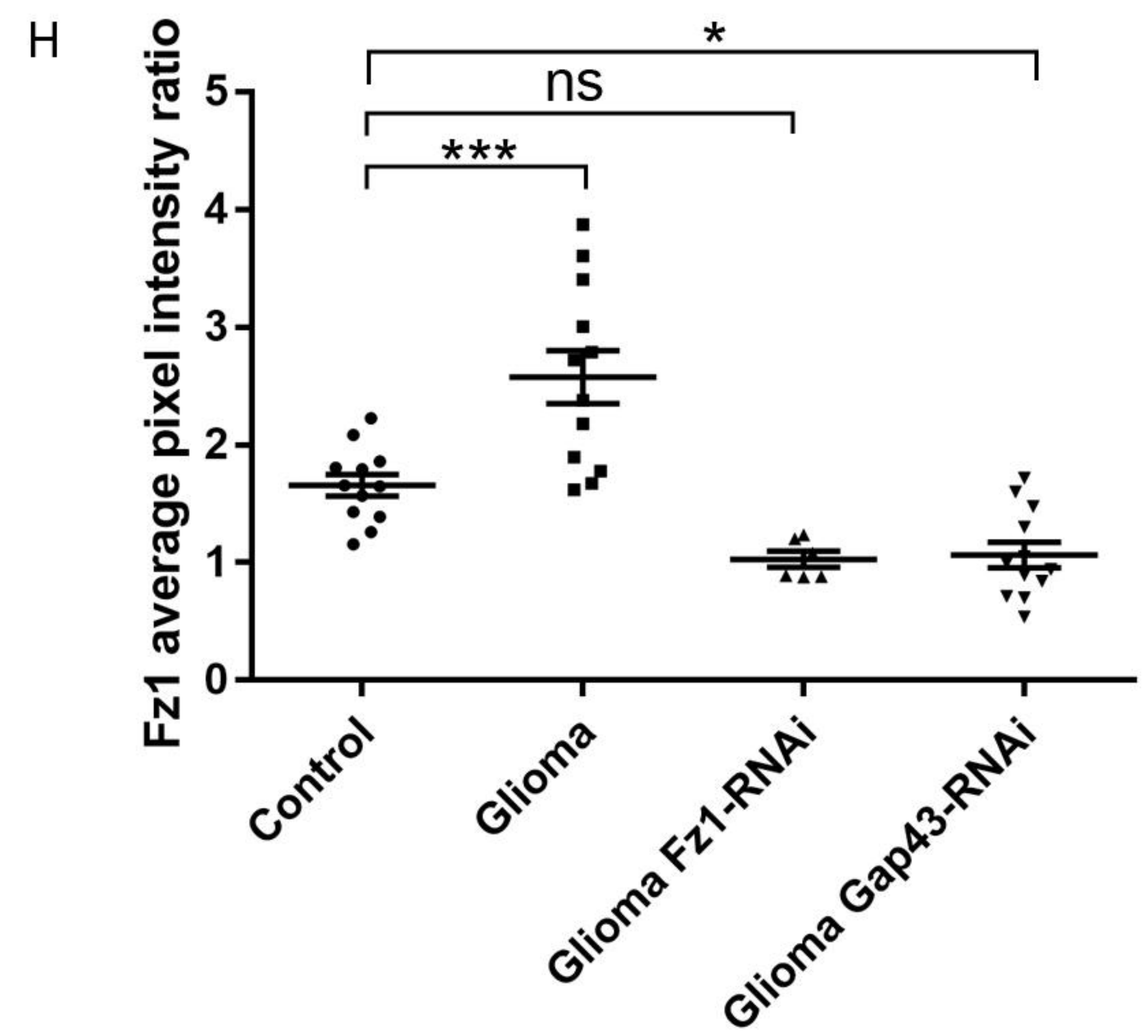
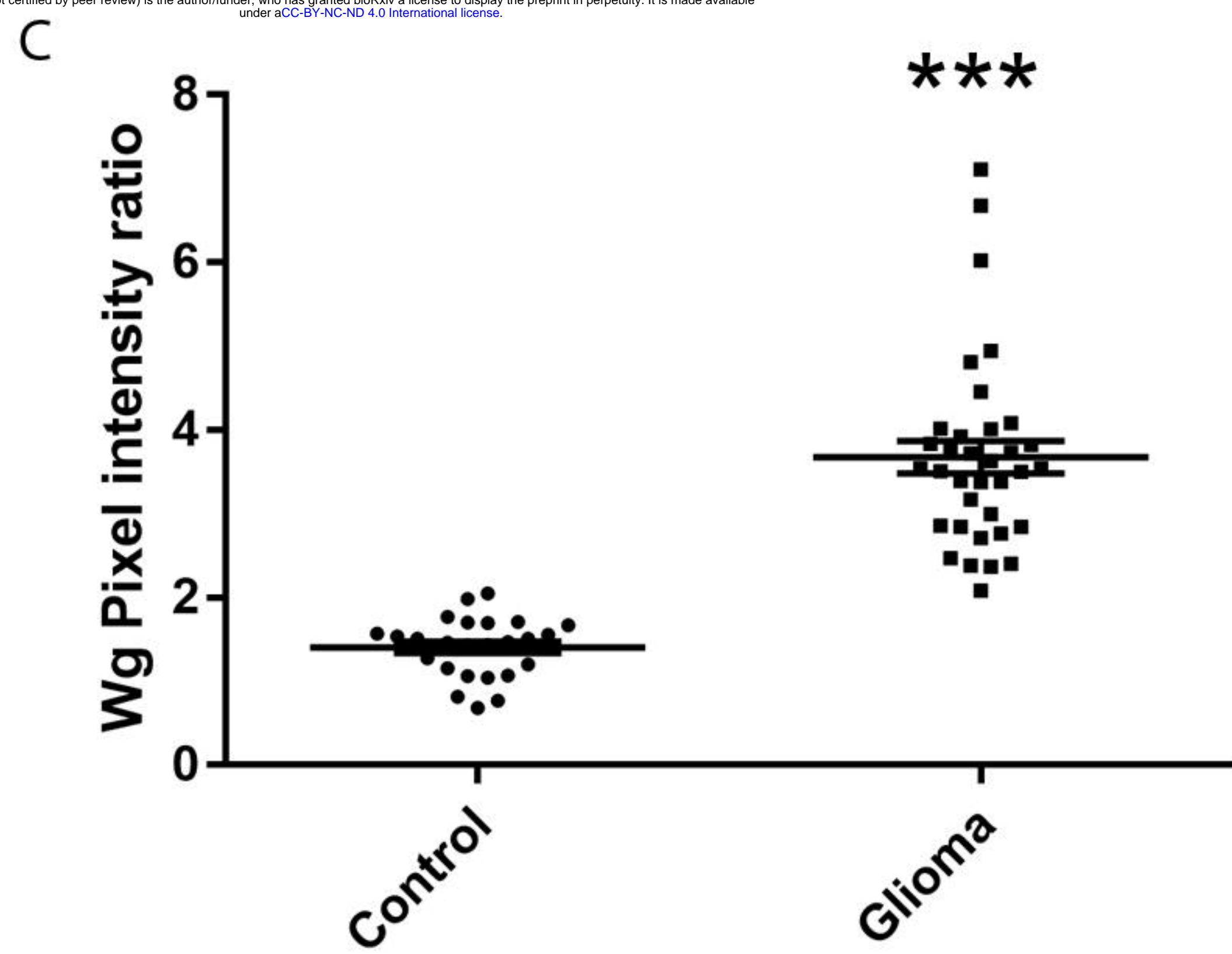
DAPI

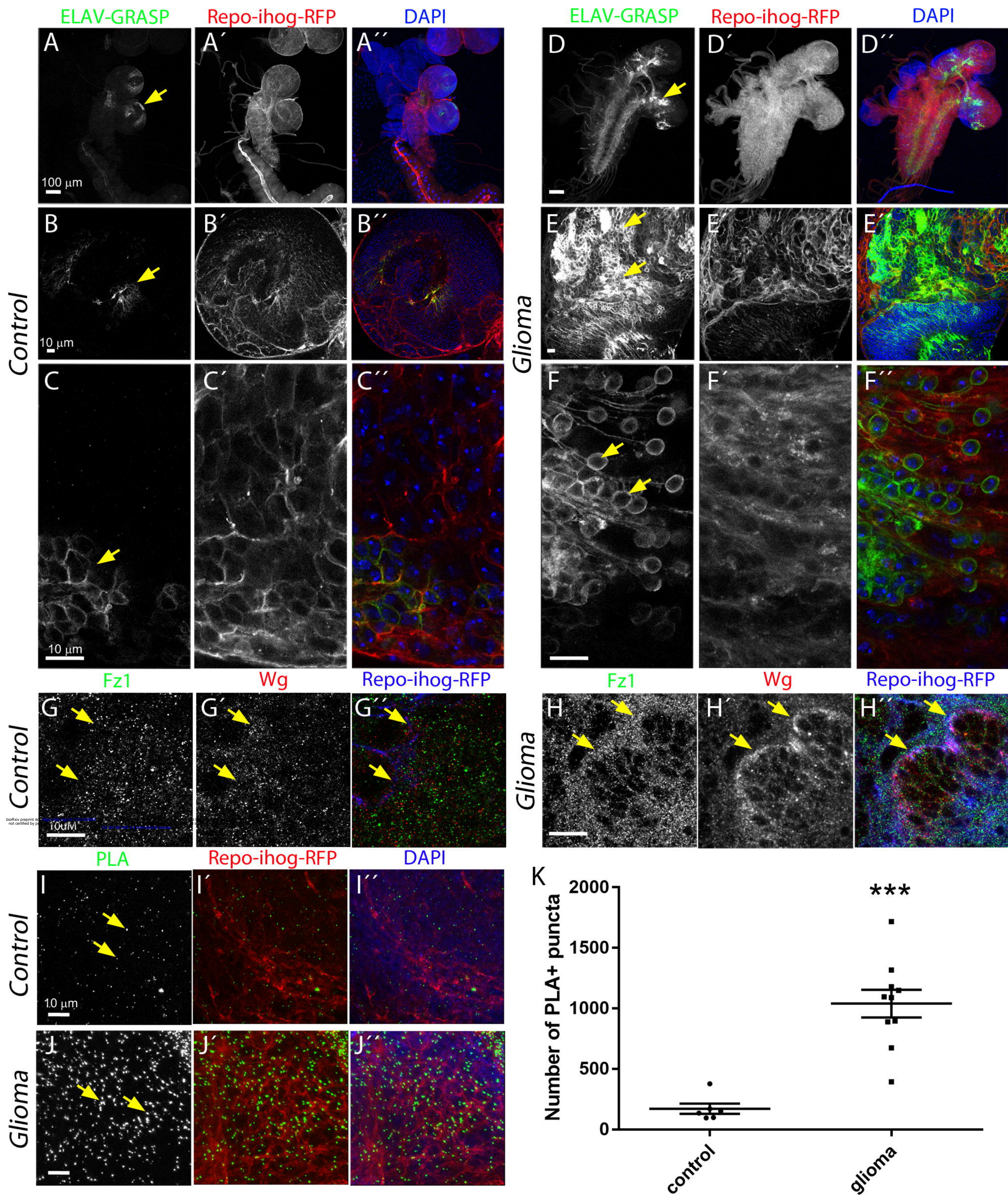
IMARIS 3D

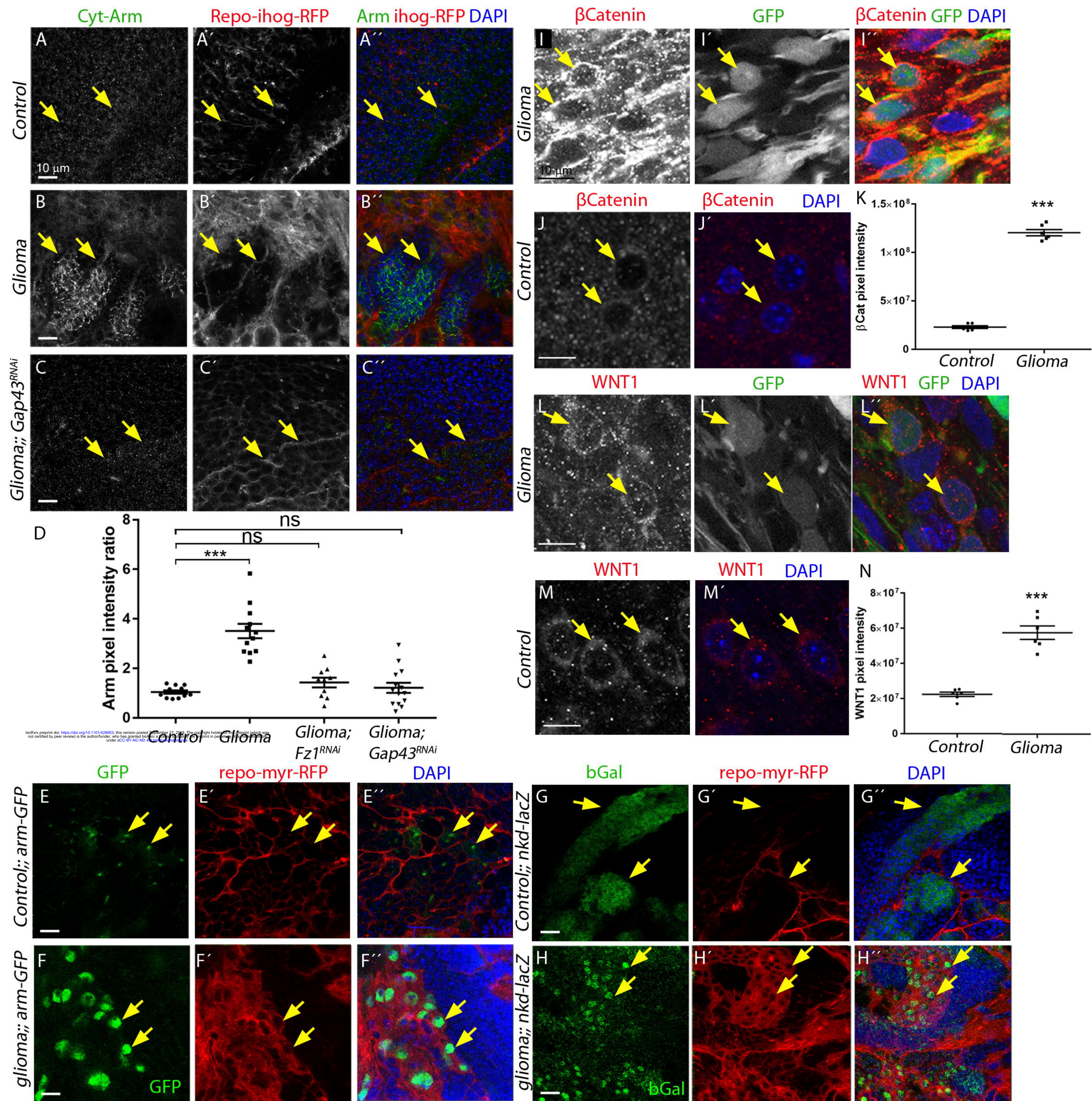




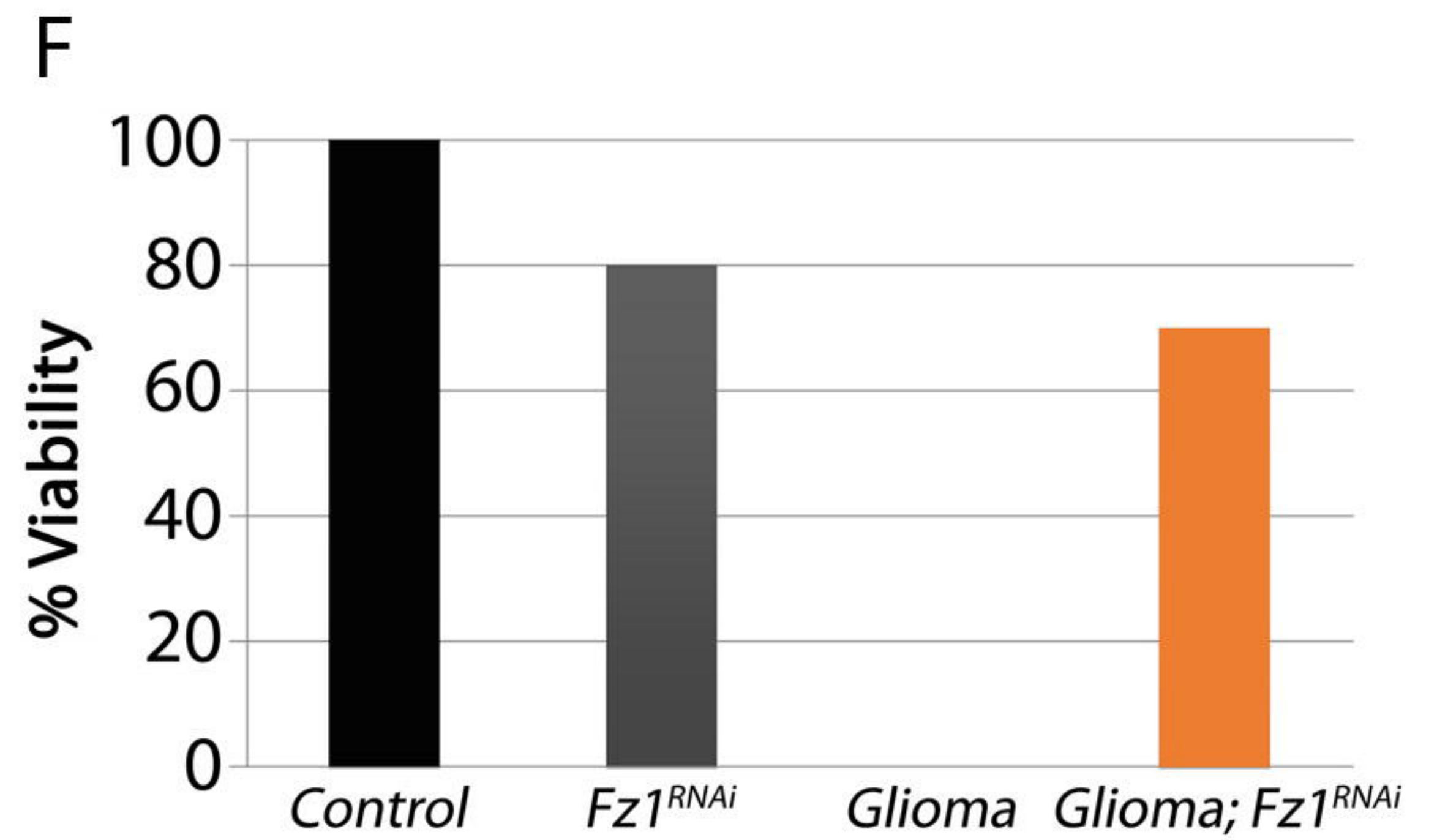
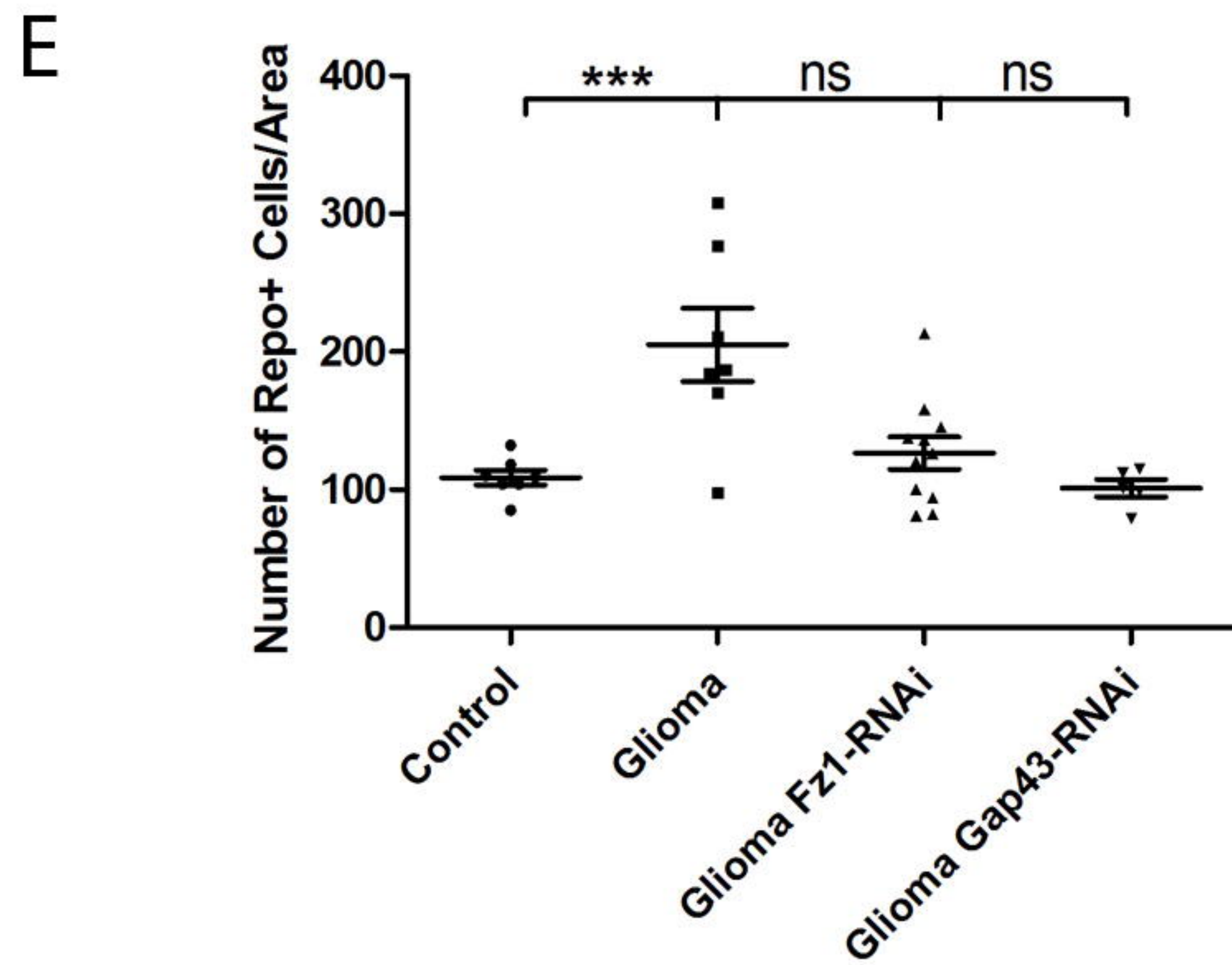
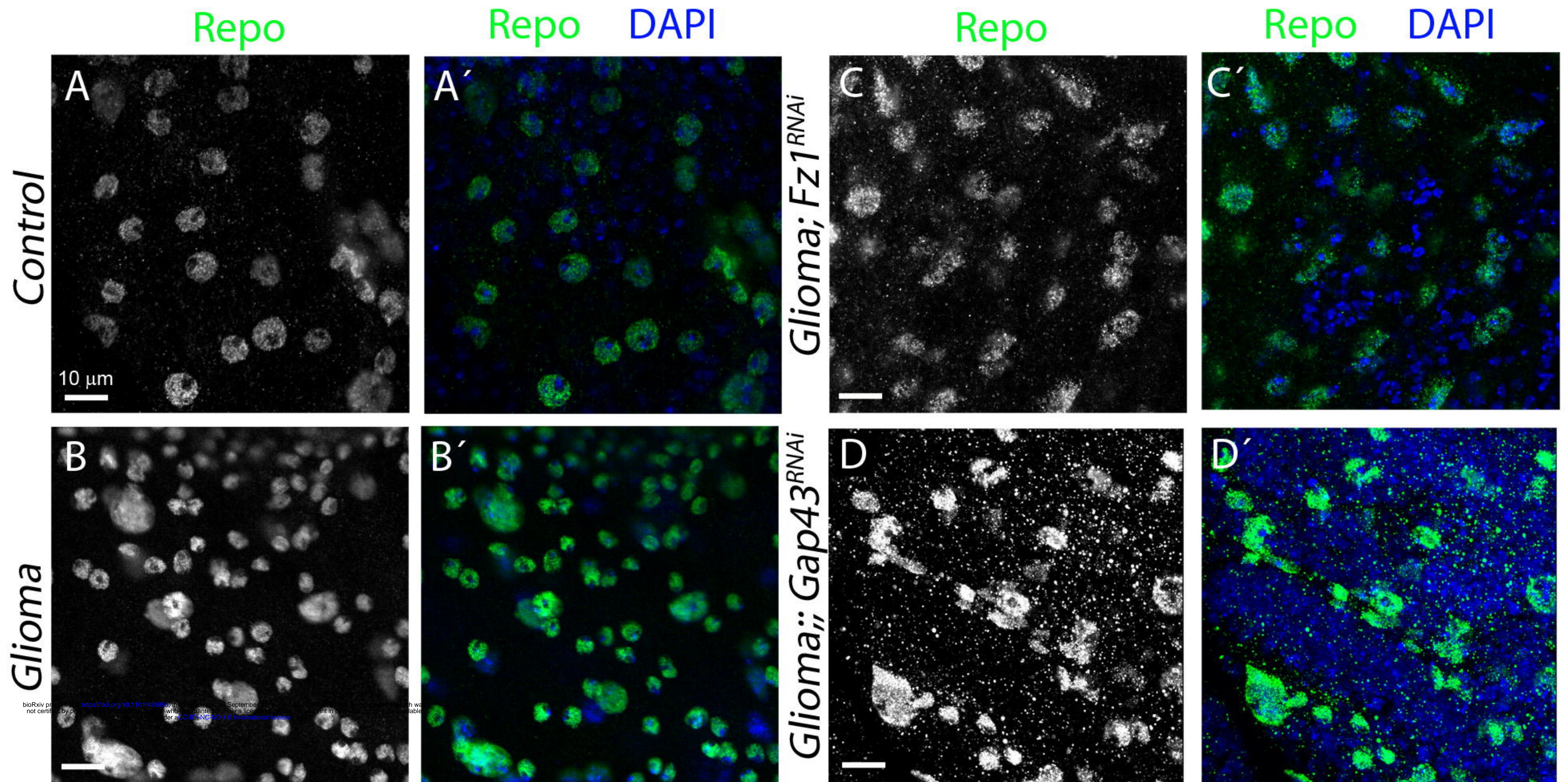
bioRxiv preprint doi: <https://doi.org/10.1101/428953>; this version posted September 27, 2018. The copyright holder for this preprint (which was not certified by peer review) is the author/funder, who has granted bioRxiv a license to display the preprint in perpetuity. It is made available under aCC-BY-NC-ND 4.0 International license.



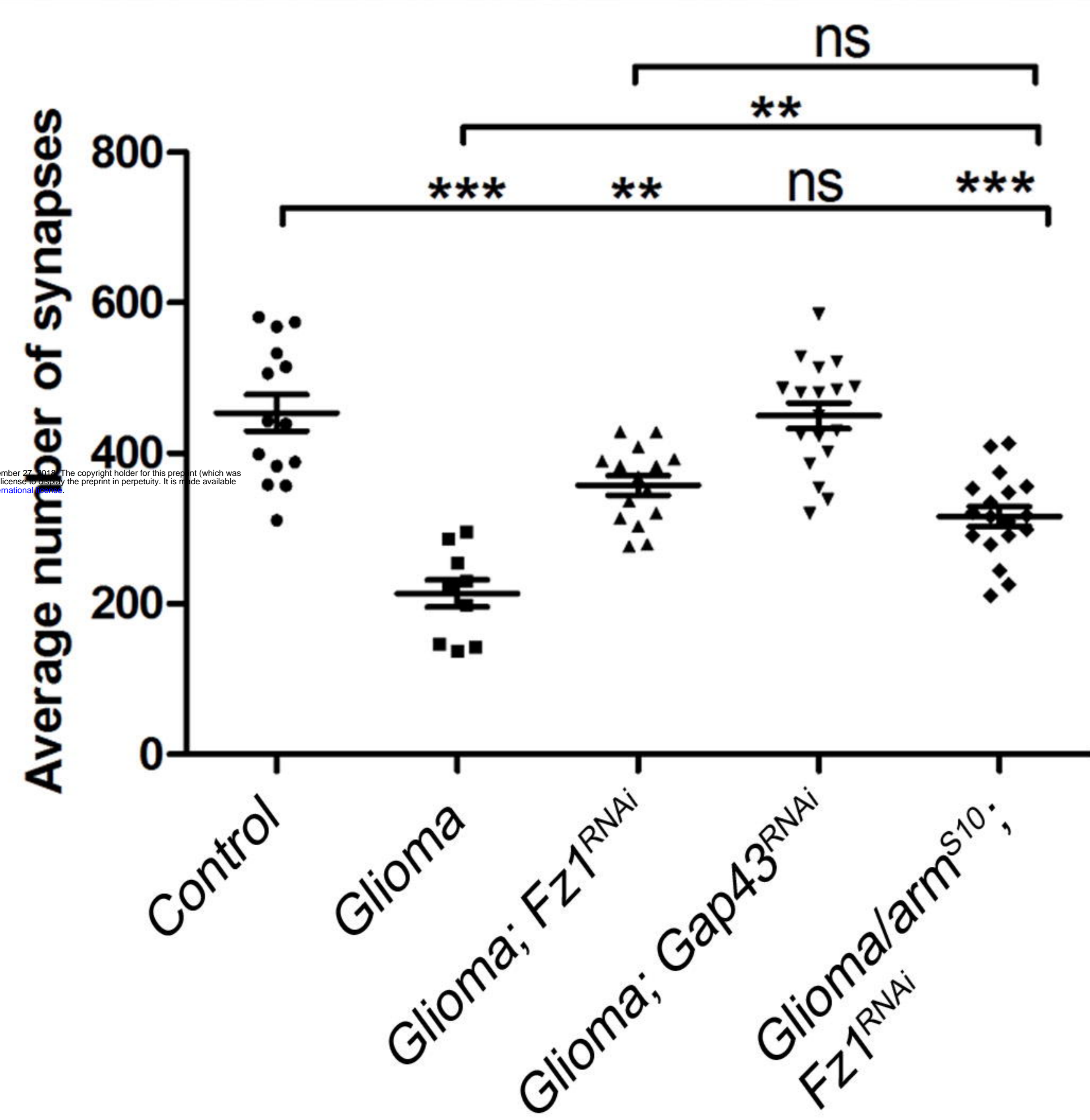
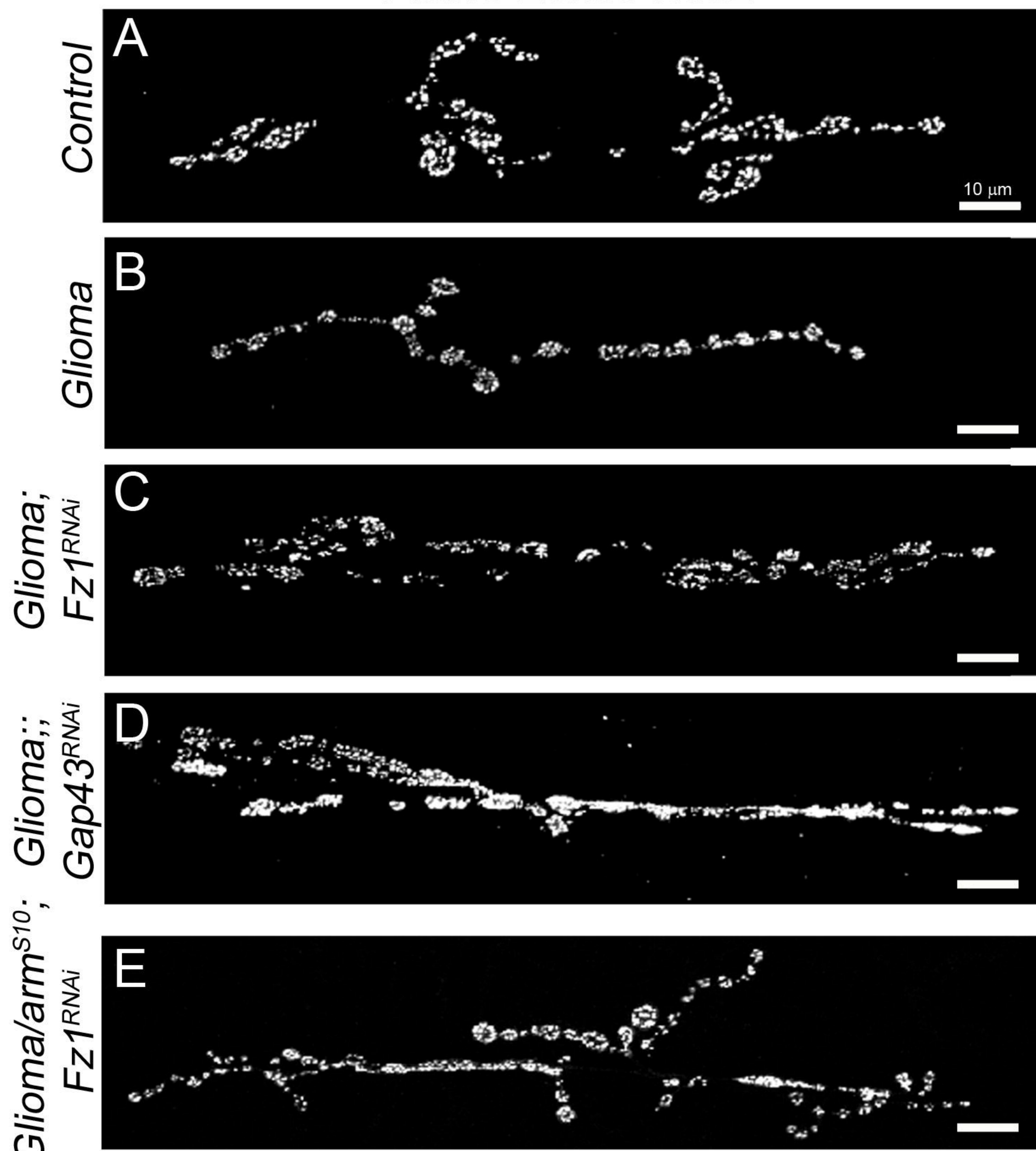








Active Zones Nc82



Repo

Repo-ihog-RFP

DAPI

